MESOPOROUS CARBON MATERIALS DERIVED FROM *ARTOCARPUS HETEROPHYLLUS* FOR WATER DESALINATION AND DEFLUORIDATION USING CAPACITIVE DEIONIZATION

Joyce Elisadiki

A Dissertation Submitted in Partial Fulfillment of the Requirements for the Degree of Doctor of Philosophy in Sustainable Energy Science and Engineering of the Nelson Mandela African Institution of Science and Technology

Arusha, Tanzania

February, 2020

ABSTRACT

Sustainable clean water for human use can be attained through cost-effective water purification technologies whereby capacitive deionization (CDI) technology is among them. To attain high CDI performance porous carbon materials with high surface area, specific capacitance, and good chemical stability are essential. In this study, high surface area mesoporous carbon has been synthesized from jackfruit peels (*Artocarpus heterophyllus*) through chemical activation method. Two different activation routes were used; carbonization followed by KOH activation and direct activation with H_3PO_4. In KOH activation route, the activation process was done by varying activation temperature from 600 to 800 ˚C and KOH to carbon ratio (KOH/C) from 1 to 3 for 1 h. In H_3PO_4 route, activation was done by varying concentration of H_3PO_4 from 10 to 35% and activation temperature from 450 to 550 ˚C for 1 h. The textural properties of the synthesized jackfruit activated carbon (JFAC) and electrochemical characteristics of the fabricated electrodes were found to be influenced by activating agent ratio/concentration and activation temperature. The synthesized JFAC possess a honey comb-like structure with plentiful mesopores at a pore size range of 3.0-5.0 nm which are beneficial for electrosorption. The BET surface area and pore volume of the carbonized jackfruit peels (JFC) increased from 607 to 2681 m^2/g and 0.52 to 2.61 cm^3/g respectively, upon activation with KOH/C ratio of 2 at 800 °C. Nitrogen adsorption-desorption studies revealed that the synthesized JFAC is mainly mesopores characterized by type IV isotherms according to IUPAC classification. Desalination experiments were carried out with 30 to 500 mg/L NaCl solution in batch mode at a flow rate of 2.5 mL/min while applying a voltage of 1.2, 1.4 and 2.0 V to the cell. The electrosorption capacity and salt-removal efficiency increased with increasing BET surface area and applied potential. Among the samples studied, carbon produced with KOH/C ratio of 1 at 700 ˚C (JFAC-1-700) exhibited the highest specific capacitance of 307 F/g, high salt removal efficiency and electrosorption capacity of 5.74 mg/g when voltage of 2 V was applied. When JFAC electrodes were studied for natural water defluoridation, it was found that JFAC CDI electrodes could remove fluoride (F^-) from natural water containing low F^- concentrations to the permissible limits set by the World Health Organization (WHO). Maximum F^- adsorption efficiency (62%) and electrosorption capacity (0.13 mg/g) were attained with applied voltage of 2 V and the pH of water remained unaffected. These results indicated that the *Artocarpus heterophyllus* peels can be the promising CDI electrode materials for low salinity water desalination and defluoridation.

DECLARATION

I, Joyce Elisadiki, do hereby declare to the Senate of The Nelson Mandela African Institution of Science and Technology that this dissertation titled "Mesoporous Carbon Materials Derived from *Artocarpus Heterophyllus* for Water Desalination and Defluoridation using Capacitive Deionization" is my own original work and that it has neither been submitted nor being concurrently submitted for degree award in any other institution.

_____ _____

Joyce Elisadiki Date

Name and Signature of the candidate

The above declaration is confirmed by:

_____ _____

Dr. Yusufu Abeid Jande Chande Date

Name and signature of supervisor 1

_____ _____

Dr. Revocatus Lazaro Machunda Date

Name and signature of supervisor 2

COPYRIGHT

CERTIFICATION

The undersigned certify that they have read and hereby recommend for examination by The Nelson Mandela African Institution of Science and Technology a dissertation entitled "Mesoporous Carbon Materials Derived from *Artocarpus Heterophyllus* for Water Desalination and Defluoridation using Capacitive Deionization" in partial fulfillment of the requirements for the Degree of Doctor of Philosophy in Sustainable Energy Science and Engineering at Nelson Mandela African Institution of Science and Technology, Arusha Tanzania.

_____ Date: _____

Dr. Yusufu Abeid Chande Jande

Name and signature of supervisor 1

_____ Date: _____

Dr. Revocatus Machunda

Name and signature of supervisor 2

ACKNOWLEDGMENT

I am grateful to Almighty God my creator for giving me the strength to accomplish my studies. I recognize the significant contribution from my supervisors Dr. Yusufu Abeid Jande Chande and Dr. Revocatus Lazaro Machunda. I owe a considerable debt to their enthusiastic encouragement, patience, motivation, wisdom, understanding, useful critiques, invaluable guidance, and continuous supervision during the course of my study.

I acknowledge Dean School of Materials, Energy, Water and Environmental Sciences (MEWES) Dr. Revocatus Machunda, Acting Head of the department of Materials and Energy Sciences and Engineering (MESE), Dr. Thomas Kivevele and all MEWES staff for their encouragement to this successful ending. I extend my sincere appreciation to Professor Tatiana and Prof. Alexander for their insightful comments, suggestions and their indefatigable spirit in helping every student. I wish their spirit could spread to every faculty member of NM-AIST.

I would also like to express my gratitude to the University of Dodoma through Higher Education Learning Student Loans Board (HELSB) for granting financial support and study leave to pursue my PhD. I also acknowledge the research grant support from European Union's Horizon 2020 research and innovation program under FLOWERED project grant agreement number 690378 and The World Academy of Sciences (TWAS) through grant number 16-529 RG/CHE/AF/AC_G-FR3240293305 dated 12th December 2016.

My heartfelt appreciation goes to Dr. Talam Enock Kibona and Dr. Agatha Wagutu who were former students at NM-AIST for introducing me to most of the laboratory facilities and continuous support during experimentation, data analysis, and manuscript and dissertation writing. I have greatly benefited from their support.

I would like to offer my special thanks to Dr. Bernard Samwel Mwankemwa my co-worker and a former PhD. student in Pretoria University for making all logistics to make sure that my samples were characterized at the University of Pretoria laboratories.

I would like to express my appreciation to MEWES laboratory scientist; Mr. Justin Lwekoramu, Miss Teresia Kimario, Mr. Paulo Sanka and Mr. Wilson Mahene for their technical support and help when I was doing my laboratory work. I also acknowledge Prof.

Marta Hatzell and Daniel A. Moreno from Georgia Institute of Technology for manufacturing the CDI cell which was used to in this study.

I express my heartfelt thanks to CDI research group pioneers at NM-AIST, Miss Tusekile Alfred and Amina Abdala, we used each other like a ladder to achieve what we have today. I can't forget MEWES cohort 5 and 6 students specifically, Robert Eliraison, Ablalah Msangi, Isack Kandola, Said Mateso, Linda Gesase, Gelion Mgaya, Christian Nabora, Fina Lesafi and Khasim Musa for their moral support, feedback, cooperation and of course friendship.

It is my honor to express my cordial thanks to my beloved husband Joseph Mkumi and my son George for their patient during my absence. Special thanks go to Miss Sara Ngomuo and my sister Omega Lyimo; they have been there for me all the time to take care of my family with excessive love. I extend my sincere thanks to my parents Mr. and Mrs. Elisadiki Lyimo, my brothers Felix, Daniel, Stephano and all loved ones for providing care and loving environment that allows me to freely pursue my studies to this level.

DEDICATION

This work is dedicated to my lovely daughter Giovanna as she was conceived and born within the course of my studies.

TABLE OF CONTENTS

LIST OF TABLES

LIST OF FIGURES

LIST OF ABBREVIATIONS AND SYMBOLS

a.u.	Arbitrary unit
AC	Activated carbon
Ag/AgCl	Silver/silver chloride
BDL	Below detection limit
BET	Brunauer-Emmett-Teller
BJH	Barrett-Joyner-Halenda
BWRO	Brackish water reverse osmosis
C	Carbon
CA	Carbon aerogel
Ca	Calcium
CDI	Capacitive deionization
CDTA	Cyclohexanediaminetetraacetic acid
ce-MoS_2	Chemically exfoliated Molybdenum disulfide
C_f	Final concentration
C_i	Initial concentration
CJF	Carbonized jackfruit peels
CNF	Carbon nanofiber
CNT	Carbon nanotube
CO_2,	Carbon dioxide
CV	Cyclic voltammetry
D	Defect
DC	Direct current
DWCNTs	Double walled Carbon nanotube
EBT	Erichrome Black T
EC	Electrosorption capacity
ED	Electrodialysis
EDL	Electrical double layer
EDLC	Electrical double layer capacitor
EDTA	Ethylenediaminetetraacetic acid
EIS	Electrochemical impedance spectroscopy
ESR	Equivalent series resistance

F^-	Fluoride
FE SEM	Field Emission Scanning Electron Microscopy
FO	Forward osmosis
G	Graphitic
G.Hdy	Gas hydrate
H	Hydrogen
HNO_3	Nitric acid
H_2O	Water
$H_3PO_{4,}$	Phosphoric acid
HCl	Hydrochloric acid
HTC	Hydrothermal carbonization
I	Intensity
I.Ex	Ion-exchange desalination
ISE	Ion selective electrode
IUPAC	International Union of Pure and Applied Chemistry
JFAC	Jackfruit peels activated carbon
K_2CO_3	Potassium carbonate
K_2O	Potassium oxide
KCl	Potassium Chloride
$KHCO_3$	Potassium bicarbonate
KOH,	Potassium hydroxide
LLE	Liquid-liquid extraction
M	Mole
MCDI	Membrane capacitive deionization
MD	Membrane distillation
MED	Multiple effect distillation
Mg	Magnesium
MSF	Multistage flash distillation
MVC	Mechanical vapor compression
N	Nitrogen
NaCl	Sodium chloride
NaF	Sodium fluoride

$NaNO_3$	Sodium nitrate
$NH_4H_2PO_4$	Ammonium dihydrogen phosphate
NHE	Normal hydrogen electrode
O	Oxygen
PTFE	Polytetrafluoroethylene
PVDF	Poly vinyldenedefluoride
RGO	Reduced graphene oxide
RO	Reverse osmosis
S	Sulfur
SCBFA	Sugarcane bagasse fly ash
S_{meso}	Mesopore surface area
S_{micro}	Micropore surface area
SPC	Specific capacitance
SSA	Specific Surface area
SWCNTs	Single-walled Carbon nanotube
TDS	Total dissolved solids
TVC	Thermal vapor compression
WHO	World Health organization
XRD	X-ray diffractometer
$ZnCl_2$	Zinc chloride

CHAPTER ONE

INTRODUCTION

1.1 Background

The need for fresh water is increasing as population, desertification, and pollution are increasing (Zhao *et al*., 2013a). Statistics show that 97.5% of the global water resources is saline water (sea and brackish water) (Demirer *et al*., 2013) which cannot be used directly for domestic purposes and only 2.5 % is fresh water in ground water, lakes and rivers. Classification of water resources according to the amount of total dissolved salt (TDS) and its percentage globally are presented in Table 1 (Husain, 2017). Out of the 2.5 % of global fresh water resource, approximately 70% is snow and ice, 30% is groundwater and less than 0.5% is surface water (Song *et al*., 2018) that have been overused by the overgrowing population. This situation creates a great worry if the available fresh water will meet the demand of the population.

Apart from water being saline, water may contain ions which are problematic when existing in higher concentrations. For example, the presence of F^- in drinking water has either positive or negative effects on teeth and bones subject to the concentration and total amount consumed. For instance, F^- concentrations between 1–1.5 mg/L make the enamel stronger, 1.5–4 mg/L lead to dental fluorosis, higher concentration (4-10 mg/L) with long term exposure cause skeletal fluorosis while low concentration (approximately 0.5 mg/L) prevents the occurrence of dental caries (Mohapatra *et al*., 2009). It is recommended that any drinking water should have a maximum permissible limit of F^- of 1.5 mg/L and desirable highest limit of 1.0 mg/L (WHO, 2011). Therefore, defluoridation of drinking water at the source or at the household level is very important to prevent and control the occurrence of fluorosis (Khairnar *et al*., 2015) especially in major fluoride belts in the world, such as areas of China, India and the Main Ethiopian Rift Valley located in Rift Valley of Africa (Brunson & Sabatini, 2013).

Worldwide, 1.1 billion people lack safe drinking water in which about 900 million are people in rural areas that have low income. Statistics shows that number of people lacking safe drinking water is expected to increase in Africa and in Asia by 2025 (Rijsberman, 2006). This calls for innovative, sustainable, cost-effective, energy efficient and environmentally friendly water desalination and defluoridation technologies to alleviate fresh water scarcity.

Table 1: Categories of water resource according to total dissolved salt and its percentage

Type	Total Dissolved salt (ppm)	Global water resource (%)
Fresh water	500 or less	2.5
Brackish water	500 to 35,000	
Sea water	> 35,000	
Brine concentrate	> 50,000	97.5

Demirer *et al*.(2013)and Husain, (2017)

Desalination is the processes that remove the amount of salt and any other minerals present in the water to produce potable water or water that is low in TDS (less than 500 ppm) whereas defluoridation is the process that removes excess fluoride from water. Diverse processes have been used in desalting saline water, to mention the few; electrodialysis methods, membrane distillation processes, reverse osmosis and capacitive deionization (CDI) (Jande & Kim, 2013b). For the fluoride removal, methods such as coagulation, adsorption, and precipitation, ion exchange, reverse osmosis, and electrodialysis have been pronounced (Tang *et al*., 2016b). Most of these methods have weakness such as high energy consumption, the need for large and costly infrastructure which results in high operational cost and sometimes employment of hazardous chemicals in the course of water treatment (Jande & Kim, 2013a; Welgemoed & Schutte, 2005). It has been reported that about 50% of the operational costs in most water desalination processes are power costs, and these costs have a direct impact on the cost of treated water (Al-Karaghouli & Kazmerski, 2013). Currently, researchers are working on a general goal to make these technologies cost-effective and more energy efficient so that societies with low income which are the vulnerable group can afford.

Currently, CDI is among the promising cost effective water desalination method due to the fact that it operates under lower power levels and it is easy to regenerate the electrodes. When compared to other desalination techniques which extract water (the majority phase) from the salt solution, CDI is energy efficiency owing to the fact that it removes the salt ions, which are the minority compound in the water (Porada *et al*., 2013b). Energy consumption in CDI has been reported to be less than 0.6 kWh/m^3 for TDS removal from ground brackish water (Welgemoed & Schutte, 2005).

Generally, CDI uses electric fields to adsorb temporally charged species such as salt ions present in aqueous solution and store them in a polarized surface (Jande & Kim, 2013a) and it

operates under two main approaches which are capacitive electrosorption and Faradaic ion storage (Zhang *et al*., 2018a). Capacitive electrosorption is the most common approach in which ions are stored within highly porous carbon material due to the formation of electrical double layer (EDL). Since CDI operates by forming EDL, its performance relies on electrode materials (Porada *et al*., 2013b) and researchers are working hard to find suitable materials that will improve its capacitive charge storage and electrosorption capacity. Usually porous carbon with good electrical conductivity, a high surface area, and high capacitance is ideal for CDI electrodes. Up to the present time, various types of carbon materials have been studied as CDI electrode materials, including carbon nanotubes (CNT) (Wang *et al*., 2011), activated carbon (AC) (Zou *et al*., 2008b), carbon nanofibers (CNF) (El-Deen *et al*., 2014a), carbon aerogel (Gabelich *et al*., 2002), graphene (Liu *et al*., 2017) together with their composites (Liu *et al*., 2015b).

Though carbon aerogels, carbon nanotubes and carbon nanofibers, have been reported with outstanding electrosorption performances, their complex synthetic routes and material cost hinders their large scale production for CDI application. For instance, the production costs for CNT electrode material is estimated to be USD 450.01 m^{-2} while the cost for producing AC electrode is USD 0.89 m^{-2} only (Chang *et al*., 2011). With this regard, AC has made through commercial CDI systems since it is considered as the most cost-effective material than the aforementioned materials (Porada *et al*., 2013b). For many years petroleum residues, coal, wood, lignite, peat and polymers have been used as a precursor for traditional production AC, but these precursors are costly and non-renewable in nature (Chen *et al*., 2011). Therefore, AC derived from lignocellulosic biomass or their by-products precursor is a potential choice owing to their availability, low-cost of the carbon precursor, renewable nature and minimal secondary environmental impact (Chen *et al*., 2011).

Several researchers have studied the possibility of producing carbon from lignocellulosic materials for various applications by taking advantage of its specific properties like volatile matter, ash and fixed carbon content (Mohamad Nor *et al*., 2013; Viswanathan *et al*., 2009). Carbon can be derived via carbonization of these lignocellulosic materials at a temperature of 400^{o}C to produce macroporous products with no significant surface area. To modify the structure of the obtained carbon, materials are activated chemically or physically to obtain AC with nanometer size pores (Enock *et al*., 2017b; Leong *et al*., 2019). Apart from the activation method, the carbon precursor and the synthesis procedures also influence the

textural and surface properties of the produced carbon. Various agricultural wastes and by-product including biogas slurry, coconut shells, seaweeds, waste coffee beans, peanut shell, seed shells, fruit peels, sugarcane bagasse and fungi have been successfully converted to porous carbon owing to their high carbon and low ash contents. The obtained carbon has shown tremendous performance in many fields including energy storage applications in the field of supercapacitor as reviewed by Enock *et al*. (2017a) , in lithium-ion batteries (Liu *et al*., 2014) and in water treatment using CDI (Quan *et al*., 2016). It is worth to note that these carbon precursors may also be used in water desalination via CDI since the principle of operation of CDI and supercapacitors are somehow the same. Both technologies are based on adsorption of ions in a double-layer, though the major purpose of CDI is salt/charged species adsorption and not energy storage as in capacitive devices (Leong *et al*., 2019).

Artocarpus heterophyllus commonly known as jackfruit is a common fruit in coastal areas of Southeast Asia and East Africa. A large amount of ripe fruit (59%) is thrown away as a waste (Inbaraj & Sulochana, 2004). The outer peels of the ripe fruit are categorized as lignocellulosic biomass with cellulose (54%), hemicellulose (23%) and lignin (3%) content suitable for qualifying it as carbon precursor (Selvaraju & Bakar, 2017). These properties together with its high carbon (>45%) and low extractives (15.3 wt%) content have driven researchers to synthesize porous carbon from this low-cost agricultural waste for various applications including removal of heavy metal such as cadmium (Inbaraj & Sulochana, 2004) and lead (Rosli *et al*., 2015), adsorption of dyes rhodamine-B (Inbaraj & Sulochana, 2006), methylene blue (Foo & Hameed, 2012) and iodine (Selvaraju & Bakar, 2017) from aqueous solution. To the best of our knowledge, jackfruit peels activated carbon (JFAC) has not been studied as electrode material for CDI. Therefore, this study has investigated the use of JFAC as electrode material for CDI cell for desalination and defluoridation applications.

1.2 Statement of the Problem

Capacitive deionization has been reported as a cost-effective, energy efficient, and a robust technology for desalination of water with a low or moderate salt content (Porada *et al*., 2013b). However, its performance depends on the materials used in making the electrodes. Various materials have been used to make CDI electrodes with ultrahigh performance. However, the complicated synthesis routes, cost of the materials and low scale yield obstructs their commercial application. Hence, using abundant, environmentally friendly and low cost biomass waste for making CDI electrode material may serve as a promising alternative to

scale up CDI technology. Jackfruit is a common fruit in coastal area and a large amount of ripe fruit thrown away as a waste. The outer peels of the ripe fruit are categorized as lignocellulosic biomass with cellulose (54%), hemicellulose (23%) and lignin (3%) content suitable for qualifying it as carbon precursor (Selvaraju & Bakar, 2017). These properties together with its high carbon content, prompted researchers to synthesis activated carbon from it for various applications. Therefore, converting this waste into value added CDI electrode materials is also considered beneficial. This study, explored the effectiveness of CDI electrodes material derived from jackfruit peels for water desalination and defluoridation applications.

1.3 Rationale of the Study

Many regions in the world including Tanzania lacks sufficient amount of potable water. This trend is expected to continue and affect the lives of billions of people due to population growth. Hence, there is a need to reclaim water from various sources to meet the demand of the population. Various water purification technologies are in the market but most of them are energy intensive and very expensive that societies with low income cannot afford. Therefore, the CDI unit with electrodes developed from biomass waste may serve as cost-effective and energy efficient technology for water defluoridation and desalination applications. Furthermore, since the CDI electrodes are developed from agricultural wastes, this will also contribute towards environmental protection through the better solid waste management system.

1.4 Objectives

1.4.1 General objective

The general objective of this work was to develop and optimize CDI electrodes from agricultural biomass wastes and evaluate their performance for saline water desalination and fluoride removal.

1.4.2 Specific objectives

(i) To synthesize and characterize activated carbon material derived from jackfruit peels for CDI applications.

(ii) To investigate the electrochemical properties of electrode fabricated from the synthesized carbon.
(iii) To evaluate performance of the jackfruit based CDI electrodes for saline water desalination and fluoride removal.

1.5 Research questions

(i) What are the characteristics of porous carbon materials derived from jackfruit peels which make them effective electrode material for the CDI process?
(ii) To what extent does the electrode fabricated from jackfruit peels attain the electrochemical properties that favor CDI performance?
(iii) What are the optimal conditions which influence the performance CDI process for saline water desalination and fluoride removal?

1.6 The significance of the research

The use of low-cost, environmentally friendly and sustainable carbon precursor for production of inexpensive CDI electrode materials is extremely important for its industrial application. This study provides simple and cost-effective CDI electrode materials derived from jackfruit peels for water desalination and defluoridation. The results of this study will contribute to the body of knowledge in the literature of water desalination and defluoridation using mesoporous carbon electrodes derived from biomass waste (i.e. Jackfruit peels). Furthermore, the use of jackfruits peels as a source of carbon will encourage *Artocarpus heterophyllus* tree planting and increase quantity fruits produced. Since a large amount of the ripe jackfruit (59%) is thrown away as waste, converting this waste into value-added material is advantageous from economic and environmental perceptions and will bring sustainable solutions to solid waste management and solve environmental challenges facing the world today.

1.7 Delineation of the study

This study aimed at investigating suitability of abundant agricultural waste from jack fruit peels in developing cost-effective electrode materials for water desalination and defluoridation by using CDI technology. Synthesis methods, characterization of materials and performance of the materials as CDI electrodes in terms of electrosorption capacities are discussed. Generally, this dissertation is divided into 5 chapters; Chapter one consists of the

background statement information, rationale of the study, objectives, research questions and the significance of the study. Chapter two presents the literature review in which major desalination technologies and biomass-based electrode materials for CDI are discussed. Chapter three covers synthesis of activated carbon from jackfruit peels, different techniques used in characterizing the developed materials, preparation of CDI electrodes and electrosorption experiment. Chapter four presents the results and discussion where by effect of different activating agent ratio, concentration and temperature on the surface area and porous structure of the formed carbon together with their electrochemical properties and electrosorption capacities of the electrodes are discussed. Chapter five presents conclusion and recommendations. Although the study thought to develop simple, low cost and more efficient materials, cost benefit analysis has not been carried out. This forms one of the limitations of this study and forms a gap for future studies of this kind. The scope of this study spanned towards developing efficient materials for water desalinization. Moreover, the efficiency of jackfruits peels, which is a common fruit in the coastal areas, has been scientifically proven by this study. However, being cost-effective in other areas where the fruit does not grow will hugely depend on the cost of availability. This equally forms the limitation of the study.

CHAPTER TWO

LITERATURE REVIEW

2.1 Introduction

The scarcity of fresh water is one among the life threatening issues of world population. To resolve this crisis, desalination have been proposed to extract fresh water from sources such as seawater and brackish groundwater to make it appropriate for various daily use such as drinking, household activities, agriculture and for different industrial and commercial applications. Various technologies are commercially available but most of them are energy intensive and very expensive that societies with low income cannot afford. This calls for the need of developing affordable and energy efficient desalination technologies. Capacitive deionization is among the future promising water purification technology that can override the energy intensive technologies. Nevertheless, finding low- cost electrode material with high electrosorption capacity is still a challenge. Therefore, research on simple methods for the synthesis of electrode materials from low-cost biomass precursors is highly needed. This chapter highlights on water purification technologies. Capacitive deionization is discussed in details, whereby various CDI electrode materials are presented with more emphasis on biomass-based CDI electrode materials. The CDI module configuration and operating conditions have also been pointed out.

2.2 Water desalination technologies

Water desalination technologies are categorized depending on its working principle or form of energy they use. These include; thermally based technologies (Ng *et al*., 2015), membrane-based (Souhaimi & Matsuura, 2011), chemically activated systems (Youssef *et al*., 2014), and electrical processes (Demirer *et al*., 2013). Description of the working principle, advantages and disadvantages of the most pronounced desalination technologies are given in the next sub-sections.

2.2.1 Thermally-based desalination methods

Thermally-based technologies rely on evaporation and condensation of saline water to obtain a solid by-product (salts) and fresh water (Demirer *et al*., 2013). These technologies include; multiple effect distillation (MED) (Desale *et al*., 2011), multistage flash distillation (MSF) (Abdul-Wahab & Abdo, 2007), thermal vapor compression (TVC) (Ettouney, 1999) and

mechanical vapor compression (MVC) (Bahar *et al*., 2004). These methods have large production capacity and are more effective in the desalination of water with very high TDS (i.e. seawaters) when compared to membrane methods. However, they are more expensive because of the large quantities of energy needed for salt water distillation.

2.2.2 Membrane-based technologies

Membrane-based technologies utilize permeable membranes which act as a filter to create two zones in which water is allowed to pass through while leaving behind the unwanted molecules such as salts, metals, bacteria, and viruses (Youssef *et al*., 2014). Reverse osmosis (RO) (Kaschemekat *et al*., 1983) and membrane distillation (MD) (Lee & Kim, 2013) are among membrane-based desalination methods. One of the major challenges of these systems is membrane fouling which leads to the deterioration of the basic membrane functions and hinders its sustainable operation. In the case of MD, Khayet (2011) pointed out challenges such as module and membrane design, poor wetting of the membrane, flux decay, low permeate flow rate and unpredictable energetic and economic costs hinders its acceptance and development. Therefore, water pre-treatment are required before being introduced into the desalination modules. Also, the high cost of membrane replacement hinders the application of membrane methods in desalinating seawater (Karagiannis & Soldatos, 2008).

2.2.3 Chemically-activated desalination systems

In these systems, a variety of chemicals are used to support desalination operations. These systems include ion-exchange desalination (I.Ex), liquid-liquid extraction (LLE) and gas hydrate (G.Hdy) (Youssef *et al*., 2014). For example in I.Ex, a physical-chemical process is used to separate ionic contaminants from salt solution by replacing them with other ions of the similar electrical charge and it have been used to soften water, and to produce high purity de-ionized water for special applications. Generally, chemically activated methods are too expensive to be used for production of fresh water for general use because it cannot be used to treat water with higher TDS (Shatat & Riffat, 2012).

2.2.4 Electrically based desalination methods

Electrically based desalination methods include

and electrodialysis (ED) in which electric potential is applied to facilitate the migration of pollutant ions to a storage location (Demirer *et al*., 2013). In ED technology electric field separates and facilitates ions from saline water to transport through the ion exchange membranes while in CDI ions are stored in the EDL formed at the interface between the oppositely charged porous electrodes and solution.

Table 2 presents the advantages and disadvantages of some well-known commercial desalination technologies together with CDI. It can be seen that each technology has some limitations which make it not to be preferred than the other. The RO, MSF and MED systems are the most implemented desalination technologies. Detailed comparisons of various desalination technologies in terms of the driving force, energy consumption and cost of purifying water are presented in Table 3. Thermal processes are quite energy intensive because large quantities of energy are required to vaporize saline water. As shown in Table 3, MED, MSF, TVC, MVC, seawater RO, and brackish water RO (BWRO) use around 1.5-27.25 kWh of electrical energy to produce 1000 liters of fresh water. RO, which is the dominant desalination technology has additional drawbacks such as low water recovery, membranes are vulnerable to bio-fouling and scaling (Quist-Jensen *et al*., 2015).

Moreover, RO is energy efficient for treating water with high salinity and less efficient for treating water with low salinity (below 5000 ppm). Thus ED and CDI are termed as efficient alternative technologies for desalinating streams with low or moderate salt content salt. Forward osmosis (FO) is reported as a promising technology for desalinating seawater with lower membrane fouling effects compared with pressure-driven membrane processes. However, its use for practical application is still in the developing stages (Cath *et al*., 2006). Therefore, environmentally friendly, economical and energy efficient technology for water desalination is required.

Table 2: Advantages and disadvantages of the desalination processes

Technology	Advantages	Disadvantages
MSF	Simple to construct and operate. Seawater desalination is possible	Energy-intensive process (requires both thermal and electrical energy) Requires huge installations which are difficult to maintain
MED	Consume low power than MSF plan	Anti-scales agents required for stopping scale build-up on evaporating surfaces.
MD	It is simple and requires the low temperature to operate	Poor wetting of the membrane, Unpredictable energetic and economic costs
RO	Low capital cost Energy efficient to treat water with high salt concentrations (> 5000 ppm) Plant size can be expanded depending on the demand at a time	Water pre-treatment is required Membranes are susceptible to fouling. Its configuration is complex Its operation and maintenance requires skilled personnel
ED	Requires DC current to separate and transport the ionic substances in the membrane Membranes last long Energy consumption is proportional to the amount salts removed.	Requires huge capital. Feasible for treating water with low salinity
CDI	Low capital cost Cost-effective and eco-friendly Safe as it uses a low DC electrical potential (0.6–2.0 V) Desalinate water with low salt concentration (10 g/L), beneficial for rural or remote communities No additional chemicals needed for regeneration of the electrodes. Power consumption depends on the amount of salt removed.	Seawater desalination is difficult

Alkaisi *et al*. (2017); Shatat and Riffat, (2012) and Thamilselvan *et al*.(2016)

Table 3: Energy consumption and cost of water for different desalination technologies

Desalination Technology	Driving force	Electrical energy consumption (kW h/m^3)	Equivalent electrical to thermal energy (kW h/m^3)	Total electricity consumption (kW h/m^3)	*Cost of water US$/$m^3$	References
MSF	Thermally	2.5 – 5	15.83-23.5	19.58–27.25	0.56 -1.75	(Al-Karaghouli & Kazmerski, 2013; Youssef *et al*., 2014)
MED	Thermally driven	2.5 - 5	12.2-19.1	14.45 – 21.35	0.52- 8	(Al-Karaghouli & Kazmerski, 2013)
MVC	Thermally driven	7–12	None	7 – 12	2 – 2.6	(Al-Karaghouli & Kazmerski, 2013)
TVC	Thermally driven	1.8–1.6	14.5	16.26	2 - 2.6	(Al-Karaghouli & Kazmerski, 2013)
BWRO	Pressure	1.5 – 2.5	None	1.5 – 2.5	0.26- 13	(Al-Karaghouli & Kazmerski, 2013)
SWRO	Pressure	4 – 6	None	4 - 6	0.45– 1.72	(Al-Karaghouli & Kazmerski, 2013)
FO	Concentration driven	3 - 8	None	3 - 8	0.80	(Moon & Lee, 2012; Youssef *et al*., 2014)
ED	Potential difference	0.7 –5.5	None	0.7–5.5	0.6 -1.05	(Al-Karaghouli & Kazmerski, 2013)
I.Ex	Chemical separation	1.1	None	1.1	1.05	(Youssef *et al*., 2014)
G.Hdy	Chemically driven	1.58	None	1.58	0.63	(Youssef *et al*., 2014)
LLE	Chemically driven	6	None	6	0.40	(Youssef *et al*., 2014)
CDI	Potential difference	0.6	None	0.6	0.11	(Gaikwad & Balomajumder, 2016; Welgemoed & Schutte, 2005)

*Cost of water depends on the size of the system and concentration of the feed solution

As an upcoming desalination technology, CDI is considered promising when compared to other desalination technologies due to its lower energy consumption per liter of water produced (Table 3) and membrane-free approach since it does not force water to pass through a membrane (Farmer *et al*., 1996; Welgemoed, 2005; Welgemoed & Schutte, 2005). Capacitive deionization uses low direct current (DC) power (either constant current or constant voltage) to polarize a pair of porous electrodes allowing ion adsorption (Jande & Kim, 2013a). The electrical energy supplied during charging of the CDI cell for adsorption of an ion can be recovered during the cell discharge in desorption phase. The energy recovery in CDI is a significant advantage when compared to other desalination technologies since energy efficiency is a key factor in desalination technology (Anderson *et al*., 2010).

Although CDI is termed as membrane free technology, it has been already proven that modifying CDI by placing ion exchange membranes (IEMs) in front of the carbon electrodes increases the salt adsorption in the system. The modified CDI system which contains IEMs is called membrane capacitive deionization (MCDI) (Zhao *et al*., 2012; Zhao *et al*., 2013b). The added IEMs prevent co-ion expulsion effect and improve the charge efficiency of the system. Improved charge efficiency leads to lower power consumption in MCDI when compared to CDI (Suss *et al*., 2015). Though MCDI has shown excellent performance, membrane cost and high contact resistance resulting from poor adhesion between the membranes and CDI electrodes limits its commercial application (Liu *et al*., 2016). Therefore, cost-effective and straightforward strategies that are analogous to the MCDI such as grafting electrodes with ion-selective functional groups (Liu *et al*., 2016; Yang *et al*., 2013) and the use of asymmetric electrodes (Lu *et al*., 2014; Yan *et al*., 2018) have been proposed to overcome the effect of co-ion expulsion and improve charge efficiency in CDI.

2.3 Fluoride removal technologies

Table 4 presents various methods that are currently used for water defluoridation. Adsorption is the most common method in which adsorbents such as born char (Brunson & Sabatini, 2013), calcium phosphate systems (Wagutu *et al*., 2018), activated alumina (Tang *et al*., 2009) and activated carbon (Yadav *et al*., 2013) are commonly used. Nevertheless, availability of low cost and sustainable adsorbent precursor at or near to areas affected by fluoride, simple methods for synthesizing adsorbent with high removal efficiency when using natural water and regeneration of the adsorbent are the most challenging issues (Barathi *et al*., 2013; Yadav *et al*., 2013). Thus, low energy consumption, environmentally friendly, easy

regeneration and cost-effective electrochemical methods are considered as an alternative water purification technology.

Table 4: Advantages and disadvantages of water defluoridation methods

Method	Advantages	Disadvantages
Coagulation/precipitation (calcium hydroxide and aluminum hydroxide)	High efficiency Chemicals used are commercially available	Expensive It's efficiency depends on pH and presence of co-ions in water Requires adjustment and readjustment of pH Results into high residual with toxic aluminum fluoride complex
Membrane filtration: RO and nanofiltration	High efficiency Remove other contaminants	Requires high capital, running and maintenance costs Produce toxic waste water by-product
Electrochemical treatments: dialysis, ED and electro-coagulation	High efficiency High selectivity	High installation and maintenance costs
Ion-exchange:	High efficiency	Costly Prone to be interfered with other ions present such as chloride, phosphate, sulfate, bicarbonate) Toxic waste water is produced during regeneration It's efficiency depends highly on water pH
Adsorption (materials used activated alumina, AC, other natural and synthetic adsorbents)	Most common and low cost method Operation is simple Adsorbents are widely available	High efficiency Require adjustment and readjustment of pH Fluoride adsorption can be interfered with some common water ions Adsorbents cannot be easily regenerated

Habuda-Stanic *et al*. (2014)

2.4 Capacitive deionization technology

2.4.1 Principle of operation

Capacitive deionization is an electrochemical technology originally developed and published by Blair and Murphy in the 1960s to desalinate water. It was known as electrochemical demineralization of water (Zhao, 2013). Its working mechanism is related to energy storage in supercapacitors. Both technologies (supercapacitor and CDI) are based on adsorption of ions in an electrical double-layer (EDL), though the major purpose of CDI is salt/charged species adsorption and not energy storage as in capacitive devices (Leong *et al*., 2019). The concept of EDL in desalination by CDI was introduced in the 1970s by Johnson and Newman (1971), who stated that the adsorption of electrolytes in double layers is responsible for the desalting phenomena. This concept of EDLs in desalination by CDI is still in use (Biesheuvel & Bazant, 2010; Jande & Kim, 2013a). More details on the evolution of CDI technology for desalination can be found in the work of Porada *et al*. (2013b).

Principally, the CDI process makes use of two fundamental mechanisms for charge storage; capacitive electrosorption and pseudocapacitive ion-intercalation. Capacitive electrosorption is the most common approach in which applied potential induces adsorption on the surface of highly porous carbon electrodes (Zhao, 2013; Zou *et al*., 2008a). The electric field is applied between a pair of porous carbon electrodes and charged ions in the salt solution are forced to move towards oppositely charged electrodes (Fig. 1) where EDL is formed near their surfaces. Within this double layer is where charged ions are stored (adsorption). To regenerate the electrodes, the electric field is removed or the polarity of the electrodes are reversed and the ions are released back into the bulk solution (desorption) (Porada *et al*., 2013b). Through this mechanism, adsorption and desorption processes depend much on the physical and structural properties of the electrode materials including microstructure, size, and distribution of pores, surface area, and chemical functional groups (Yasin *et al*., 2017).

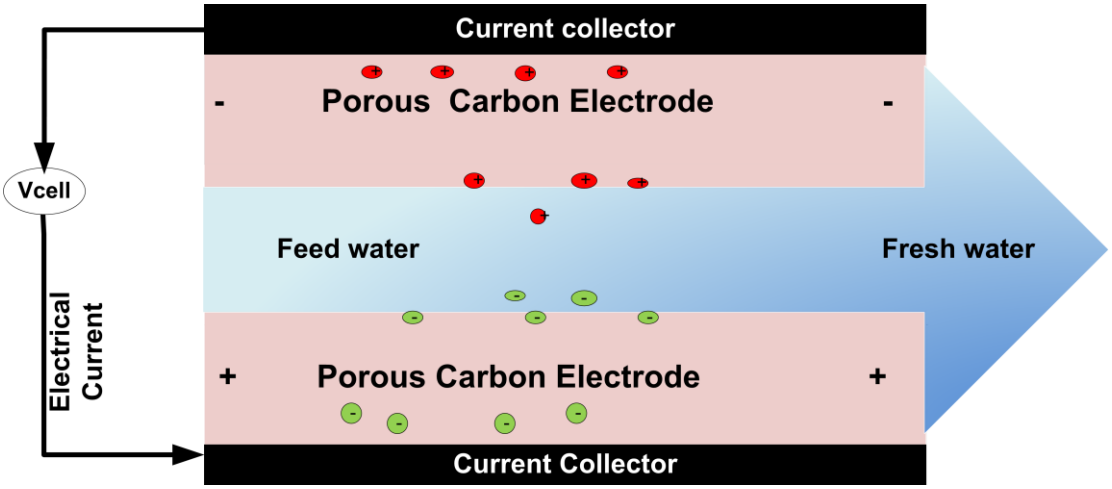

Figure 1: Schematic diagram of a CDI cell in a charging cycle

With the electrosorption mechanism CDI can complete hundreds of adsorption-desorption cycles in an oxygen-free electrolyte. When oxygen is present, however, degradation of the desalination performance can occur over time due to oxidation of the positively charged electrode (Gao *et al*., 2016; Srimuk *et al*., 2017b). Oxidation results in increased concentration of oxygen-containing surface functional groups within the micropores of the carbon anode leading into decreased salt adsorption capacity (Cohen *et al*., 2013). This effect is the major limitation on the CDI cell life cycle. Thus, studies on long term performance of CDI electrodes are highly encouraged. Various strategies have been implemented to mitigate electrode oxidation and thus improve the CDI electrodes life cycle. These strategies include purging inert gases such as nitrogen or argon to the feed water (Cohen *et al*., 2013), reduction of cell potential as carbon oxidation takes place between 0.7 and 0.9 V (vs. normal hydrogen electrode (NHE)) (He *et al*., 2016; Lee *et al*., 2010), and increase of the concentration of negatively charged surface groups at the anode by chemical treatments (Gao *et al*., 2013; Gao *et al*., 2015). Furthermore, addition of metal oxides to the carbon electrode (Srimuk *et al*., 2017b) and the use of thin polymeric ion exchange membrane sheaths for the anode (Omosebi *et al*., 2014), have shown good results in inhibiting electrode oxidation reactions.

Pseudocapacitive ion-intercalation is an approach in which ions from salt water interchange reversibly with those of the electrode by Faradaic reactions on the surface of the electrode. During pseudocapacitive ion intercalation process novel electrode materials (Jaehan Lee *et al*., 2014) apart from carbon are used. These materials offer Faradaic reactions to replace ion electrosorption by ion intercalation or surface redox reactions (Srimuk *et al*., 2017a). In this mechanism, intercalation electrodes are used, and ions are stored in the crystallographic sites

of the intercalation host compounds due to its redox activity (Porada *et al*., 2017). Materials such as MXene (Srimuk *et al*., 2016), chemically exfoliated Molybdenum disulfide (ce-MoS_2) (Xing *et al*., 2017) are some of the materials that have been studied for CDI and presents pseudocapacitive desalination. More information about application of intercalation materials in CDI can be found in the review paper by Singh *et al*. (2019)

Through CDI, drinking water can be produced by controlling the dissolved salts level and converting low saline water into potable water by attracting contaminants (charged species) and store them in porous electrode (Tang *et al*., 2015). Capacitive deionization technology has been used for water softening, removal of nitrates, fluoride, ammonium ions and removal of heavy metals such as lead, cadmium and ferric ions from water (Mahendra S. Gaikwad & Balomajumder, 2016). Recently, the use of CDI has been expanded to other fields including in monoethanolamine-based post-combustion CO_2 capture to minimize energy consumption during CO_2 regeneration in the stripper (Jande *et al*., 2014), and in energy harvesting from CO_2 emission (Paz-Garcia *et al*., 2015; Paz-Garcia *et al*., 2014). Other applications of CDI may include insulin purification (Jung *et al*., 2012) and oil recovery (Janssen *et al*., 2013). Due to the potential of CDI in a wide range of applications, research on improving its performance is vital. Since the performances of CDI primarily depend on the electrode materials, the material selection for CDI electrodes is the key factor in the cell's ion removal efficiency.

2.4.2 Electrode materials for CDI

Electrode plays an important role in the CDI process as it is the place where ions are stored. In general, carbon materials with tunable structural properties and high electrical conductivity and of low cost are promising electrode materials for CDI. Furthermore, electrode materials should at least have high salt adsorption capacity, high specific capacitance (i.e., high charge efficiency), enough mechanical strength to sustain the hydrodynamic forces in the cell and other forces resulting from the assembly process. Materials should also possess resistance to bio-fouling, ability to undergo charging and discharging cycles, hydrophilic properties, no chemicals that are harmful to human beings, and no rust causing agents (Huang *et al*., 2013; Porada *et al*., 2013b). Table 5 summarizes the salt adsorption capacity of various CDI electrode materials. The electrosorption capacity varies from 0.25 to 79.4 mg/g whereby most of the composite materials exhibit superior desalination performance when compared to their single component carbon materials. The

factors such SSA, pore size, specific capacitance, initial concentration, applied voltage, mode of operation are widely reported to affect electrosorption capacity of the material. It is evident that the performance of CDI depends on the electrode materials and the synthesis methods have great influence on the properties of the resulting carbon. Though materials such as CNT–graphene hybrid aerogels (Sui *et al*., 2012), CNT/Graphene composites and three-dimensional (3D) graphene-based materials, exhibited high electrosorption capacity and termed as good CDI electrode materials, they suffer from drawbacks such as the complicated preparation methods and a high manufacturing cost. Therefore, developing simple, cost-effective and more efficient electrode materials will be the solution towards improving salt removal performance and scaling up of CDI systems (Kong *et al*., 2016). Activated carbon derived from biomass or their by-products is a potential choice for fabrication of CDI electrodes owing to the availability and low-cost of the carbon precursor, renewable nature and minimal secondary environmental impact (Chen *et al*., 2011). Owing to the increased interest in biomass-based CDI electrodes, there is a need to discuss the methods that have been used to make porous carbon from biomass for CDI applications and compare their performance with other novel studied CDI electrode materials.

Table 5: Comparison of electrosorption capacity among different CDI electrode materials from various studies

Material	Synthesis method	BET SSA (m^2 g^{-1})	Pore size/volume	SCP (F/g)	SR (mV/s)	CDI MO	AP (V)	Ci of NaCl (mg/L)	EC (mg/g)	Reference
DWCNTs		415				Batch	2	23	0.55	(Li *et al*., 2011)
SWCNTs		453				Batch	2	23	0.75	(Li *et al*., 2011)
CNT sponges,	chemical vapor deposition	60–80				Batch	1.2	60	4.5	(Wang *et al*., 2011)
CNT/Graphene	Reduction of GO combined with CNT	391	0.49 cm^3/g	220	5		2	780	26.42	(Wimalasiri & Zou, 2013)
CNT/graphene hybrid aerogels	supercritical CO2 drying of graphene–CNT hybrid hydrogel precursors obtained from heating aqueuos mixtures of GO and CNTs with Vitamin C	435				Batch	1.6	4000	79.4	(Sui *et al*., 2012)
Graphene	Modified hummers' method	77				Batch	2	23	0.46	(Li *et al*., 2011)
Graphene	Modified Hummers method	14.2	7.42 nm	75.18	70	Batch	2	50-450	1.85	(Li *et al*., 2009)
Microporous graphene	Activating GO with KOH	3513		20.1	2	Batch	2	74	11.86	(Li *et al*., 2015)
Graphene/carbon nanotube composites	modified exfoliation approach	479.5		230	10	Batch	2	114	1.41	(Zhang *et al*., 2012b)
Sponge-templated graphene	Sponge -templated	305		57	10		1.5	~212	4.95	(Yang *et al*., 2014)
Graphene-like nanoflake	Hummers' method	222.01				Batch	2.0	~110	1.35	(Li *et al*., 2010)
3D graphene with hierarchically	template-directed method and an in situ	824		151.7	1	Batch	1.2	500	14.7	(Wang *et al*., 2016)

Material	Synthesis method	BET SSA (m^2 g^{-1})	Pore size/volume	SCP (F/g)	SR (mV/s)	CDI MO	AP (V)	Ci of NaCl (mg/L)	EC (mg/g)	Reference
porous structure	defect etching strategy									
3D porous graphene	Silica particles as templates	2680	1.76 nm	~70	5	Single Pass	1.4	300	14.32	(El-Deen *et al*., 2016)
N-doped graphene sponge	Direct freeze drying of GO	526.7	3.13 cm^3 /g	286.86	5	Batch	1.5	500	21.0	(Xu *et al*., 2015)
Nitrogen-doped porous carbon spheres	Fast microwave-assisted approach using sucrose as the precursor	1640.50	0.79 cm^3/g	290.7	1	Batch		1000	14.91	(Liu *et al*., 2015a)
Carbon aerogel	Polymerization of RF using ambient drying technique followed by pyrolysis	910		83	10	Batch	1.2	500	5.62	(Quan *et al*., 2017)
CA		400 to 1100				Batch	1.2	50	1.4	(Farmer *et al*., 1996)
CA/AC composite	CAs- prepared by supercritically drying and carbonizing the gel of resorcinol and furfural in isopropanol, and AC was a commercial product			90	2	Batch	1.2	1000	17	(Kohli *et al*., 2012)
Ordered Mesoporous carcon	Modified sol–gel process involving nickel salts	1491	3.7nm	192	1	Flow through	0.8	46	0.93	(Lixia *et al*., 2009)
Ordered Mesoporous carcon	Direct carbonization of silica/triblock	844	0.90 cm^3 /g	133	1	Batch	1.2	25.6	0.68	(Zou *et al*., 2008a)

Material	Synthesis method	BET SSA (m^2 g^{-1})	Pore size/volume	SCP (F/g)	SR (mV/s)	CDI MO	AP (V)	Ci of NaCl (mg/L)	EC (mg/g)	Reference
	copolymer									
TiO_2 nanofibers/AC				380	10	single-pass	1.2	292	17.7	(El-Deen *et al*., 2014b)
Hierarchical porous carbon materials	One-step pyrolysis of EDTA and KOH activation	2185.71	1.368 cm^3/g	182	50	Batch	1.4	40	34.27	(Chao *et al*., 2015)
AC	Ground of commercial AC gradules	968	0.59 cm^3/g	107	1	Batch	1.2	25	0.25	(Zou *et al*., 2008a)
Polyaniline AC	Activation of polyaniline with KOH	1484	1.38	90	1	Batch	1.4	600	14.9	(Zornitta *et al*., 2017)
N, P, S co-doped hollow carbon polyhedron derived from MOFs-based core-shell nanocomposites	Calcination of ZIF-8@PZS)	929		333	1	Batch	1.2	500	22.2	(Zhang *et al*., 2018b)
MOF-derived porous carbon rods/reduced graphene oxide composite (PC/rGO).	carbonization of Fe−MOF/GO	713	-	218	2	Batch MCDI	1.2	1000	37.6	(Shi *et al*., 2018)

SSA= Specific surface area, SCP= specific capacitance, SR= scan rate, MO= Mode of operation, AP= Applied potential, EC= Electrosoption capacity, Ci= initial salt concentration

2.5 Biomass-based carbon electrode materials for CDI

Generally, biomass is defined as the biological materials from plants or animals together with their waste and residues (Chew & Doshi, 2011). As the need for activated carbon in various applications increase, the use of sustainable biomass waste derived carbon has received much attention. This is because they are of low-cost (˷0.50 €/kg) (Marsh & Reinoso, 2006), environmentally friendly, obtained easily and are facile to prepare. To date, different are used to synthesize activated carbon from biomass for various applications, including energy storage and water treatment. The methods include salt templating, pyrolysis, activation and hydrothermal carbonization of natural or waste biomass materials. Various biomass materials including watermelon peels (Zhao *et al*., 2017), coconut shells (Yeh *et al*., 2015), peanut shells (Quan *et al*., 2016), loofa sponge (Feng *et al*., 2018), basswood (Liu *et al*., 2018a), sugarcane bagasse (Lado *et al*., 2016) and cotton leaves (Li *et al*., 2016) have been studied as electrode materials for CDI. Different precursors, synthesis procedures and conditions produce carbon with different porous structures, surface area, pore size distribution, and chemical functional groups. Various methods that have been used to synthesize porous carbon from biomass for CDI electrodes are disused in the next sub-section.

2.5.1 Pyrolysis and activation process

Generally, activated carbon is produced by thermal activation/pyrolysis of carbonaceous materials at temperatures lower than 1000 °C followed by activation of the resulting black char (Fig. 2). The pyrolysis process takes place in an inert atmosphere whereby tarry, gaseous products evolve and solid black char remain. Pyrolysis conditions play a crucial role on the surface and textural properties of the activated carbon generated. For instance; Lado *et al*. (2016) prepared activated carbon from sugarcane bagasse fly ash (SCBFA) through a thermal activation/pyrolysis process at different temperatures (200-800 °C). The obtained carbon was then used to prepare CDI electrodes for the purpose of desalinating brackish water. It was reported that, an increase in pyrolysis temperature results in an increase in BET surface area and the micropores structure. It was also reported that thermally treated SCBFA at 200 ^{o}C exhibited the highest specific capacitance of 55 F/g and electrosorption capacity of 6.2 mg/g compared to other samples. The improved performance was associated with increased surface oxygen groups (revealed by XPS analysis data, see Fig. 3) that significantly enhanced electrode wettability when compared to carbon produced at higher pyrolysis temperature. It

was further noted that temperatures >300 °C lead to higher SSA but also to the decrease in surface oxygen groups due to the decomposition of surface oxygen groups.

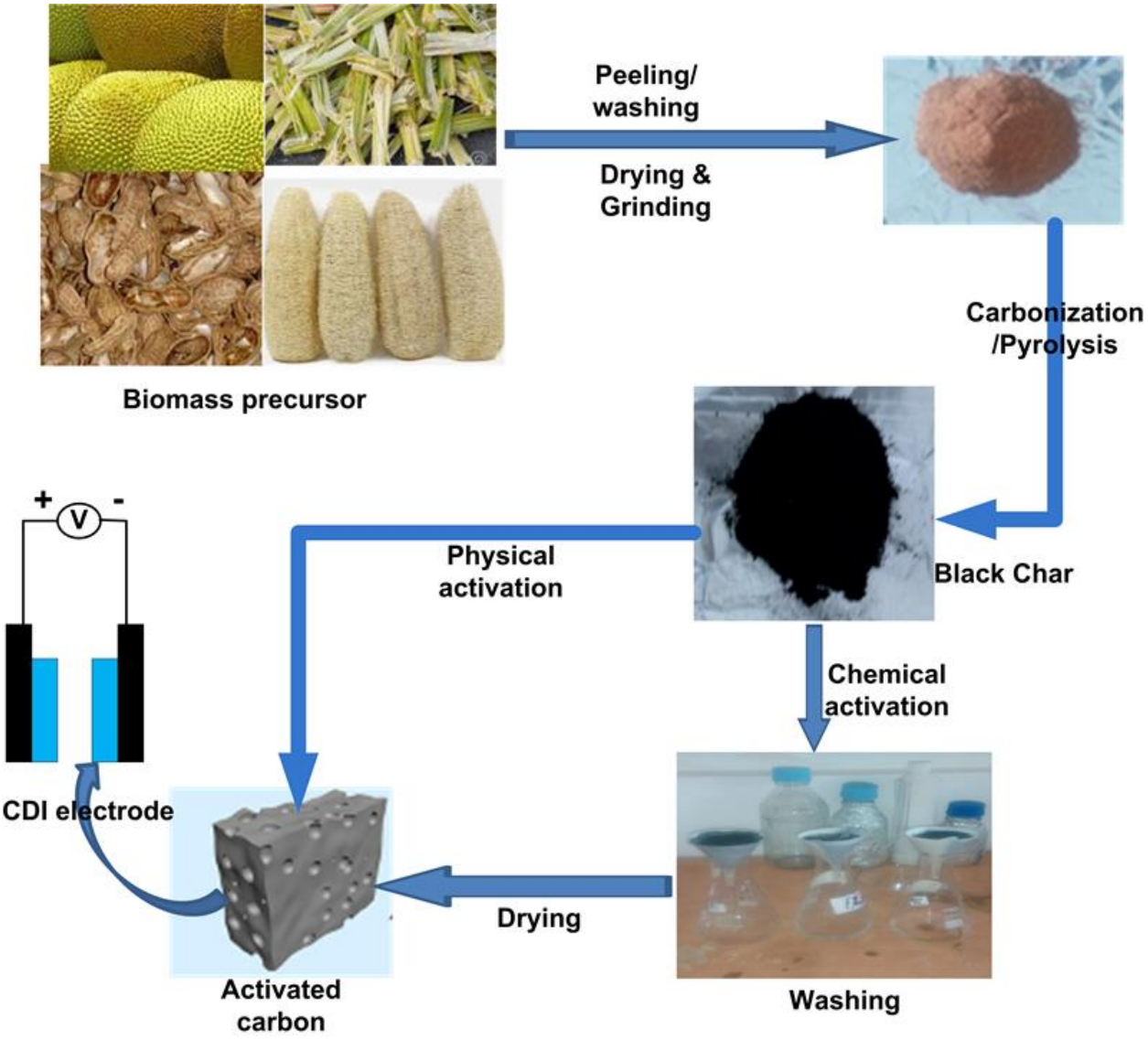

Figure 2: A schematic illustrating the synthesis of activated carbon from biomass precursor through pyrolysis and activation process for CDI electrodes

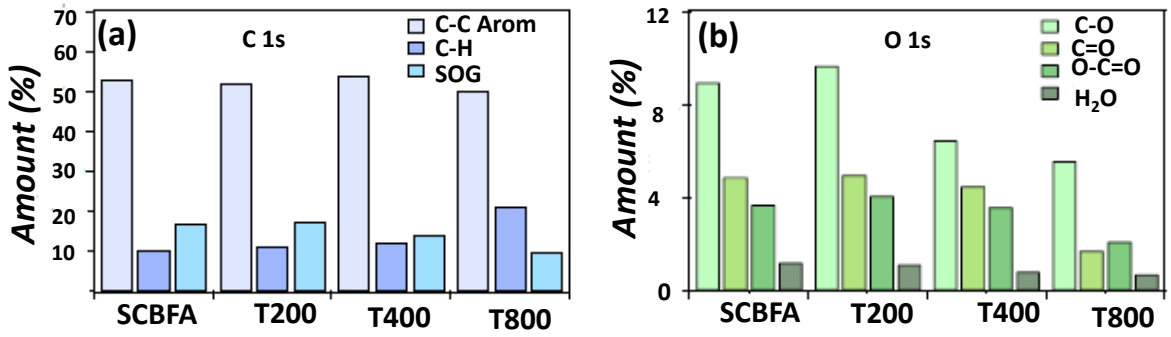

Figure 3: Analysis of surface functional groups of carbon derived from sugarcane bagasse fly ash from XPS spectra based on the (a) C 1s (b) and O 1s Reprinted from (Lado *et al*., 2016) copyright (2016), with permission from Elsevier

Pyrolysis has been a common method to produce porous carbon; however, the carbon produced usually possesses low specific surface area (SSA) and poor porous structures. Therefore, an activation strategy is employed to increase the SSA and adjust the porous structures (Manocha *et al*., 2013). The activation process may be chemical activation (with $ZnCl_2$, H_3PO_4, HNO_3, KOH, and KHCO3 to mention the few) at a certain activating agent/carbon ratio in an inert atmosphere or physical activation (with CO_2 or steam) or a combination of both. Compared to physical activation, chemical activation is usually preferred since it is a faster process, produces activated carbon with high specific surface area, well-developed porosity, wide pore distribution and produces high carbon yield (Hui & Zaini, 2015).

During the chemical activation process, the raw carbon materials are carbonized at temperatures below 1000 °C, followed by the activation at temperatures between 950 °C and 1000 °C (Jia & Zhang, 2016) in an inert atmosphere. The degree of impregnation, which is the weight ratio of the activating agent and dry carbon material (activating agent/C) is an important factor in chemical activation. It is reported that a slight increase in the degree of impregnation results in an increase in the total pore volume of the product and specifically an increase in the volume of smaller pores. However, further increase of the impregnation ratio increases the number of pores with larger diameter and decreases the volume of the smaller pores (Dehkhoda, 2016). For instance, Quan *et al*. (2016) prepared hierarchical porous biomass carbon by pyrolysis and KOH activation of a natural waste peanut shell. It is noted that the SSA and specific capacitance increases from 962 to 1827 m^2/g and 44.9 to 83.2 F/g respectively as the ratio of KOH/C increased from 1.0 to 3.0. The decrease in surface area and capacitance with low KOH/C ratio was due the fact that KOH does not react with the

carbon precursor sufficiently resulting in a small SSA and fewer transportation channels for adsorption and diffusion of salty ions and thus, lower specific capacitance at KOH/C ratio of 1. Furthermore, Feng *et al*. (2018) synthesized porous carbon through carbonization and KOH activation of lignocellulosic loofa sponge (*Luffa cylindrical* (LS)) and observed that specific surface area, pore volume, electrochemical properties, and electrosorption capacity were enhanced by KOH/C ratio.

Activation temperature is another factor which affects the physicochemical characteristics of the resulting carbon material after the activation process. For example; Zhao *et al*. (2017), prepared micro/mesoporous carbon sheets from watermelon peel as a carbon precursor with a high specific surface area ranging from 872 to 2360 m^2/g by activating the samples with $KHCO_3$ in the ratio of 1: 8. The authors proved that both specific surface area and pore size increased with activation temperature. The electrodes fabricated from the carbon activated at 800 °C showed high deionization capacity of 17.38 mg/g and faster salt adsorption rate at 1.2 V in a 500 mg/L NaCl solution with good regeneration behavior when compared to the carbonized sample. The specific capacitance of the electrode fabricated from an activated sample was reported to be 224 F/g, which was higher than that of electrodes made from an unactivated sample (176 F/g). The authors concluded that improved specific capacitance was due to the improved SSA, better wettability and good porosity of the produced carbon.

Moreover, Yeh *et al*. (2015) prepared high surface area activated carbon from coconut shell by combining chemical (KOH) and physical (CO_2) activation methods. The two-step activation process influenced the SSA and the mesopore to micropore ratio of the produced carbon. Furthermore, they realize that KOH activation generally etch the carbon surface to generate micropores, while CO_2 activation resulted in an increase in surface area and creates more mesopores. The fabricated electrodes show improved desalination performance (9.72 mg/g) due to the high surface area and the high ratio of mesopore to micropore resulted from controlling the KOH impregnation ratio and the CO_2 activation time, compared to electrodes fabricated with the commercial activated carbon used without further activation (1.89 mg/g).

2.5.2 Hydrothermal carbonization

Hydrothermal carbonization (HTC) is a thermochemical conversion technique which uses subcritical water to convert biomass materials into porous carbon s through fractionation of the feedstock (Jain *et al*., 2016; Wang *et al*., 2018). Hydrothermal carbonization is attractive

because it uses a low temperature, can transform wet biomass without pre-drying, has low production cost and carbonization medium used is environmentally friendly (Xie *et al*., 2018). Generally, in HTC a mixture of water and carbon precursor is thermally treated at moderate temperatures of 180-250 °C and through autogenous pressure. This process lowers the content of oxygen and hydrogen in the feedstock through dehydration and decarboxylation (Titirici *et al*., 2015; Wang *et al*., 2018). Li *et al*. (2017) utilized watermelon as a carbon precursor to prepare carbonaceous aerogels (CAs) through the HTC route.

Moreover, a simple hydrothermal and calcination process was used for growing metal oxide (MO) nanoparticles on CAs by using the metal ion solution as precursors to obtain functionalized flexible carbonaceous aerogels/metal oxide (CAs/MO) hybrids. The CAs/MO with open porous morphology were then used as CDI electrode material for the recovery of Cu(II) from aqueous solutions. The CDI results (with 50 mg/L Cu(II) at 1.2 V) revealed that the addition of TiO_2 nanoparticles enhanced the capacitive performance of CAs-based material significantly. Other studies reported the combination of HTC method with chemical activation to further improve the porosity of the produced carbon. For instance, Xie *et al*. (2018), synthesized porous carbon from citrus peel by hydrothermal reaction followed by carbonization, using a small quantity of activating agents ($ZnCl_2$, KOH, and H_3PO_4) in hydrothermal step. The carbon produced from different activating agents acquired different structural, electrochemical and electrosorption properties. Carbon activated with $ZnCl_2$ shows improved properties compared to carbon activated with KOH and H_3PO_4. It was realized that addition of $ZnCl_2$ in the hydrothermal stage improves the degradation of cellulose and the aromatization of carbon matrix leading to highest SSA and pore volume of 323 m^2/g and 0.197 m^3/g respectively, highest specific capacitance, charge efficiency and the good desalination performance.

Furthermore, when C-Zn was used in asymmetric CDI with C-Zn as anode material and AC as counter electrode material, the electrosorption capacity of 16 mg/g and salt adsorption rate of 0.67 mg g-1 min-1 were achieved. Yan *et al*. (2017) prepared activated carbon from *Lentinus edodes* through hydrothermal method (M-HTC) followed by activation via $ZnCl_2$ (M-HTC-Zn) at elevated carbonization temperature. The authors discovered that the sample prepared through hydrothermal and $ZnCl_2$ activation exhibits a more porous structure and enhanced electrosorption capacity compared to M-HTC sample and the commercial activated carbon. Moreover, Zhang *et al*. (2018c) synthesized porous carbon from waste biomass

corncob with a 3D honeycomb-like structure via hydrothermal carbonization followed by with KOH activation. The resulting carbon was utilized as CDI electrode material to remove chromium (VI) from the aqueous solution. Zhang *et al*. (2018c) revealed that, KOH activation and activation temperature improved both the SSA and pore volume. In both studies combination of HTC and chemical activation effectively improved the SSA, the pores of biomass-based carbon as well as their electrosorption capacity.

2.5.3 Salt templating

Salt templating is another method used in converting biomass into activated carbon. It is a simple and effective route for the production of heteroatom doped porous carbon materials. In this method, a precursor containing heteroatom is added into the carbon precursor and mixed with a low melting point salts to allow doping of heteroatoms into carbon skeletons prior pyrolysis (Zhang *et al*., 2017a). The low melting point salt acts as a solvent and a template at the same time. This approach is used to synthesis heteroatom-doped carbons with tunable surface area, pore structure and pore volume which cannot be achieved by using the conventional chemical or physical activation methods (Fechler *et al*., 2013). The presence of heteroatoms such as nitrogen, boron, phosphorus, and sulfur in carbon materials help to improve electrical conductivity and wettability resulting in the enhanced electrochemical performance of carbon materials (Deng *et al*., 2015b). Nitrogen is more appropriate because its atomic size and valence bond are similar to those of carbon atoms (Liu *et al*., 2015a). Nitrogen-doping carbon material (N-doped) have been observed to have more defects which creates more accessible surface area and increase charge adsorption sites, thus enhancing capacitive performance (Liu *et al*., 2015c) Low cost nitrogen-containing precursors such as chitosan (Deng *et al*., 2015b), sucrose (Liu *et al*., 2015a), glucosamine and glucose (Porada *et al*., 2015) have been recommended for synthesis N-doped carbon materials. Porada *et al*. (2015), utilizes a bottom-up salt template approach to synthesize nanoporous heteroatom-doped carbons from sustainable biomass precursors (glucose and glucosamine) with different heteroatom dopants (e.g., nitrogen or sulfur). The authors used 2-thiophenecarboxylic acid as a sulfur source and both $ZnCl_2$ and cesium acetate as a salt template and activating agent. By varying salts and activation temperature; carbon with different elemental composition, yield (~80% for $ZnCl_2$ and ~50% for cesium acetate) surface morphology, pores structure, and surface area was obtained. The carbon with 1.0 wt% N (N- doped carbon) yielded high

surface areas of up 2830 m^2 /g, salt adsorption capacity of 15.0 mg/g at 1.2 V in 5 mm NaCl solution, but low charge efficiency when compared to the commercially activated carbon.

Apart from the salt templating method, heteroatom doped porous carbon can be produced by functionalizing the activated carbon derived from biomass (through any of the methods above) with a heteroatom dopant source. For instance, Zhao *et al*. (2018) synthesized nitrogen-doped porous carbon (NPC) with a nitrogen content of 1.66 wt.% with micro-mesoporous structure from soybean shell precursor through a $KHCO_3$ assisted pyrolysis approach. The prepared N-doped carbon was further functionalized with sulfonic groups in an aryl diazonium salt solution and sulfonyl functionalized NPC (S-NPC) was obtained. The FT-IR spectra (Fig. 4) of carbonized soybean shells (NC), NPC and S-NPC samples proves that S-NPC was successful functionalization due to the presence of the characteristic absorption band of S=O at 1150-1040 cm^{-1} and 650-575 cm^{-1} groups on the surface. The presence of $-SO_3^-$ groups improved the specific capacitance of S-NPC (215.3 F/g) when compared to the capacitances of NPC (165.2 F/g) and NC (156.5 F/g). The desalination capacity of NPC assembled CDI was higher (16.0 mg/g) compared to that of S-NPC (15.5 mg/g) when using 40 mg/L NaCl solution at applied voltage of 1.2 V. The superior CDI performance of NPC was associated with high surface area (1036.2 m^2/g) and its porous structure. Furthermore, S-NPC exhibit much faster adsorption rates of 0.44 mg g^{-1} min^{-1} compared to NPC electrodes (0.26 mg g^{-1} min^{-1}). When using 1000 mg/L NaCl solution, S-NPC achieved an electrosorption capacity of 43.3 mg/g, which was greater than that of the recently reported novel carbon-based CDI electrode materials as presented in Table 5.

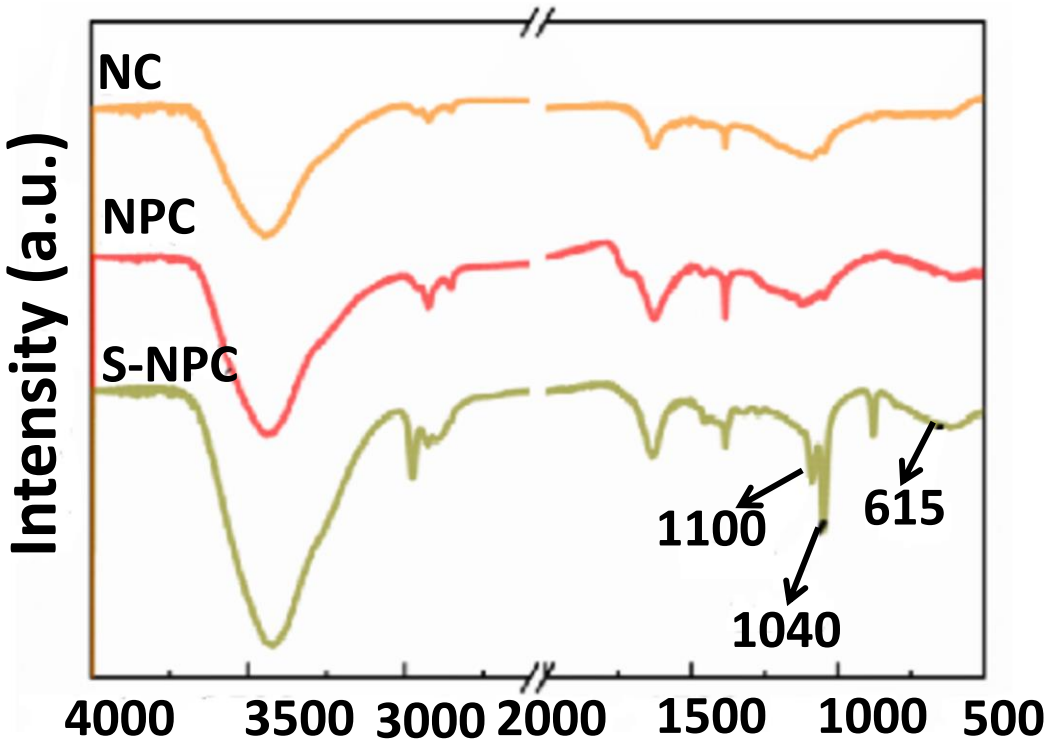

Figure 4: FT-IR spectra of NC, NPC, and S-NPC derived from soybeans shells. Reprinted from (Zhao *et al*., 2018) copyright (2019), with permission from Elsevier.

Though different methods of preparing porous carbon from some biomasses for CDI electrodes together with the characteristics of the resulting carbon have been described in the previous sub-sections, more materials, methods and their performance are summarized in Table 6. From Table 6, the synthesis route is an important factor that controls surface properties of the biomass-based carbon electrodes. It can be further observed that high surface area > 2500 m^2/g carbon and pore size suitable for electrosorption can be obtained from biomass precursor. From Table 6, porous carbon electrode derived from biomass has achieved the highest electrosorption capacity of 57.13 mg/g when used for removal of Cu(II) from $CuCl_2$ solution (Li *et al*., 2017) . Also, biomass-based electrodes achieved the electrosorption capacity of 38 mg/g through MCDI (Sriramulu *et al*., 2019) which is almost the same as that of metal organic framework (MOF)-derived porous carbon rods/reduced graphene oxide (PC/rGO) composite electrode (37.6 mg/g) (Shi *et al*., 2018) materials used in MCDI and 22.5 mg/g (CDI) when using NaCl solution feed solution. The reported electrosorption capacity of biomass-based CDI electrode materials is comparable to other novel materials such as 3D intercalated graphene sheet–sphere nanocomposite architectures (22.1 mg/g) (Khan *et al*., 2018), N, P, S co-doped hollow carbon polyhedron derived from MOFs-based core-shell nanocomposites (22.2 mg/g) (Zhang *et al*., 2018b) and TiO_2

nanofibers/AC composite (17.7 mg/g) (El-Deen *et al*., 2014b). It is also reported to be higher than that of commercial activated carbon (14.3 mg/g) (Porada *et al*., 2013a), carbon aerogel (5.318 mg/g) (Gabelich *et al*., 2002) and CNTs-RGO (0.88 mg/g) (Li *et al*., 2013) and other carbon materials as summarized in Table 3. These results revealed that biomass-derived materials could be used to prepare cost-effective and high-performance CDI electrodes.

Table 6: Synthesis methods, structural characteristics and salt adsorption performance of different porous carbon derived from biomass in CDI electrodes

Source of carbon	Synthesis Method	SSA* (m^2/g)	Pore size (nm)	Scan rate (mV/s)	SC* (F/g)	C_i*(mg/L)	CDI mode of operation	Voltage (V)	EC* (mg/g)	Reference
Watermelon peel	Pyrolysis and activation with $KHCO_3$	872-2360	0.50–33	1	224	500 NaCl	Batch	0.8-1.4	17.38	(Zhao *et al.*, 2017)
Watermelon soft tissue	hydrothermal reaction followed by calcination	282.1		20	120.4	50 mg/L CuCl2	Batch	1.2	57.13	(Li *et al.*, 2017)
Soybean shell	$KHCO_3$-assisted pyrolysis and solution reaction method	1036	-	2	165	40 NaCl	Batch	1.2	16	(Zhao *et al.*, 2018)
Pomelo peel	Dual activation strategy by using $NH_4H_2PO_4$ and $KHCO_3$	2726	0.89	1	207	1000 NaCl	Batch	1.4	20.78	(Xu *et al.*, 2017)
Sugarcane bagasse fly ash	Thermal treatment/pyrolysis	240-491		1-10	33-55	550 NaCl	Batch	1.2	2.9-5.3	(Lado *et al.*, 2016)
Peanut shells	Pyrolysis and KOH activation	962-1827	1.4 - 3.8	10	44.9 - 83.2	20 NaCl	Batch	1.2	0.22-1.96	(Quan *et al.*, 2016)

Source of carbon	Synthesis Method	SSA* (m^2/g)	Pore size (nm)	Scan rate (mV/s)	SC* (F/g)	C_i*(mg/L)	CDI mode of operation	Voltage (V)	EC* (mg/g)	Reference
Glucose and glucosamine	Bottom-up salt template approach/hydrothermal carbonization (HTC)	880-2830			67-132		Single-pass	1.2	6 -15.5	(Porada *et al*., 2015)
Coconut Shells	Commercial AC	917-1040		5–50		50 NaCl	Batch	1.6	2.75 - 3.75	(Wang *et al*., 2013)
		700-1400		1 − 100	3.94-0.06	5800 NaCl	Single pass	3	-	(Endarko *et al*., 2016)
Coconut Shells	Chemical (KOH) and physical (CO_2) activation	2105		5	181.8	30 NaCl	Batch	0.2 - 1	2.12-9.72	(Yeh *et al*., 2015)
Raw-cotton	Pyrolysis followed by NH_3 treatment and annealing at high temperature.	690-2680	0.8-4	10-200	16.4- 109.9	500 NaCl	Batch	1.2	4.9 - 16.1	(Li *et al*., 2016)
Woody biomass	modified chemical activation method using KOH	971-1675	1.91-2.97	0.5-2	197-240	500 NaCl	Batch	1.2	5.07-5.39	(Dehkhoda *et al*., 2016)
Natural basswood	Simple carbonization and physical activation process	839	2.17	1	87.1	100 NaCl	Batch	1.2	5.7	(Liu *et al*., 2018a)

Source of carbon	Synthesis Method	SSA* (m^2/g)	Pore size (nm)	Scan rate (mV/s)	SC* (F/g)	C_i*(mg/L)	CDI mode of operation	Voltage (V)	EC* (mg/g)	Reference
Loofa sponge *(Luffa cylindrica)*	Carbonization and KOH activation	2062	0.5–4	1	270	2500 NaCl	Batch (*MCDI)	1.2	38	(Sriramulu *et al*., 2019)
Dried mushrooms (*Lentinus edodes*)	Hydrothermal + $ZnCl_2$ activation	-	-	1	247.6	500 NaCl	Batch	1.2	12.9	(Yan *et al*., 2017)
wheat straw carbon	KOH activation followed by sol-gel coating process with SiO_2 thin film	1206	3.8	10	156.8	~30 NaCl	Batch	-	2.67	(Quan *et al*., 2018)
Corncob	hydrothermal carbonization coupled with KOH activation	952	2.96	10	452	30 of chromium (VI) solution.		2	-	(Zhang *et al*., 2018c)
Citrus Peels	hydrothermal synthesis with $ZnCl_2$ activation	323		1	120	500 NaCl	Batch	1.5	16	(Xie *et al*., 2018)
Tea Waste	Chemical modification with concentrated sulfuric acid and	-	-	-	-	10 of chromium Cr(VI)	Batch	1.2	0.77	(Gaikwad & Balomajumder, 2017b)

Source of carbon	Synthesis Method	SSA* (m^2/g)	Pore size (nm)	Scan rate (mV/s)	SC* (F/g)	C_i*(mg/L)	CDI mode of operation	Voltage (V)	EC* (mg/g)	Reference
	thermal treatment					10 of fluoride			0.74	
						100 of Cr(VI)			2.83	
						100 of fluoride			2.49	
Wasted coffee grounds	pyrolysis process using KOH	1856	1.73	180.3	10	292 NaCl	Batch	1.4	16.50	(Qian *et al.*, 2019)

*SSA= Specific surface area, *SPC = Specific capacitance, Ci = initial concentration of NaCl/ NaF/ Cr(VI) and *EC = Electrosorption capacity
*MCDI=Membrane CDI

2.6 Electrochemical properties of CDI electrodes

Since the main component of CDI systems is the electrode which shares many similarities with supercapacitors, some electrochemical performance metrics from the field of supercapacitor have been adopted to characterize CDI electrodes. The electrochemical analysis methods such as cyclic voltammetry (CV), electrochemical impedance spectroscopy (EIS) and galvanostatic charge-discharge cycles (Jin, 2015) are used to evaluate electrochemical properties of the electrodes. In the arena of CDI, CV and EIS have been used to study electrochemical properties of electrode materials using an electrochemical workstation with the three-electrode cell in 0.2-1 M NaCl solution at different scan rates.

Cyclic voltammetry plots are used to express the capacitive behavior while Nyquist plots convey the electrical conductivity of the electrode materials. Most reported CV curves for CDI electrodes exhibits ideal rectangular shape without any oxidation or reduction peak, demonstrating that the capacitance results from an ideal electrical double layer capacitor (EDLC) behavior at the electrolyte-electrode interface (Zhao *et al*., 2017). By integrating the area under the CV curves, the specific capacitance (SPC (F/g)) which shows the charge storage capacity per unit mass of the electrode is obtained (Liu *et al*., 2019a).

Electrochemical impedance spectroscopy analysis is used to characterize the electrical conductivity and capability of the electrode material in storing the electrical energy (Frackowiak & Beguin, 2001). It is presented by a Nyquist plot derived from real (abscissa X-axis, Z') and imaginary impedance data (ordinate Y-axis, Z") at different frequencies (Jin, 2015). Nyquist plots (Fig. 5), generally comprise of three regions; a semi-circle in the high-frequency region between points A and B, Warburg line with a 45^{o} inclination at middle frequencies between points B and C, and a nearly vertical line in the low-frequency region beyond point C (Mei *et al*., 2017). The diameter of the semi-circle (R_B-R_A) represents the charge-transfer resistance of the electrodes and the solution interface and a straight/vertical line represent the double layer capacitive behavior of the electrode while the Warburg region is related to the resistance in the porous structure of the electrode (Prabaharan *et al*., 2006). The intercept at the real axis (R_A) represents the equivalent series resistance (ESR), which include the ionic resistance of salt solution, intrinsic resistance of electrodes and contact resistance at the interface of the carbon materials and the current collectors (Zhang *et al*., 2012a; Zhao *et al*., 2017). The intersection between the vertical line and the Z_{re} axis (R_C) is termed as the internal resistance or the overall resistance of the electrode.

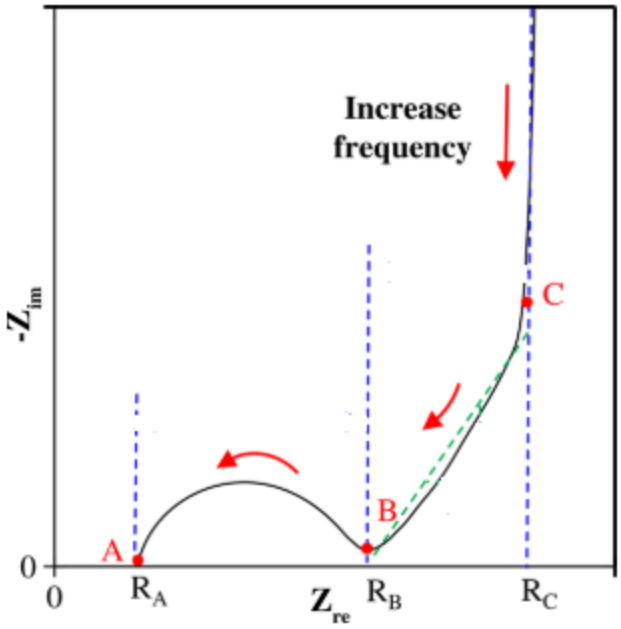

Figure 5: Schematic diagram of Nyquist plots for EDLC electrodes (Mei *et al*., 2017)

It is reported that, SPC mainly depends on the SSA of carbon electrodes and that there is a linear relationship between the specific capacitance and BET surface area of activated carbon (Enock *et al*., 2017a). Conversely, this does not hold for all carbon precursors as shown in Table 7 and plotted in Fig. 6a. Some carbon materials exhibit low specific capacitance despite the fact that they possess high specific surface areas. This might be due to other material surface properties and some other variables including; concentration of the electrolyte, scan rate, voltage window, mass of active material, the surface area of the electrode and the technique used will result in discrepancies observed in the measured capacitance values. The relationship between specific capacitance and electrosorption capacity is presented in Fig. 6b. It can be noted that there is a slight correlation between specific capacitance and EC. Similar trend was observed by Saleem and Kim (2018) when studying the effect of different parameters on the performance and optimization of a CDI desalination process. Materials with lower specific capacitance also exhibited lower EC and vice versa. Therefore, materials with high specific capacitance are good electrode materials for CDI.

Table 7: The BET surface area, specific capacitance and EC of activated carbon derived from biomass

Material	BET surface area (m^2/g)	Specific capacitance (F/g)	Electrolyte concentration (NaCl in M)	Scan rate (mV/s)	EC (mg/g)	Reference
Peanut shells	1362	83	1	10	1.96	(Quan *et al*., 2016)
Watermelon	2360	224	0.5	1	17.38	(Zhao *et al*., 2017)
Sugar cane bagasse fly ash	353	55	0.2	1	4.30	(Lado *et al*., 2016)
Coconut shell	2105	182	1	5	9.72	(Yeh *et al*., 2015)
Raw cotton	2680	110	1	10	16.10	(Li *et al*., 2016)
Basswood	839	87	1	1	5.70	(Liu *et al*., 2018a)
Loofa sponge	1819	186	1	5	22.50	(Feng *et al*., 2018)
Mushroom (LE)	-	248	1	1	12.90	(Yan *et al*., 2017)

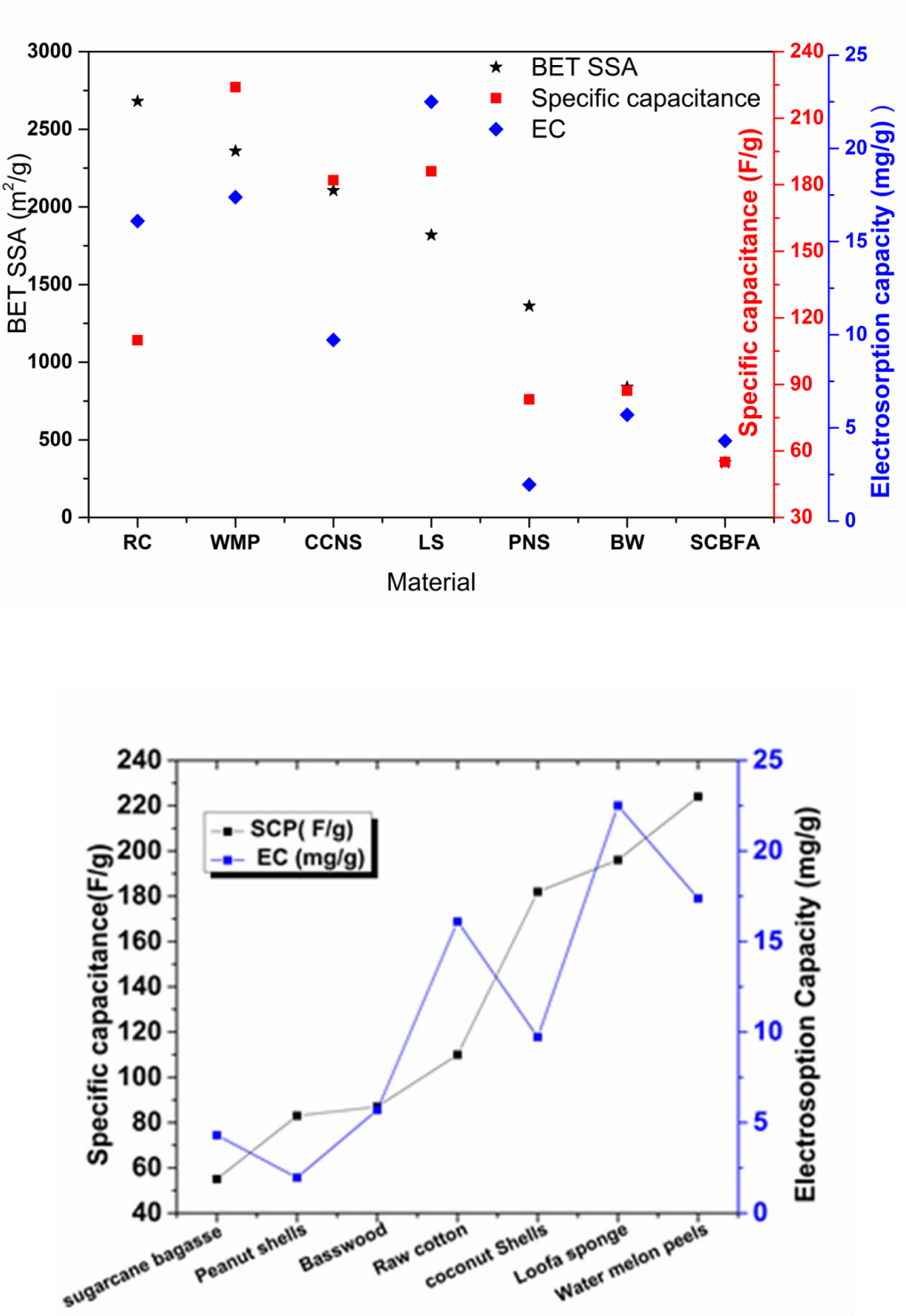

Figure 6: (a) BET surface area, specific capacitance and electrosorption capacity (b) relationship between the specific capacitance and electrosorption capacity of some of the reported biomass-based CDI carbon electrodes as presented in Table 5

2.7 The CDI module configuration and operating conditions

The performance of a CDI system depends on the nature of electrode material, module configuration/geometry, operational mode (Suss *et al*., 2015) , operational parameters (applied electrical potential and flow rate) and the solution conditions that is concentration and type of ions present in the solution (Kong *et al*., 2016). Since changing any of these parameters influence the deionization performance significantly, thus there is a need to study and set out optimal conditions that affect the performance of CDI.

2.8 CDI module configuration

Literature has reported four different geometries or configurations for a CDI system; flow-by mode, flow-through mode, electrostatic ion pumping and desalination by wires or wire-CDI (Zhao, 2013). Flow-by mode is the traditional CDI configuration in which two oppositely charged porous carbon electrodes are placed together with a small gap in between which allows water flow along the electrode (Fig. 7a). In flow-through configuration the influent water is allowed to flow directly through electrode pores, i.e. perpendicular to the surface of the electrodes (Fig. 7b). Electrostatic ion pumping (Fig. 7c) refers to a configuration in which electrodes are stacked and desalinated water is collected at the bottom side after feed water have been pumped in from the top side.

Wire-CDI configuration (Fig. 7d) utilizes two movable carbon rod electrode wires which are dipped into the stream of water that is to become freshwater (Porada *et al*., 2012a). Once potential difference is applied between the two wires, one serve as cathode and adsorbs cations and the other wire serve as the anode and adsorb anions. When wires are being saturated with ions they are then removed and dipped into another water stream whereby electric field is removed and ions are released to form a brine solution. To the moment there is no clear conclusion on the question of which among these geometries are the most promising as each of the architectures/geometry has unique advantages over the other. Therefore, flow by mode was adopted in this study due to its simplicity in operation and for testing the performance of the system.

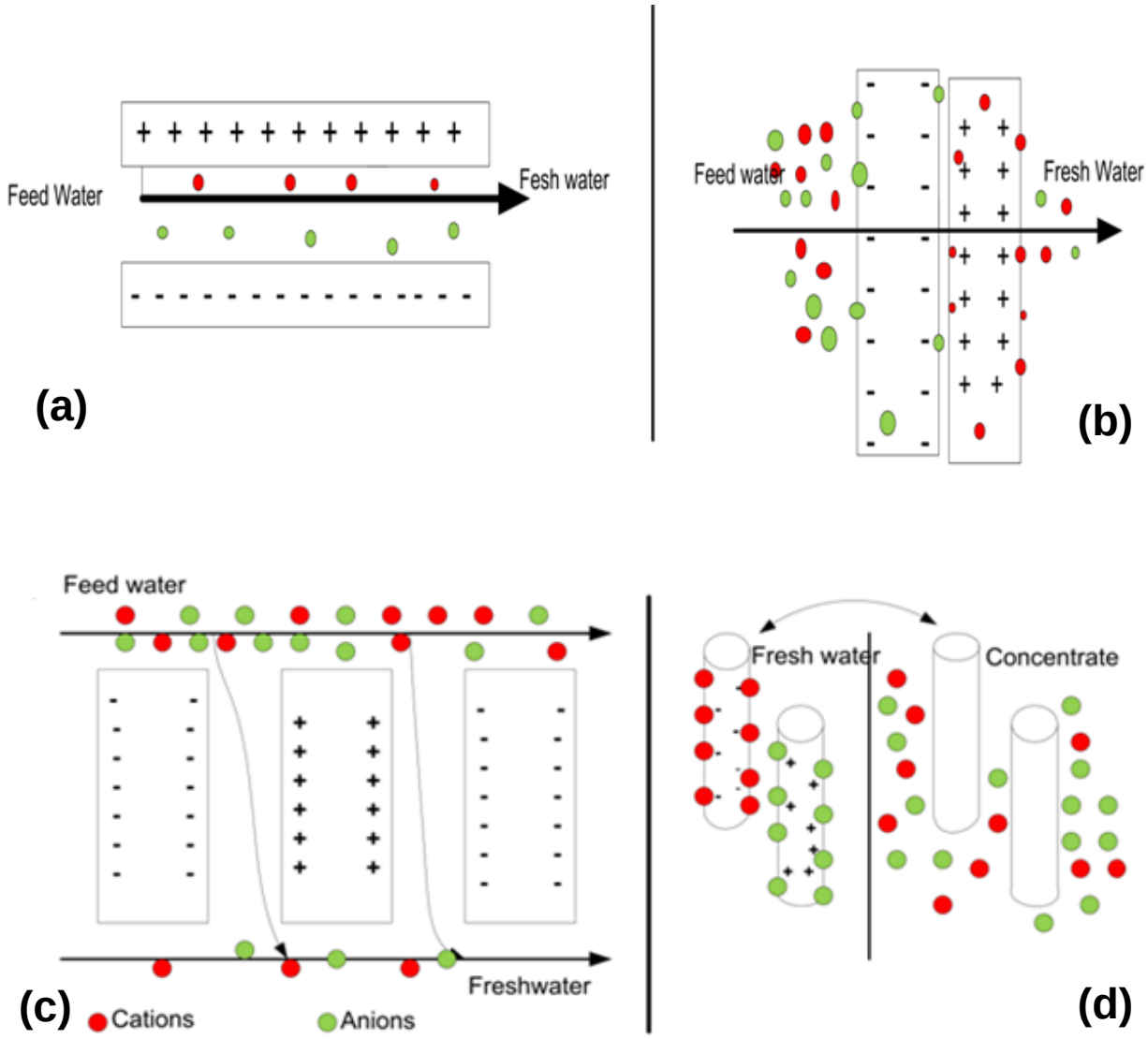

Figure 7: CDI system geometry. (a) Flow by mode, (b) Flow through mode (c) Electrostatic ion pumping, (d) Desalination with wires (Zhao, 2013)

2.9 CDI mode of operation

Capacitive deionization can be operated either in a batch mode in which water is recycled till equilibrium is reached or in a single pass mode where small amount of water passes through the CDI cell once only (Jande & Kim, 2014). Furthermore, CDI units can be operated using either constant current or constant voltage (Jande, 2015; Jande & Kim, 2013a). In desorption stage of a CDI operated at constant voltage, the cell is short-circuited or the cell voltage is reversed or reduced and the stored ions (ion desorption) are released out of the transport channel and the new cycle begins (Fig. 8a). Operation at a constant cell voltage has been reported to have some disadvantages because the effluent salt concentration changes in time,

when voltage is applied the concentration of salt in the effluent water decreases fast to a minimum value, thereafter the concentration again increases and the electrodes attain salt adsorption capacity slowly. Short-circuiting the cell at the beginning of the desorption stage leads to fast ion release from the electrodes and an abrupt increase in the effluent salt concentration (Porada *et al*., 2012b). This is because, at the begining of the adsorption step, the EDLs are uncharged, and thus the driving force over the channel is at a maximum (no loss of cell voltage in the EDLs) (Zhao, 2013). This results in very low water recovery (amount of pure water divided by the total waste water fed). To evade this problem it is recommended to charge the CDI cell at constant current. When CDI is charged at constant current it can either be discharged by being short-circuited (zero voltage application) (Fig. 8b) or by applying reversed constant current (Fig. 8c) as presented by Jande and Kim (2013a).

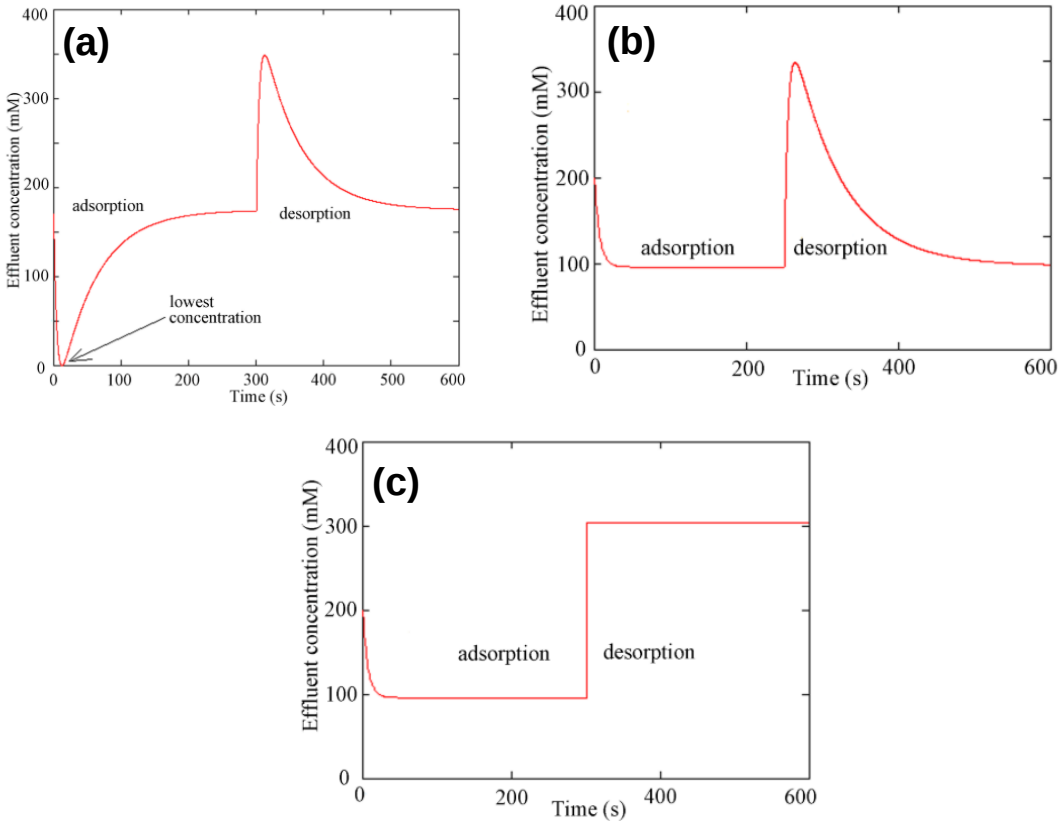

Figure 8: Theoretical variation of effluent concentration with time when CDI cell is (a) charged at constant voltage (b) charged at constant current but discharged at zero voltage (c) charged at constant current (Jande & Kim, 2013a)

2.10 Water defluoridation with CDI

Various researchers have utilized CDI for water defluoridation applications. Tang *et al*. (2015) studied fluoride and nitrate removal from brackish ground waters by batch mode CDI and developed a simplified one dimensional model for electrosorption of these ions. In their experiments, they utilized CDI module with 100 pairs of cell consisting of activated carbon electrodes to study electrosorption of mixed solution of NaCl and NaF or $NaNO_3$. Tang *et al*. (2015) concluded that contaminants such as F^- and NO_3^- can removed from water or solution and stored in the porous electrodes, even in the presence of significant concentrations of other ions. They further developed a model which shows CDI system can utilize 52 kJ (0.0144 kWh) to treat 11.7 L water containing 20 mg/L of F^- and 2 g/L NaCl (Tang *et al*., 2015). Literature pointed out that by varying pump flow rate or the electrical current when operating the CDI in constant current mode it is possible to control the concentration of F^- in the effluent water stream to a preferred level of 0.5−1.5 mg L^{-1} (Tang *et al*., 2016a). The same group studied defluoridation with single-pass constant-voltage CDI mode. They realized that that the system was effective in removing fluoride from low salinity ground waters (Tang *et al*., 2016b).

Furthermore, Gaikwad and Balomajumder (2017a) studied simultaneous removal of F^- and chromium from a binary solution and find out that increasing flow rate and applied voltage enhanced removal efficiency and electrosorption capacity of each ion with good electrode regeneration properties. However, most of this literature investigated electrosorption of F^- theoretically and the ones which conducted experiments utilized synthetic water. Therefore, there are limited numbers of literature showing the application of CDI in fluoride removal from natural water. Therefore, studies to investigate the fluoride removal from natural water with CDI using cost-effective electrode materials are essential.

2.11 Availability of CDI systems for commercial/industrial purposes

Due to its advantages, including low operations cost, low maintenance simplicity of the system and high water recovery many companies worldwide embarked on producing commercial CDI systems for water purification, including Voltea in Sassenheim, Netherlands (Voltea, 2015), ENPAR Technologies Inc. in Ontario, Canada (Idropan-dell'Orto, 2015), Reticle in California, United States of America (Jande *et al*., 2014) and Idropan dell'Orto Depuratori S.r.l in Milan, Italy, AquaEWP, Pionetics Linx (Nkuna, 2017) and O_2&B in

Korea. These companies are installing CDI systems in various parts of the word. For example, O_2&B Company from Korea manufactured and installed CDI water treatment systems in various places in Tanzania including Mbande in Dodoma, Lemanda in Arusha and Chato in Geita. Information about the capacity and performance of these systems in Tanzania are limited. Therefore, researchers need to work closely with this company to study the performance of the system in long run.

CHAPTER THREE

MATERIALS AND METHODS

3.1 Materials

Jackfruit peels were collected from local vendors in the Arusha region, Tanzania. Chemicals used in this study were of analytical grade and used without purification. The chemicals included potassium hydroxide (KOH), phosphoric acid (H_3PO_4) 85 wt. % in H_2O, sodium chloride (NaCl), hydrochloric acid (HCl), polytetrafluoroethylene (PTFE), 99.9% ethanol, glacial acetic acid and cyclohexanediaminetetraacetic acid (CDTA) all purchased from Sigma Aldrich. Poly vinyldenedefluoride (PVDF) and carbon black (TIMICA SUPPER C65), were purchased from MTI Corporation.

The activities and procedures that were used in the synthesis of porous carbon, development of electrodes and evaluation their performance are summarized in the flow chart Fig. 9.

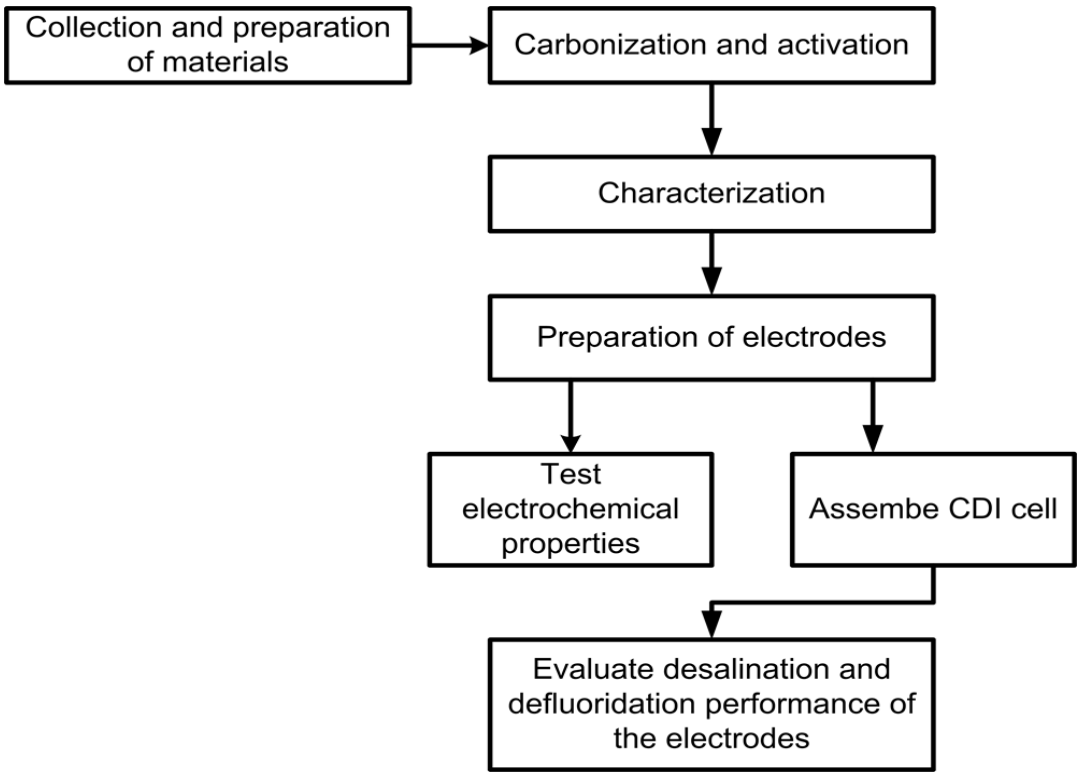

Figure 9: Flow chart of the activities involved in this study

3.2 Synthesis of porous carbon from jackfruit peels

Synthesis of activated carbon from jackfruit peels was done as illustrated in Fig. 10. Specifically, jackfruit peels were cut into small pieces then washed several times using tap water and finally distilled water to remove the adhering dirt. The cleaned peels were sun-dried for one week and then oven-dried at 100 ºC overnight to remove the moisture. Dry peels were grounded into powder and two routes (KOH and phosphoric acid activation) were used to synthesis the porous carbon.

3.2.1 KOH activation

In the first route 20 g of the grounded sample was placed in a ceramic boat crucible and carbonized at 400 ºC for 1 h in a horizontal tube furnace (CTF 12/65/550) under a constant flow of nitrogen gas. The obtained black char was named as carbonized jackfruit peels (JFC). Then 10 g of CJF was mixed with 5 M KOH solution in KOH: Carbon mass ratio (KOH/Carbon) of 1:1, 2:2 and 3:1 and stirred at 80 ºC for 2 h then, oven-dried at 110 ºC for 12 h. The dried mixture was activated at 600, 700 and 800 ºC at a heating rate of 10 ºC min^{-1} for 1 h in a tube furnace under flow of nitrogen gas. The samples were left in the furnace to cool naturally before taken out of the furnace. Samples were then washed using a 1M HCl solution so as to remove inorganic constituents to open the pores and repeatedly washed with hot distilled water to remove the chlorine ions from the sample surface as reported elsewhere (Rosas *et al*., 2010) until effluents reached neutral pH. The obtained samples were dried at 100 ºC for overnight and stored for further use. The obtained carbon materials were named as JFAC-x- y, where x is the mass ratio of activating agent and carbon and y is the activation temperature.

3.2.2 Phosphoric acid activation

In the second route 10 g of grounded sample were mixed with 150 ml of phosphoric acid with concentration of 10 and 35% and stirred at 85 ºC for 2 hr. The resulting slurry was oven-dried at 120 ºC overnight and then packed in a ceramic boat crucible and activated at 450 ºC and 550 ºC for 1 h in a horizontal tube furnace under a constant flow of nitrogen gas and were left in the furnace to cool naturally before taken out. The obtained sample was washed repeatedly with hot distilled water until the pH of effluent reached a constant pH. The sample was dried overnight at 100 ºC in a vacuum oven. The samples were named $_{P}$JFAC-z-y where z is the

concentration of phosphoric acid and y is the activation temperature and stored for next experiments.

Figure 10: Schematic diagram for the synthesis of activated carbon from jackfruit peels

3.3 Characterization of JFAC

3.3.1 Elemental analysis

The elemental composition (C, N, H, S) of the dried jackfruit peels and the resulting activated carbon samples were determined by elemental analyzer (Flash 2000 Organic elemental analyzer, Thermo Scientific). The oxygen content was obtained by the difference based on percentage of (C + H + N + S + O) = 100 % as previously reported by Hou *et al*. (2015).

3.3.2 Surface morphology and textural properties

The surface morphology of the samples was investigated using Zeiss Ultra Plus Field Emission Scanning Electron Microscopy (FE SEM). Automated gas sorption (Nova 4200e Quantachrome porosimeter, UK) was used to measure nitrogen adsorption and desorption at liquid nitrogen temperature (77 K). Prior to nitrogen adsorption studies, samples were degassed at 120 ºC for a period of 3 h. The Specific surface area was determined from sorption studies using the Brunauer-Emmett-Teller (BET) method, pore size distributions were evaluated through the Barrett-Joyner-Halenda (BJH) method while the micropore surface area was determined by the *t*-plot method. The diffraction patterns of the synthesized

samples were measured by automated PANalytical X'PERT PRO X-ray diffractometer (XRD) system using Cu- Kα radiation (λ = 1.54060 Å.) from Bragg angle (2θ) 5 to 80º. Structural parameters including the interlayer spacing, (d_{002} and d_{100}) and microcrystalline dimensions; (stack height (L_c) and stack width (L_a)) were evaluated by the application of Bragg's Law eqn (1) and the Debye–Scherrer Equation (2)

$$n\lambda = 2d\sin\theta \quad (1)$$

$$L_{c,a} = K\lambda / \beta_{c,a}\cos\theta \quad (2)$$

The mean number of layer planes in the microcrystalline (Np) was obtained from the ratio L_c/d_{002} while the ratio L_c/L_a was used to calculate the relative density of edge and basal planes in the microcrystalline. Where n = 1, λ is the wavelength (1.5406 Å) of the X-ray radiation and θ is the Bragg angle representing the position of the (002) and (100) diffraction peaks, K is the shape factor equal to 0.89 and 1.84 for L_c and L_a, respectively, and $\beta_{c.a}$ is the full width at half maximum of the symmetrically shaped diffraction peaks (Enock *et al*., 2017b; Mohd Nor *et al*., 2015). Raman spectroscopy studies were used to investigate the vibrational mode of the samples using a T64000 Raman spectrometer at an excitation wavelength of 514 nm.

3.4 Electrochemical measurements

The electrochemical performance of different JFAC based electrodes were carried out by AUTOLAB Potentiostat/Galvanostat (PGSTAT204, AUT50663 Metrohm) in a three electrodes cell system. The working electrode with dimensions of 1 cm × 1 cm was prepared by pressing 80 wt. % JFAC, 10 wt. % conducting carbon and 10 wt. % PVDF on a pre-cleaned piece of nickel foam which served as a current collector. PVDF act like a binder while carbon black was added to enhance electrical conductivity of the JFAC electrode. Saturated Ag/AgCl (KCl) was used as reference electrode and platinum wire as a counter electrode. All electrochemical properties were measured in 1M NaCl solution at room temperature. The specific capacitances *C* (F/g) were obtained by integrating the area of CV curves using equations (3) and (4).

$$C = \frac{Voltammetric\,Ch\arg e}{Potential\,window \times mass\,loading}, \text{ which can further be written as} \quad (3)$$

$$C = \frac{\int IdV}{2m.\Delta V.S} \quad (4)$$

where, $\int IdV$ is the total voltammetric charge obtained by integration of negative and positive sweep in cyclic voltammograms, I is current (A), ΔV is the potential window, S is the sweep rates(Vs^{-1}), and m is the mass of active materials in the working electrodes (g) (Chen *et al*., 2010). The conductivity of the electrodes were evaluated by EIS analysis in the frequency range of 10 mHz to100 kHz.

3.5 Fabrication of JFAC based electrode for CDI cell

The JFAC based electrode was prepared by mixing 80 wt. % activated carbon (JFAC), 10 wt. % conducting carbon and 10 wt. % PTFE. Then 15-25 ml of 99.9% ethanol were added to the mixture and stirred for a few minutes until a thick paste was formed. The paste was pressed to a desired thickness of 1 mm, cut into pieces of 4 cm $\times$ 4 cm then dried at 60ºC overnight in a vacuum oven. Finally, the electrodes were assembled into a CDI cell to investigate its electrosorption capacity. The total mass of both JFAC electrodes used in the electrosorption experiments was approximately 0.4–0.8 g.

3.6 Electrosorption experiments

The electrosorption experiments were carried out with laboratory scale CDI reactor in a batch mode to evaluate the desalination performance of JFAC electrodes. The experimental setup (Fig. 11) consisted of CDI cell (drawings of its parts and their dimensions (in inch) are presented in Figures 12 and 13, DC power source, peristaltic pump, feed tank and conductivity meter. A pair of JFAC electrodes of 4 cm $\times$ 4 cm, placed on titanium sheets current collectors were assembled in CDI cell and separated by 1 mm thick plastic mesh placed between the carbon electrodes to ensure electrolyte flow and prevent short circuit. Rubber gaskets were added to seal up the cell and all the components were covered with a plexiglas sheet and tighten with screws. During desalination experiment, 30 ml of NaCl feed solutions with varying concentrations (30-500 mg/L) were supplied to the CDI cell using a peristaltic pump (MasterflexLive™, L/S® series) and circulated feed return to the feed tank with a flow rate of 2.5 ml/min. Potentials of 1.2, 1.4 and 2.0 V were supplied to the CDI cell by potentiostat/galvanostat (Vertex.1A.EIS (1A/10V/1MHz EIS, Ivium Technologies, The Netherlands, equipped with IviumSoft electrochemistry software) at electrode terminals to

study the efficiency of salt-removal at these potentials. Conductivity meter was used to measure conductivity change in the feed tank after every 5 minutes. The relationship between conductivity and concentration was obtained according to a calibration curve made prior to the experiment. The conductivity change of NaCl feed solution was continuously measured with a portable digital conductivity meter (GMH 3400 series) in the feed tank.

The salt adsorption capacity Γ (mg/g) was calculated from equation (5):

$$\Gamma = \frac{(C_f - C_i) \times V}{m} \tag{5}$$

where C_f and C_i are final and initial concentrations in mg L^{-1}, V is the volume in litres and m is the total mass of the active material in both electrodes in grams (Leong & Yang, 2016).

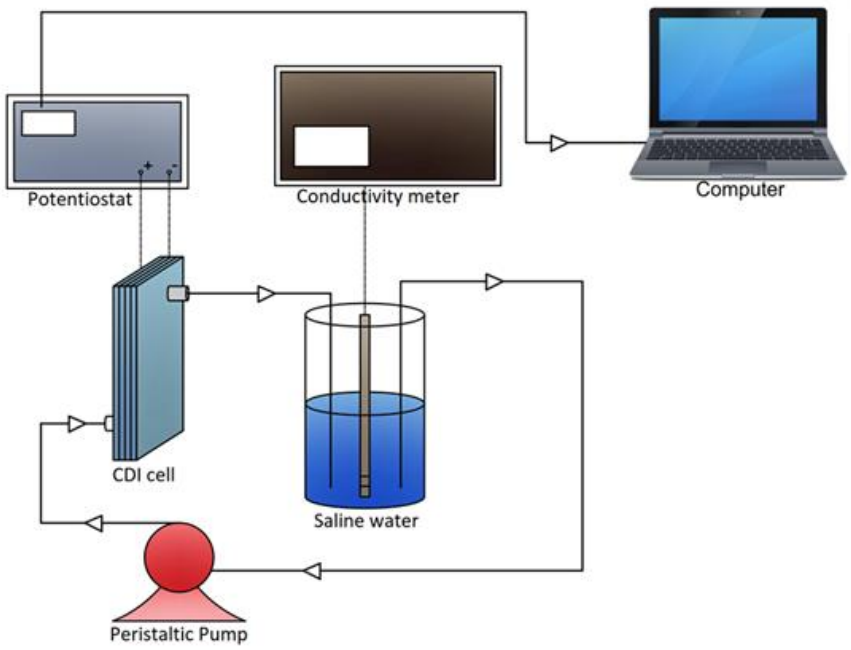

Figure 11: Schematic diagram of the CDI experiment set up

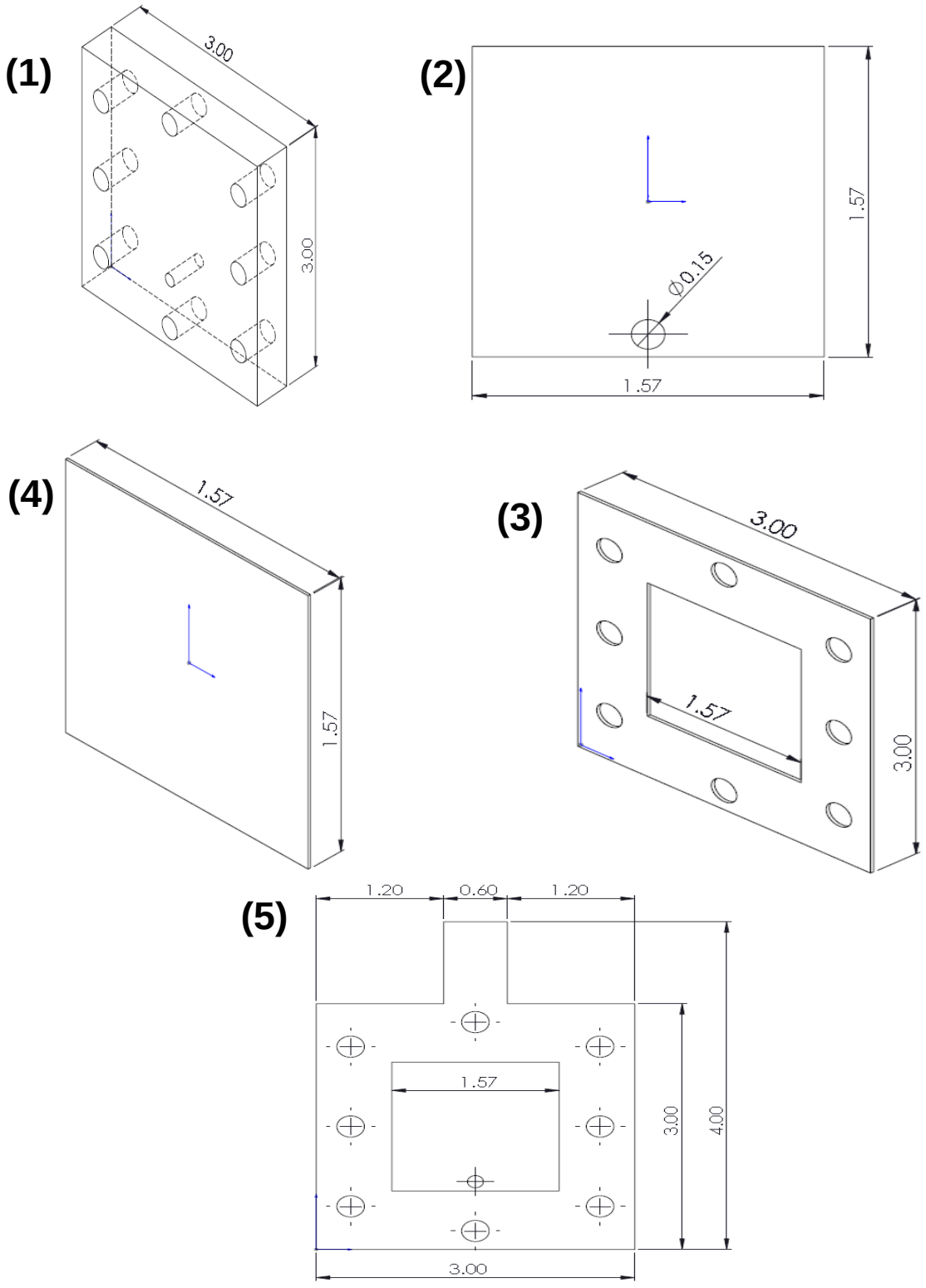

Figure 12: Parts of CDI cell (1) End-plate- plexiglas sheet (2) Porous carbon Electrode (3) Spacer/separator (4) Gasket (5) Current collector

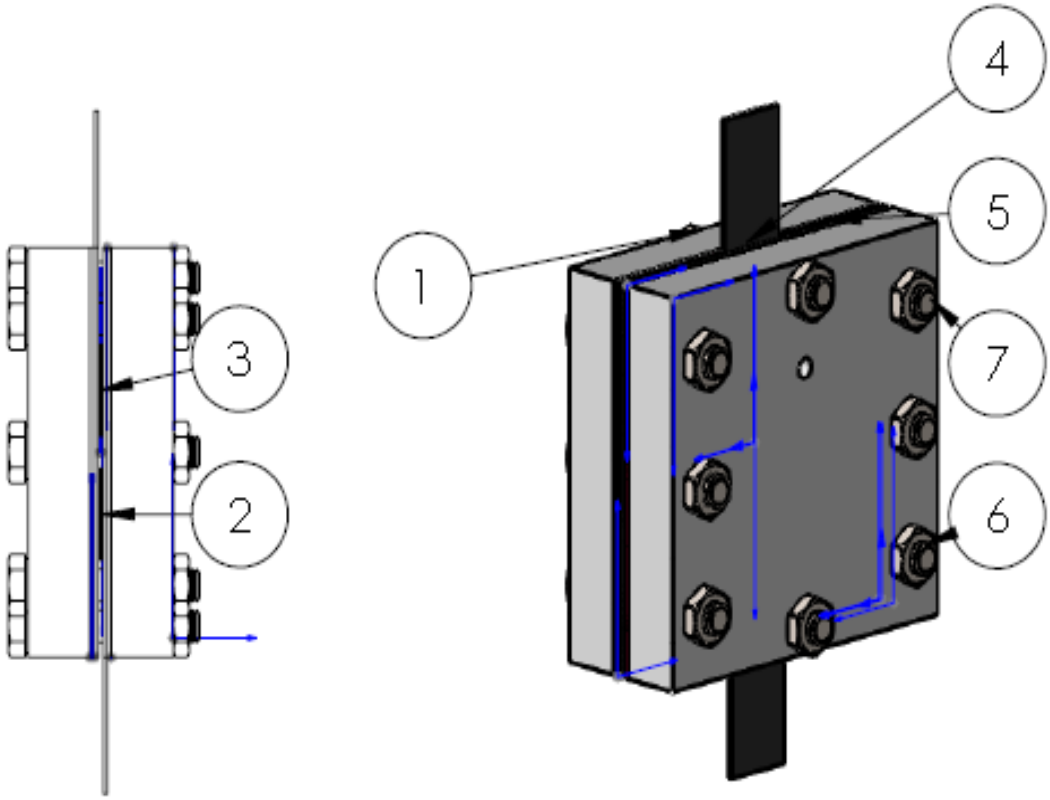

Figure 13: Drawing showing CDI cell after being assembled (number 6 and 7 represents bolts and hexagon thin nuts respectively)

Charge efficiency (ʌ) which is the ratio of salt adsorption over charge transfer in a CDI-cycle was calculated using equation 6

$$\Lambda = \frac{\Gamma \times F}{M_w \times \Sigma} \tag{6}$$

Where $\sum$ is the specific charge stored during the adsorption curve (C g^{-1}) obtained from measured data for current and time during charging step, F is the Faraday's constant of 96485 (C mol^{-1}) and, M_w (g/mol) is molecular weight of salt solution used.

The total energy consumption (E in joules) of a purification cycle was calculated from equation 7. The obtained energy in joule was then converted into kWh/m^3 of water desalinated.

$$E = V\int Idt \tag{7}$$

3.7 Water characterization

Water samples were collected from the tap (mainly derived from groundwater sources) in our institution laboratory. Ion selective electrode (ISE) coupled with Mettler Toledo Seven Compact pH/Ion S220 meter was used to measure the concentration F^-. Before F^- measurements total ionic strength buffer (TISAB II) was mixed with treated and untreated water in the ratio of 1:1. Glacial acetic acid (57.0 ml), NaCl (58.0 g) and cyclohexanediaminetetraacetic acid (CDTA (4 g)) were mixed in 500 ml of distilled water to prepare TISAB II. Solution pH was adjusted to 5.3–5.5 by adding about 150 ml of 6 M NaOH and distilled water was then added to make it 1L. Hanna HI 9829 Multi-parameter was used to measure pH, electro-conductivity (EC) and total dissolved solids (TDS). Total hardness as Ca-$CaCO_3$ was determined using a titration method with ethylenediaminetetraacetic acid (EDTA) with Erichrome Black T (EBT) indicator and ammonium buffer. Calcium hardness and magnesium hardness as $CaCo_3$ and concentration of Ca^{2+} and Mg^{2+} were determined by method 8030 Calcium and Magnesium; Calmagite Colorimetric Method with DR 2800 spectrophotometer according to the Standard Methods for Water and Wastewater Analysis (Eaton *et al*., 2005).

CHAPTER FOUR

RESULTS AND DISCUSSION

4.1 Elemental analysis of raw material and JFAC

Table 8 shows the results of elemental analysis of dried jackfruit peels (DJFP) and the synthesized JFAC. The dried raw jackfruit peels contain contains 44.11 % of carbon, 49.89% of oxygen, 5.71 % of hydrogen, 0.32% of sulfur and nitrogen was below the detection limit (BDL) of the equipment. Jackfruit peels are suitable precursor for preparation of activated carbons because of their high carbon content. After carbonization, the carbon content increased to 74.36% while oxygen, hydrogen, and sulfur decreased to 21.77, 3.87 and 0.27% respectively. Introduction of activating agent and temperature lead to further increase in carbon content from 74.36 to 92.12% as activation temperature increased to 700 °C for samples activated with KOH/C ration of 1. With further increase in temperature to 800 °C the carbon content decreases to 54.31%. Similar trend is observed for carbon samples activated with KOH/C ratio of 3. For samples activated with KOH/C ratio of 2, the carbon content increase with increase in activation temperature. The increase in carbon content with increase in activation temperature may be due to an increasing degree of aromaticity as previously reported by Fierro *et al*. (2006). Generally, carbonization and the activation processes increase the carbon content of JFAC when compared to the carbon of the raw material. On the other hand, activation process decreases the content of sulfur.

Table 8: Elemental analyses of raw materials and the synthesized JFAC

Sample	Elemental analysis (%)				
	C	H	N	S	O*
DJFP	44.11	5.71	BDL	0.32	49.86
JFC	74.36	3.87	BDL	0.27	21.50
JFAC-1-600	90.64	1.24	BDL	0.14	7.98
JFAC-1-700	92.12	0.55	BDL	0.07	7.26
JFAC-1-800	54.31	0.26	BDL	0.00	45.43
JFAC-2-600	61.84	0.87	BDL	0.05	37.24
JFAC-2-700	70.33	1.26	BDL	0.00	28.41
JFAC-2-800	85.36	0.24	BDL	0.10	14.30
JFAC-3-600	60.21	1.05	BDL	0.00	38.74
JFAC-3-700	83.13	0.56	BDL	0.23	16.08
JFAC-3-800	72.72	0.36	BDL	0.00	27.17

O* estimated by difference

4.2 Surface morphology of JFAC

SEM images of JFAC samples activated with KOH and H_3PO_4 at different temperatures are shown in Figures 14 to 17. It can be seen that after carbonization at 400 ºC less porous carbons with a layered structure and block like structures that agglomerated on the surface were produced as shown in Fig. 14a. This is associated with incomplete carbonization resulting from low activation temperature used as reported previously by Huang *et al*. (2014). At low carbonization temperature, tar derived from the degradation of lignocellulosic materials block the pores and hinders the formation of new pores, resulting in low specific surface area and total pore volume as shown in Table 9. With the introduction of the activating agent and increasing activation temperature Fig. 14(b-d), JFAC samples develop more pores and surface roughness increased. As shown in Fig. 15 (a-c) and Fig. 16 samples JFAC-1-700, JFAC-1-800, JFAC-2-600, JFAC-2-700 and JFAC-2-800, acquired the honey comb like structure. The honey comb structure is beneficial for ion adsorption (Matsubara *et al*., 2010). Significant differences in morphology were observed in JFAC-3-600 (Fig. 15d), JFAC-3-700 (Fig. 15e) and JFAC-3-800 (Fig. 15f) in which enlarged pores appear on the surface. This might be due to the breakage pores resulted from increasing activating agent ratio as previously observed by Zou *et al*. (2018).

From high resolution SEM images Fig. 16(a-f), it can be seen that the selected JFAC samples exhibited some connected pores. This might have been caused by the intercalation of potassium between carbon layers during the activation process as described herein Eqn (8) (Hui & Zaini, 2015; Otowa *et al*., 1993; Wang & Kaskel, 2012). The KOH activation process consists of several reactions as shown in Eqn (9)–(14). At 400 ºC KOH first dehydrates to form K_2O Eqn (9) followed by water gas reaction Eqn (10)-(11) and then carbonate formation Eqn (12). The carbonates decompose into CO_2 and K_2O and disappear at temperatures higher than 700 ºC Eqn (13). The metallic potassium (K) produced after reduction of K_2O by carbon at the temperature around 800 ºC Eqn (14) intercalate into the carbon matrix, thereby widening the atomic layer of carbon. During washing, the intercalated metallic K and other compounds containing K are removed resulting into expanded carbon lattices that cannot return to their previous structure therefore pores that are essential for the large surface area are created .

$$6KOH + 2C \rightarrow 2K + 3H_2 + 2K_2CO_3 \quad (8)$$

$$2KOH \rightarrow K_2O + H_2O \quad (9)$$

$$C + H_2O \rightarrow CO + H_2 \quad (10)$$

$$CO + H_2O \rightarrow CO_2 + H_2 \quad (11)$$

$$CO_2 + K_2O \rightarrow K_2CO_3 \quad (12)$$

$$K_2CO_3 \rightarrow K_2O + CO_2 \quad (13)$$

$$C + K_2O \rightarrow 2K + CO \quad (14)$$

Figure 16 shows SEM image of samples activated with phosphoric acid. It can be seen that the surface of the produced pJFAC consists of irregular pores with a tunnel shape and honey comb-like structure. The observed tunnels resulted evolution of volatile matters after decomposition of the material during activation process. Furthermore, sample pJFAC-10-550 (Fig. 16b) displayed a more hierarchical structures which resemble the honey-comb holes in which the corner lines of the hole openings can be observed clearly. Additionally, as we increase concentration of phosphoric acid to 35% the material (sample pJFAC-35-450 (Fig. 16c)) developed pores with bamboo-like structures. As activation temperatures increased to 550 ºC the bamboo-like pore structure were destructed and the material acquires irregular pores (pJFAC-35-550 (Fig. 16d)).

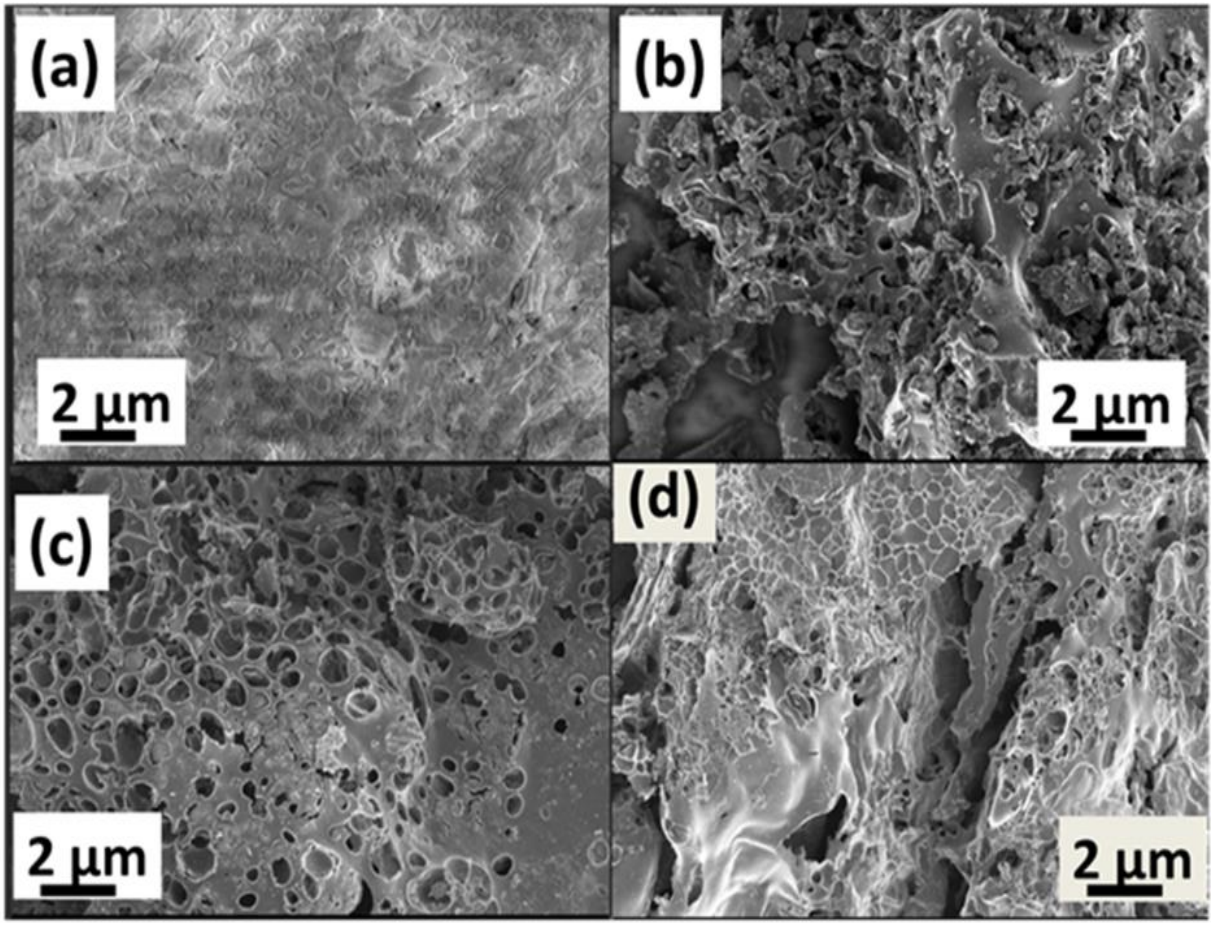

Figure 14: SEM image for (a) JFC, (b) JFAC-1- 600, (c) JFAC-1- 700, (d) JFAC-1- 800 at low resolution

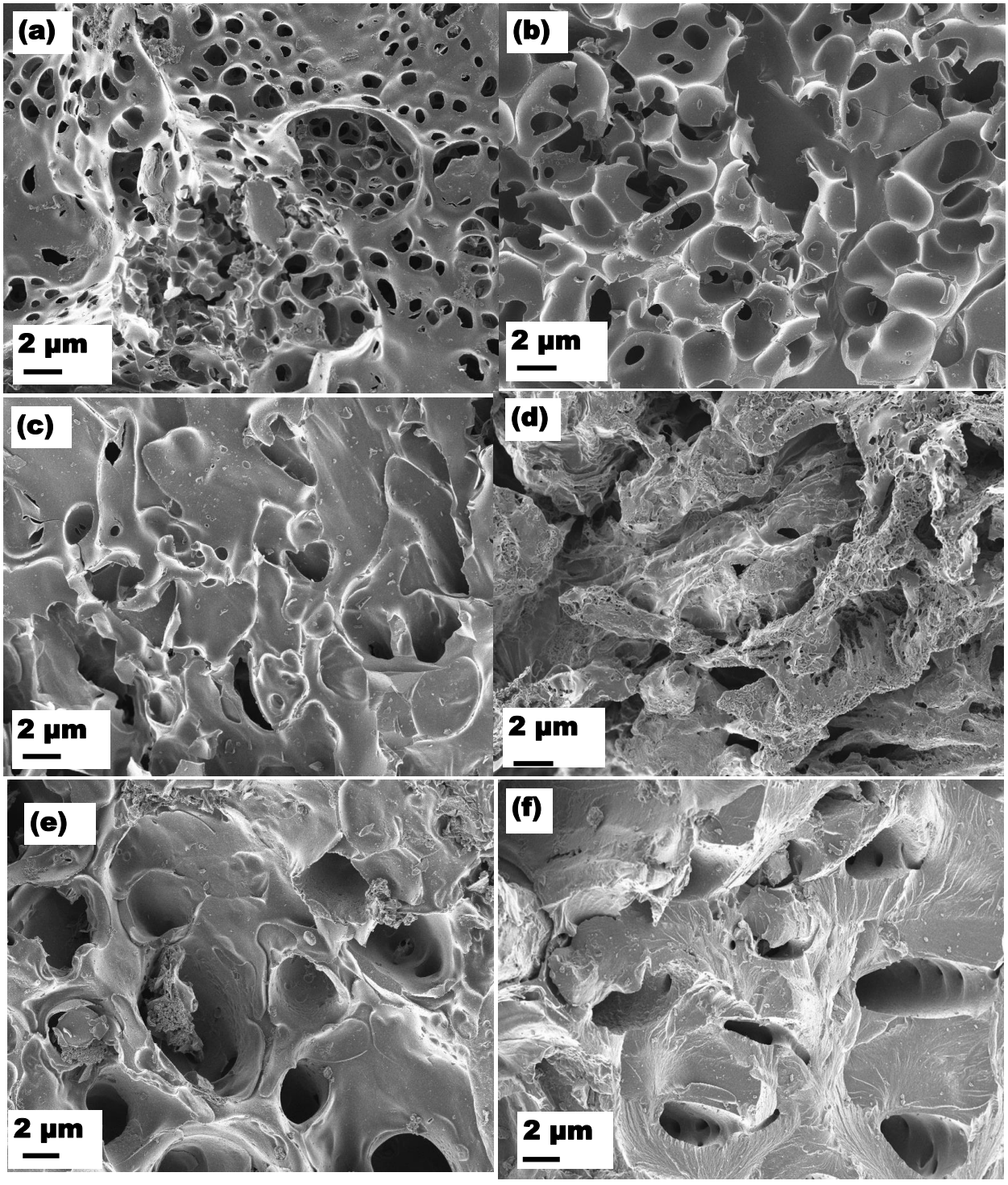

Figure 15: SEM images of (a) JFAC -2-600 (b) JFAC -2-700 (c) JFAC -2-800 (d) JFAC -3-600 (e) JFAC -3-700 (f) JFAC -3-800

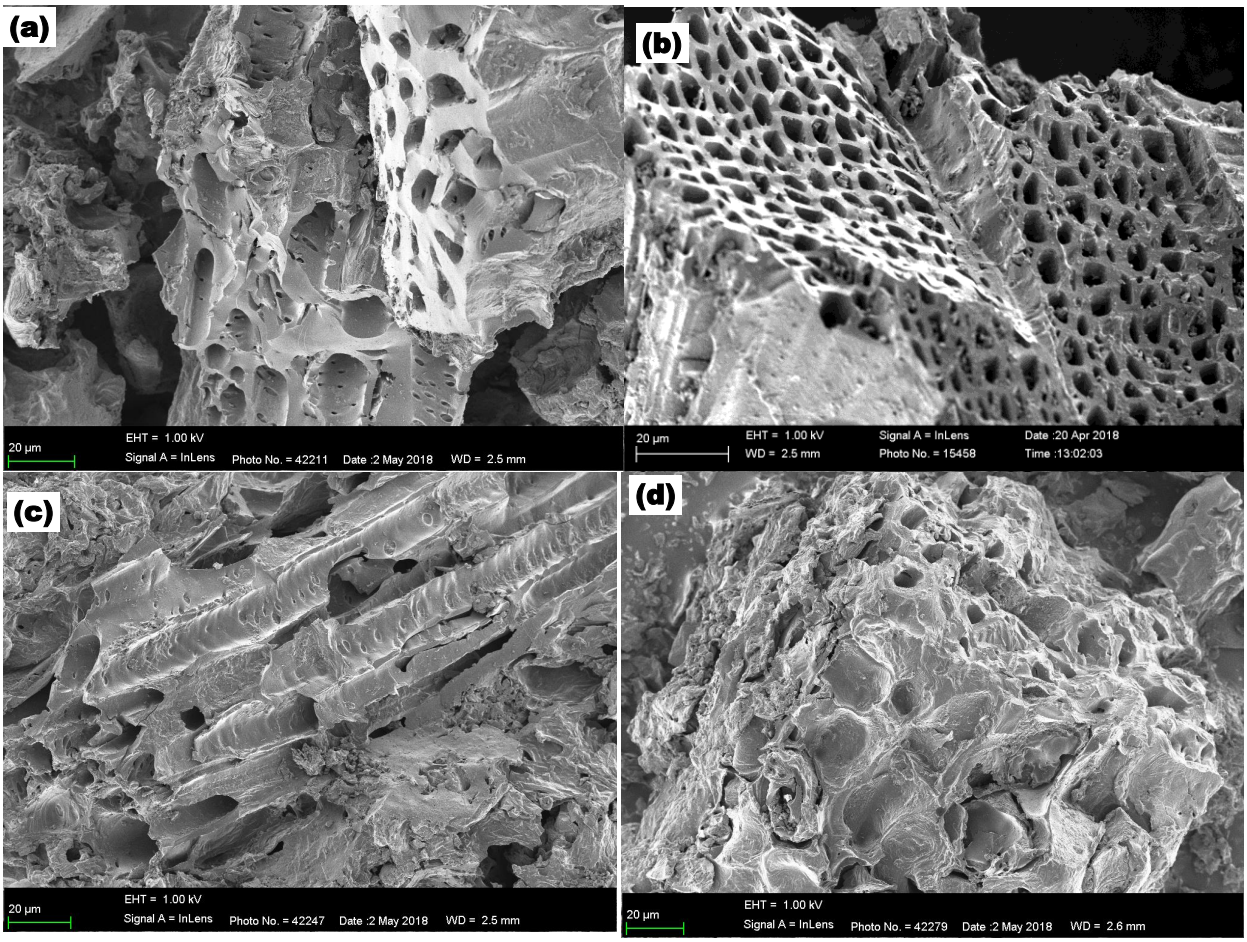

Figure 16: SEM images of (a) $_{P}$JFAC-10-450 (b) $_{P}$JFAC-10-550 (c) $_{P}$JFAC-35-450 (d) $_{P}$JFAC-35-550

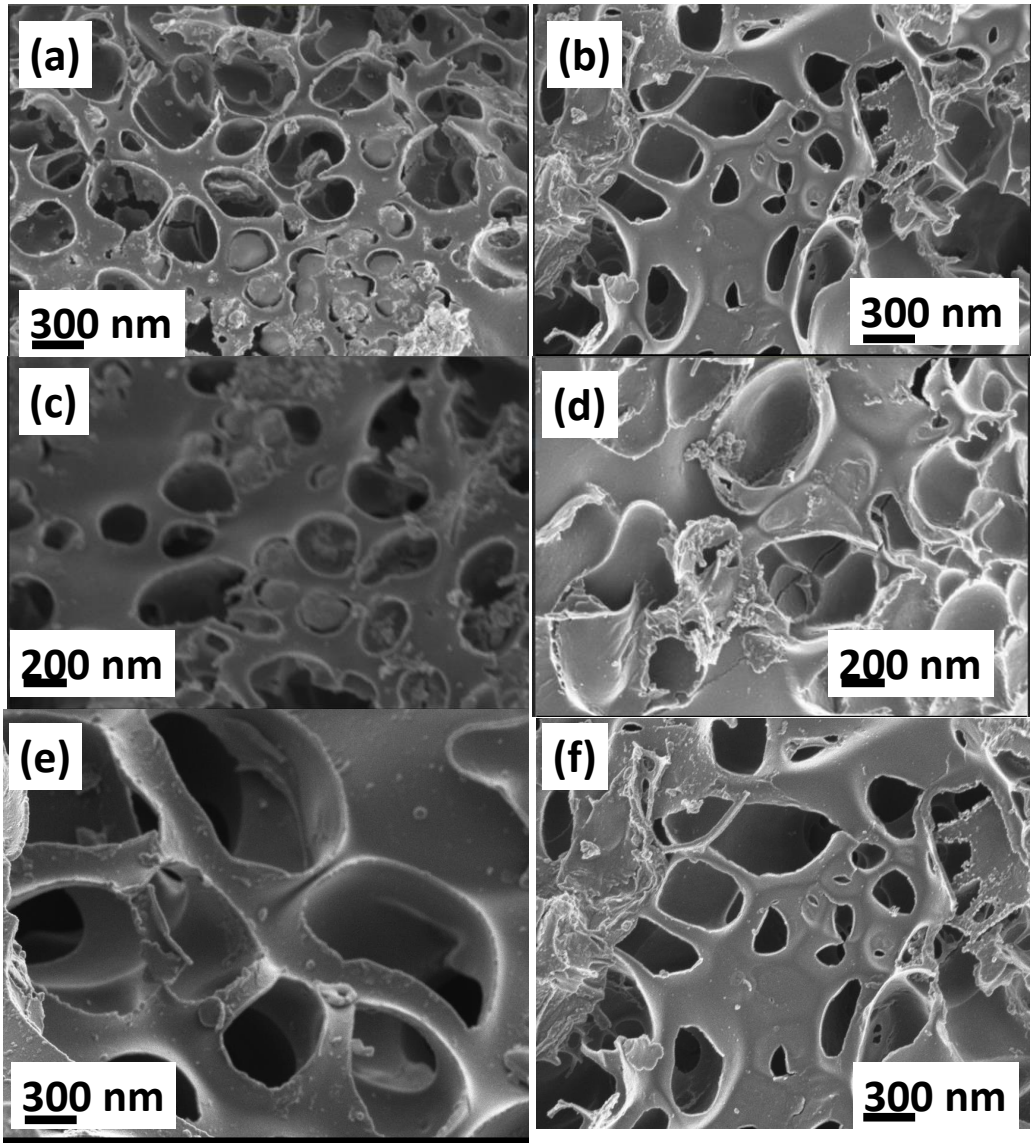

Figure 17: SEM image for JFAC-1-700 (a, c) and JFAC-1-800 (b, d), (e) JFAC-2-600 (f) JFAC-3-600 at high resolution

4.3 Textural characteristics of JFAC

4.3.1 Surface area and pore structure

In order to classify the pore structure of materials and the adsorption mechanism, the adsorption of inert gases is conducted before liquid sorption experiments. Fig. 18 shows the nitrogen sorption isotherms and BJH pore size distribution plots of JFAC materials. From Fig. 18a, Fig. 18b and Fig. 18c, it is observed that the adsorbed volume increased remarkably from 200 to around 2400 cm^3 for JFC and JFAC-2-800 respectively, revealing the enhanced specific surface area and pore volume. Specifically, JFAC-2-800 exhibited the highest N_2 adsorption capacity with highest S_{BET} of 2681 m^2/ g as shown in Table 9. In Fig. 18a, as

activation temperature increases from 700 to 800 ºC the quantity of nitrogen adsorbed by JFAC-1-800 decreases indicating a reduction of both surface area and pore volume. Carbonized jackfruit carbon sample did not show significant changes in the volume of gas adsorbed, indicating that the material has a little amount of pores. The slope of the nitrogen isotherm curve increased as activation temperature increases, suggesting the development of a porous structure in the carbon as previously reported by Im *et al*. (2014). According to the IUPAC classification, JFC and JFAC-1-600, JFAC-2-600, JFAC-2-700, JFAC-3-600, JFAC-3-700 and pJFAC-10-450 carbon samples exhibit type I isotherm (from Fig. 18a, Fig. 18b and Fig. 18c) in which no abrupt uptake of adsorbed volume occurs at the lower relative pressure evidencing that the materials only consists of a small amount of micropores. Furthermore, JFAC-1-700, JFAC-1-800, JFAC-2-800 JFAC- 3-800, pJFAC-10-550, pJFAC-35-450, and pJFAC-35-550 exhibit type IV isotherm with a small hysteresis loop at the higher relative pressure range (P/P_o >0.4), suggesting the presence of considerable amount of mesopores in the sample as previously reported by Zornitta *et al*. (2017).

The pore size distribution of JFAC was calculated from the N_2 desorption data with BJH methods. Figure 18 (d-f) shows the pore size distribution of JFAC samples. From Fig. 18d one can observe that as activation temperature increases to 700 ºC, the differential volumes also increase indicating that the materials developed more pores. However, when the temperature increased to 800 ºC, differential volume decreased suggesting that pores were collapsing. All samples show that, most of the pores are less than 50 nm and have a high differential pore volume at a pore size range of 3.0-5.0 nm. This indicates that JFAC samples possess mesopores as classified by IUPAC. Presence of mesopores in the sample is of paramount importance due to the fact they not only contribute to the large surface area but also provide wider transport channels to micropores resulting into improved electrosorption performance as confirmed in previous studies by Noked *et al*. (2009).

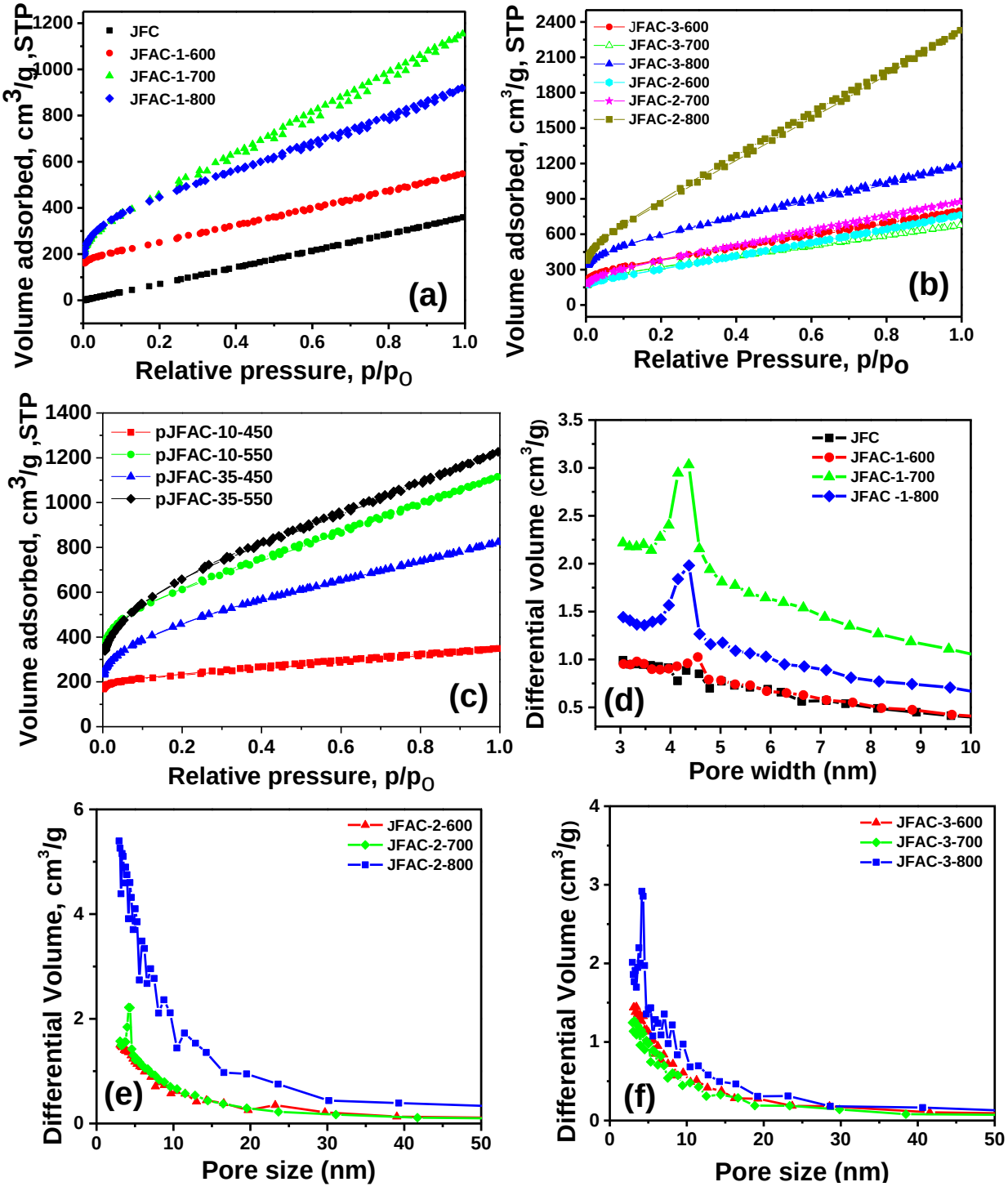

Figure 18: (a-c) Nitrogen adsorption/desorption isotherms of JFAC (d-f) Pore size distribution calculated from desorption isotherm using the BJH method

Table 9 presents the textural characteristics; BET surface area, micropore and mesopore volume and surface area, average pore size and the total pore volume of JFAC obtained from the nitrogen adsorption/desorption studies. For samples activated with KOH, it can be seen that different KOH/C ratio and activation temperatures have different effects on the surface

and pore structure of JFAC. For samples with KOH/C ratio of 1, the BET surface area and pore volume increased from 607 to 1955 m^2/g (Fig. 19a), and 0.52–1.34 cm^3/g as temperature increased from 400 to 700 ºC respectively. Moreover, as activation temperature increases to 800 ºC, BET surface area and pore volume decreased to 1579 m^2/g and 0.85 cm^3/g respectively. It is reported that at higher activation temperature, the activation process would occur more complete leading to more pores that are beneficial for the large surface area (Zhang *et al*., 2017b). However, with KOH/C ratio of 1, as activation temperature increases from 700 to 800 °C, surface area and pore volume decreased. This might be due to a sintering effect which occur at high temperature followed by shrinkage and realignment of the structure of carbon as previously reported by Prahas *et al*. (2008), Kumar and Jena (2016) and Mohanty *et al*. (2005).

Also, from Table 9, it can seen that BET surface area, micropore surface area (S_{micro}), mesopore surface area (S_{meso}), total pore volume (V_T) and average pore diameter (P_d) of all JFAC samples activated with KOH/C ratio of 2 and 3 increases with increase in activation temperature. This signifies that as activation temperature increases, the rate of reaction between carbon and KOH increases, consequently generating new pores. Sample JFAC-2-800 exhibits a largest BET surface area of 2681 m^2/g, the pore size of 2.23 nm and a high pore volume of 2.6 cm^3/g followed by JFAC-3-800 with a pore size of 4.16 nm, a BET surface area of 1993 m^2/g, and a pore volume of 1.09 cm^3/g. The BET surface area, pore size and pore volume of JFAC-3-700 are 1350 m^2/g 3.47 nm and 0.75 cm^3/g respectively. Yet, JFAC-3-600 has a surface area of 1067 m^2/g with a pore size of 2.93 nm. Increasing KOH/C ratio from 2 to 3 significantly decreases the BET surface area and pore volume while pore diameter increases at higher temperatures i.e 700 and 800˚C. This is due to the fact that at high activation temperature the activation process occurs more completely (Zhao *et al*., 2017) and the decomposition rate becomes faster, leading to more pore opening and widening as previously reported by Deng *et al*. (2015a). Figure 19b and 19c shows the variation of BET surface area and activation temperature while Fig. 20 shows the variation of BET surface area with activating agent ratio/concentration at a certain activation temperature. For KOH activated samples (Fig. 20a), the increase in BET surface area and KOH/C ratio has no specific trend. For samples activated with H_3PO_4, it can be noted that BET surface area increased with both increase in concentration of H_3PO_4 and activation temperature (Fig. 20b). An increase in the specific surface area represents an increase in the number of adsorption sites that favors enhanced electrochemical properties and electrosorption capacity. From

these results it is evident that, type of activating agent and the synthesize route yield materials with different characteristics. Generally, the activation temperature, phosphoric acid concentration, and KOH/C ratio are the key factors in determining the surface and textural properties of the produced JFAC. From Table 9 it can be seen that all carbon samples have the average pore sizes ranging from 2.93 to 4.16 nm which is within the mesoporous range according to IUPAC classification. It can also be noted that the BET surface area and total pore volume of activated carbon from jackfruit peels (JFAC-2-800) obtained in the present study are larger than those reported by Prahas *et al*. (2008) and Foo and Hameed (2012). Therefore, JFAC is anticipated to have a superior capacitance and electrosorption capacity due to their large surface area and pore size which are among important factors in identifying good electrode materials for CDI.

Table 9: Summary of the textural characteristics of the JFAC samples

Carbon	[a]S_{BET} (m^2/g)	[b]S_{micro} (m^2/g)	[c]S_{meso} (m^2/g)	[d]P_d (nm)	[e]V_{micro} (cm^3/g)	[f]V_{meso} (cm^3/g)	[g]V_T (cm^3/g)
JFC	607	179	428	3.05	0.06	0.46	0.52
JFAC-1-600	888	437	451	3.06	0.21	0.32	0.53
JFAC-1-700	1955	766	1189	3.05	0.32	1.02	1.35
JFAC-1-800	1579	788	791	3.05	0.29	0.56	0.85
JFAC-2-600	965	274	691	3.23	0.19	0.63	0.82
JFAC-2-700	1405	603	802	3.22	0.23	0.64	0.87
JFAC-2-800	2681	425	2256	3.23	0.41	2.20	2.61
JFAC-3-600	1067	483	584	2.93	0.29	0.36	0.65
JFAC-3-700	1350	674	676	3.47	0.23	0.52	0.75
JFAC-3-800	1993	1005	988	4.16	0.47	0.62	1.09
$_p$JFAC-10-450	736	543	193	3.04	0.27	0.24	0.51
$_p$JFAC-10-550	2076	1224	852	3.23	0.55	0.34	0.89
$_p$JFAC-35-450	1594	942	652	3.24	0.39	0.22	0.61
$_p$JFAC-35-550	2309	1310	999	3.23	0.53	0.44	0.97

a-BET surface area, b-Micropore surface area, c-Mesopore surface area, d-Average pore diameter, e-Micropore volume, f-Mesopore volume and g- Total pore volume

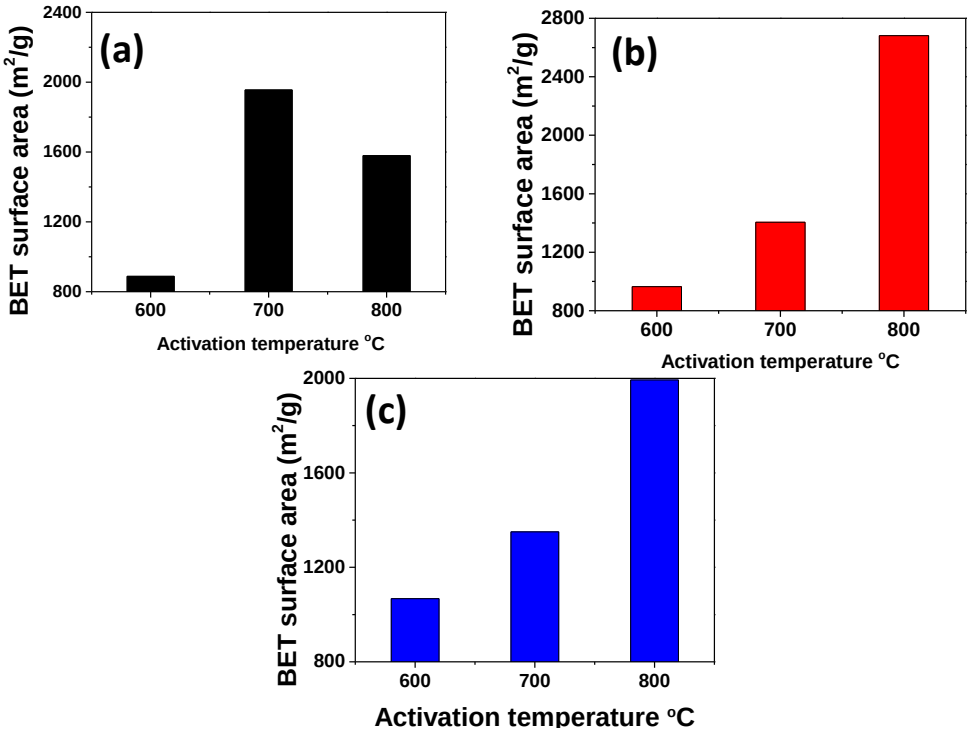

Figure 19: Variation of BET surface area with activation temperature at KOH/C ratio of (a) 1(b) 2 (c) 3

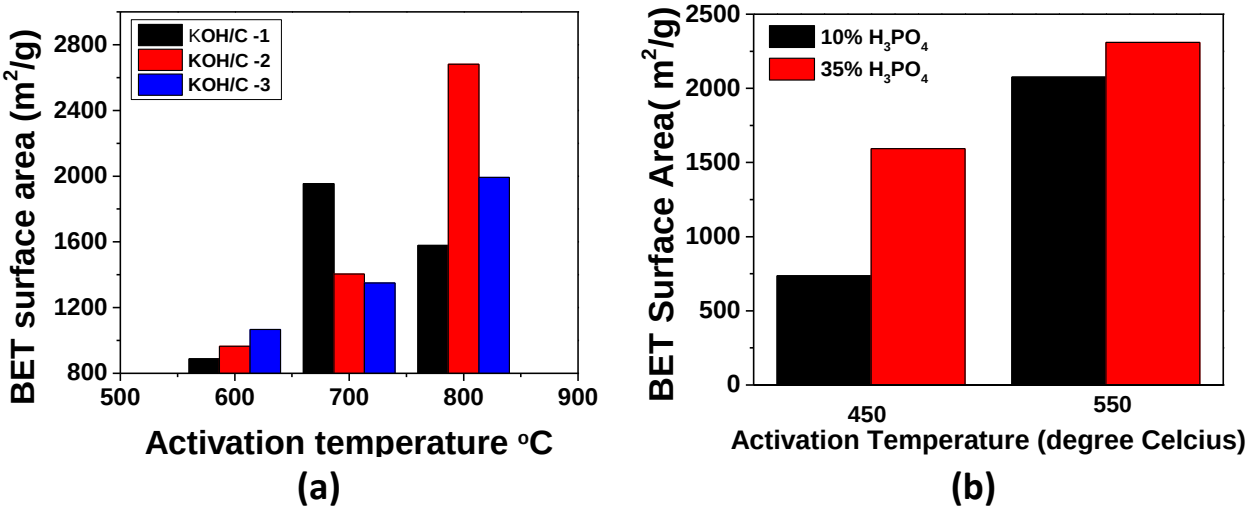

Figure 20: Variation of BET surface area with (a) KOH ratio (b) H3PO4 at a different activation temperature

4.3.2 X-ray diffraction studies

X-ray diffraction patterns of unactivated carbon (JFC) and activated carbon samples at different temperature and KOH/C ratio are shown in Fig. 21(a-c). Two broad peaks positioned at around 20-25º and 40-45º which are indexed with (002) and (100) planes of the

graphitic-like carbon with the amorphous character were observed. This indicates that all JFACs are pure carbon samples. Presence of these peaks confirms the destruction of carbon matrix in the structure of lignocellulosic material as previously reported by Anton *et al*. (2016). Furthermore, the occurrence of the broad peak at around 2θ =20-25° and 40-45° suggests that the structure of the formed JFAC is mainly amorphous. However, in the JFC sample the peaks are not much visible. This could be associated with the presence of impurities/ inorganic substances in the carbon precursor which disappeared during the activation process and probably when washing the sample with HCl.

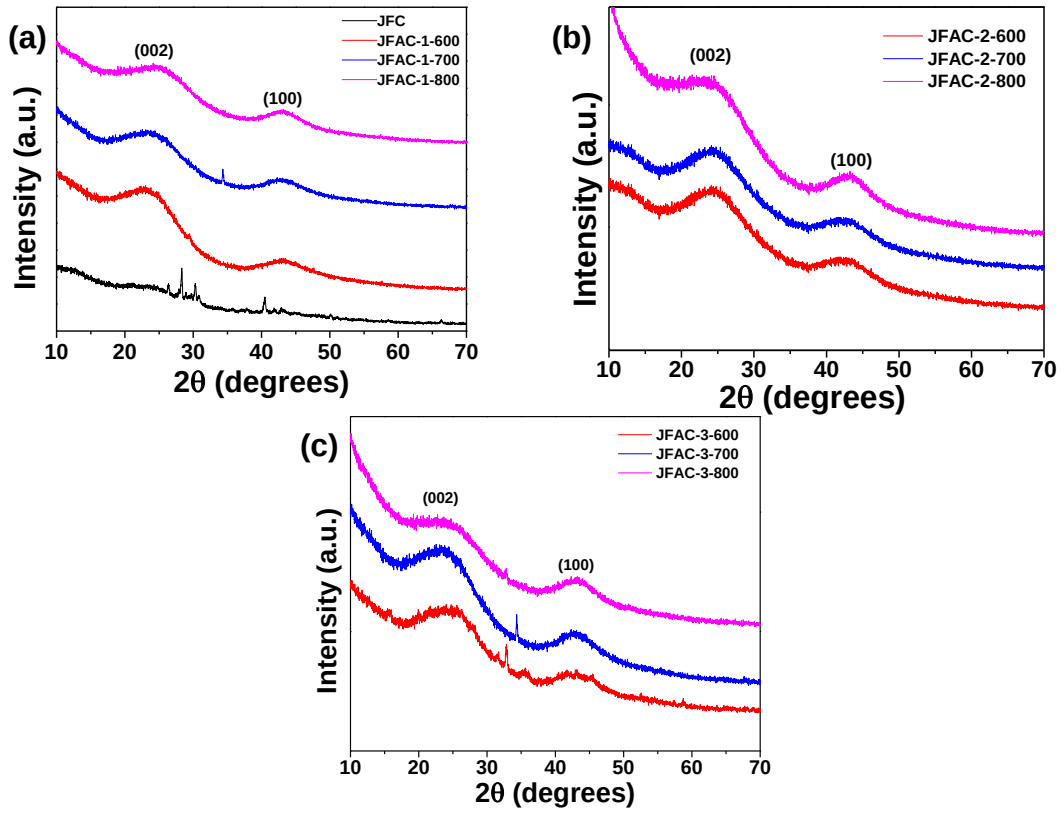

Figure 21: XRD patterns of the JFAC samples at different KOH/C ratio and activation temperature

The structural parameters calculated from X-ray diffraction data are shown in Table 10. It can be seen that there is no significant variation in d_{002} and d_{100} values of all JFAC samples implying that, the activating temperature and KOH/C ratio did not affect the microcrystalline orientation. The calculated interlayer spacing (d_{002}) varies from 3.63-3.91 are slightly higher than the normal graphitic dimensions of 3.35 Å. These results show that synthesized JFAC carbon consists of turbostratic (fully disordered) structures as previously reported by Girgis *et al*. (2007). The JFAC samples show stack height (L_c) value varied from 19.35-20.84 Å, the

stack width (L_a) value ranging from 50.43-50.81 Å and a constant L_c/L_a value of 0.41 for samples activated with KOH/C ratio of 1 and 0.38 for samples activated with KOH/C ratio of 2 and 3. Both parameters i.e. microcrystalline size and orientation are very important as they have a significant influence on the formed electric double layer and on the specific capacitance value of the material (Nabais *et al*., 2011).

Table 10: Interlayer spacing, microcrystalline dimension, and ratios of Lc/La and Np of all JFAC samples

	Interlayer spacing (Å)		Microcrystalline dimension (Å)			
Sample	d_{002}	d_{100}	L_c	L_a	L_c/L_a	N_p
JFC	3.68	2.20	19.35	50.43	0.38	5.26
JFAC-1-600	3.91	2.09	20.84	50.77	0.41	5.32
JFAC-1-700	3.80	2.10	20.81	50.81	0.41	5.47
JFAC-1-800	3.77	2.09	20.83	50.70	0.41	5.53
JFAC-2-600	3.69	2.19	19.35	50.48	0.38	5.24
JFAC-2-700	3.70	2.12	19.35	50.69	0.38	5.23
JFAC-2-800	3.63	2.12	19.35	50.71	0.38	5.32
JFAC-3-600	3.70	2.14	19.35	50.65	0.38	5.22
JFAC-3-700	3.68	2.12	19.35	50.72	0.38	5.25
JFAC-3-800	3.75	2.12	19.35	50.70	0.38	5.15

4.3.3 Raman spectroscopy

Raman spectroscopy is a nondestructive method for characterizing amorphous, crystalline and nanocrystalline materials (Ferrari & Robertson, 2000). It is one of the most useful characterization methods in understanding the development of structural order in carbon material. Figure 22 shows the Raman spectra of JFC and JFAC. From the spectra of Fig. 18(a-c), two important bands located at around 1351 cm^{-1} and 1587 cm^{-1}, corresponding to D and G bands, respectively were observed. The D band is associated to the disordered carbonaceous structure, while the G band is related to the ordered graphitic structure. The D band is due to the breathing mode of k-point phonons of A_{1g} symmetry and the G band is assigned to the zone center phonons of E_{2g} (Ferrari & Robertson, 2000).

The intensity ratio of D band to G band (I_D/I_G) expresses the degree of graphitization of the carbon samples. The I_D/I_G ratio of samples synthesized with KOH/C ratio of 1 (Fig. 22a) varies from 0.85 to 0.95 as activation temperature increases from 600–800 ºC, correspondingly. Similarly, with JFAC-2 samples (Fig. 22b), it can be seen that the value of I_D/I_G increases slightly from 0.84 to 0.88 as activation temperature increases to 700 ˚C and then dropped to 0.85 as temperature increase further to 800 ˚C. This slight increase in the I_D/I_G ratio indicates that the activation temperature destroys a part of the graphite structure leading to more defects as reported previously by Lu *et al*. (2018). More defects are advantageous as they may lead to the improvement of the ion storage during the CDI process since they can generate more accessible pore volumes and surface area.

However, as we increase the KOH/C ratio to 3, the I_D/I_G ratio did not increase significantly (Fig. 22c). The I_D/I_G ratio increases from 0.84 to 0.87 as activation temperature increased from 600-700 ºC and then decreases to 0.84 as activation temperature increases to 800 ºC indicating that activation temperature increases the degree of graphitization of the material. For samples activated with phosphoric acid (Fig. 22d) the I_D/I_G ratio of samples pJFAC-10-450 and pJFAC-10-550 decreases from 0.91 to 0.85 as activation temperature increased from 450 to 550 ˚C respectively. The I_D/I_G ratio of pJFAC-35-450 and pJFAC-35-550 samples is 0.89, indicating that the activation temperature did not affect the degree of graphitization of these samples.

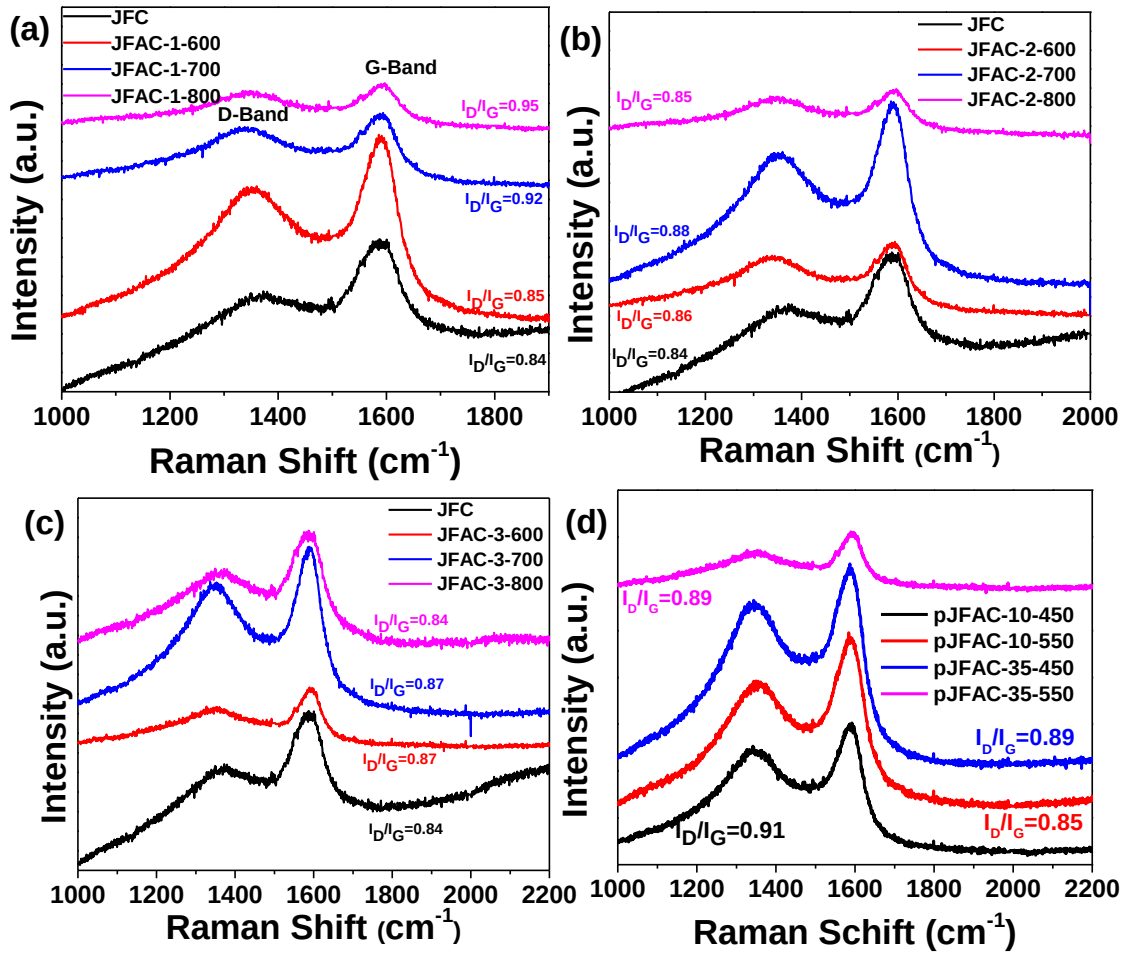

Figure 22: Raman spectra of JFAC at different activation temperature and (a) KOH/C ratio (b) H_3PO_4 concentration

4.4 Electrochemical performance

Cyclic voltammetry is a vital tool to assess the potential of electrode materials used in supercapacitor as well as CDI for EDL formation due to the comparable working principle of supercapacitor and CDI (Li *et al.*, 2010). CV tests were carried out to assess the EDL behavior of the fabricated ACJF electrodes as presented by CV curves in Fig. 23(a-d). It can be observed that all CV curves exhibit nearly a quasi-rectangular shape and no faradic peaks were observed in the working potential of −1.0 V to 0.0 V. This suggests that ions were removed from the solution by formed EDL instead of electrochemical reactions.

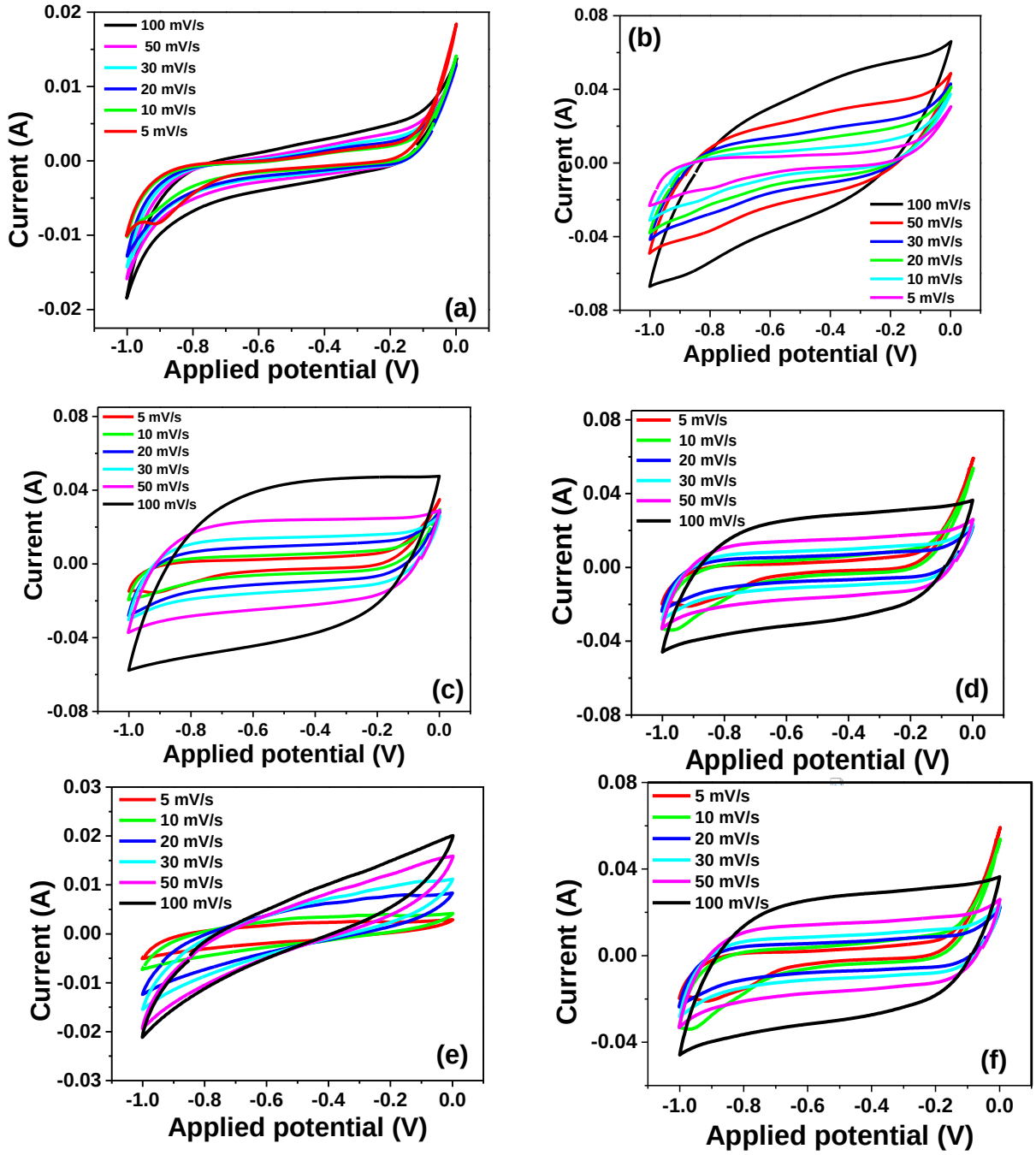

Figure 23: CVs of (a) CJF, (b) JFAC 1-700, (c) JFAC -2-800, and (d) JFAC-3 -800 electrodes at various scan rates in 1 M NaCl aqueous solution

The calculated specific capacitances (C) based on the integrated area of CV curves of the JFAC electrodes at different scan rates are presented in Fig. 24 (a-d). It is observed that the specific capacitance decreased with increase in scan rate. This can be explained as follows: at low scan rates, the ions get sufficient time to diffuse into pores of JFAC. This result in excessive ions' migration reaction, leading to higher capacitance at low scan rates, compared to high scan rates (Yasin *et al.*, 2018).

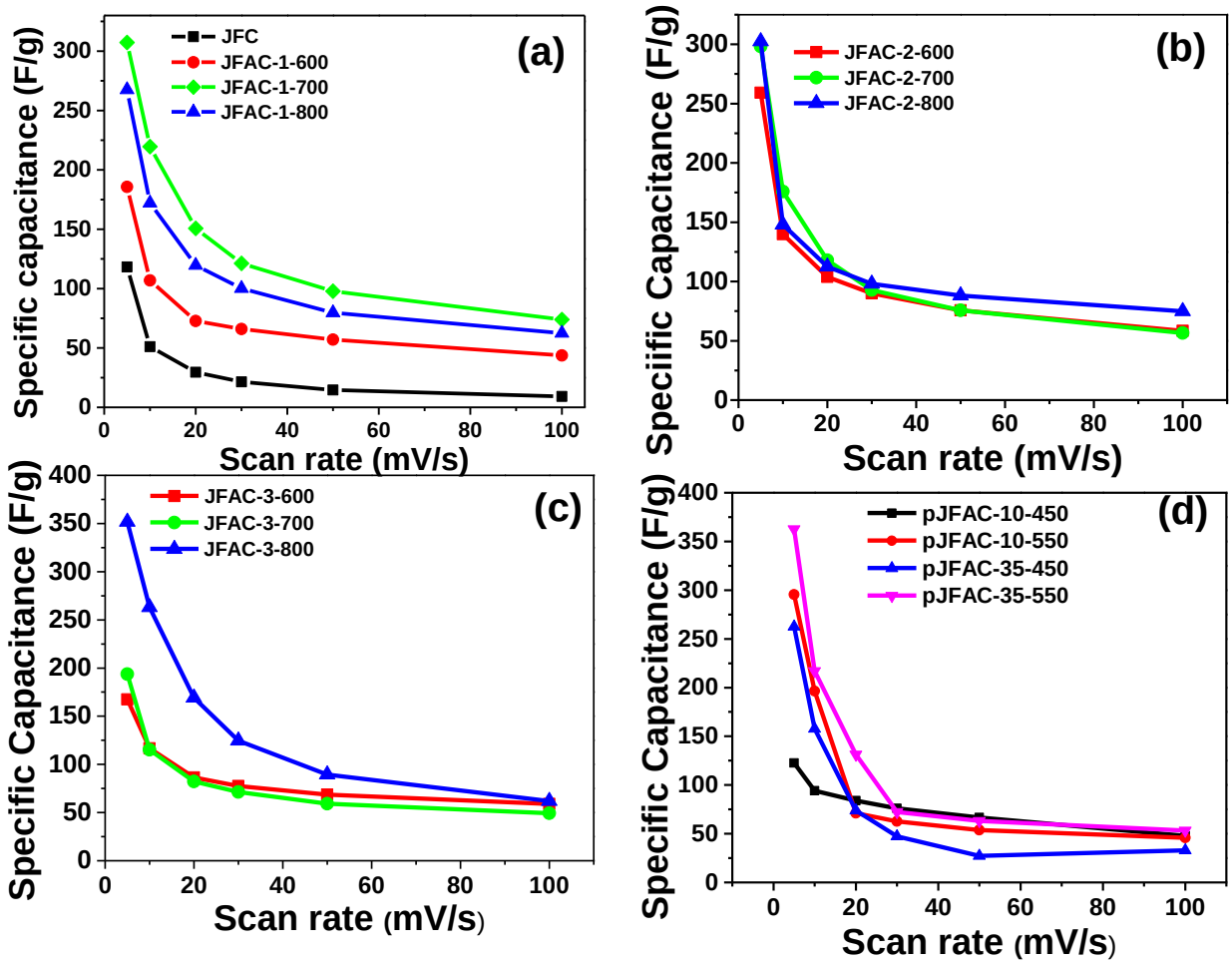

Figure 24: (a-d) Comparison of specific capacitance for the obtained ACJF electrodes in a 1 M NaCl aqueous solution at different scan rates

At a scan rate of 5 mV/s, pJFAC-35-550 exhibited largest specific capacitance of 362 F/g, followed by JFAC-3-800 (352 F/g), JFAC-1-700 (307 F/g), JFAC-2-800 (302 F/g), JFAC-2-700 (298 F/g) and JFC was the least with a specific capacitance of 118 F/g. The enhanced specific capacitance of pJFAC-35-550, JFAC-2-800, JFAC-1-700 and JFAC-3-800 is due to the richer porosity and the higher specific surface area (Fig. 25 (a-d)) developed by the activation temperature. With the increase in the activation temperature, the electrical resistance of JFAC is reduced and the charge transfer becomes easier, which can be proved by EIS measurement shown in Fig. 26. The enhanced Specific surface area provides more electro-active sites for the Faradaic reaction and increases the double layer charges. When the scan rate is increased to 50 mV/s, the specific capacitance decreases to around 15-90 F/g for all JFAC samples. These results indicate that most of JFAC electrodes have good capacitance and rate capability.

It is further observed that specific capacitance increased with increase in activation temperature except for JFAC-1-700, in which the specific capacitance increases as activation temperature increases to 700 ºC and decreases as temperature was further increased to 800 ºC (Fig. 25a), the explanation for this may be backed up with SEM image Fig. 14d, that as temperature increase to 800 ºC, the pores were destructed and probably, affect its capacitive performance. Theoretically, the specific capacitance of the carbon electrode increases with the increase in the surface area of carbon (Adinaveen *et al*., 2013). But this is not the case for our results; JFAC-2-800 exhibited the largest BET surface area (2681 m^2/g) but did not attain the largest specific capacitance as shown in Fig. 25b. Literature report that the large BET surface area does not always provide a large EDL capacitance because the carbon material may contain closed pores and dead-end pores, which contribute a large percentage to the surface area but are difficult for ions to access (Liu *et al*., 2019b). Furthermore, poor wettability of pure porous carbon materials may also cause difficulty for the materials to be well wetted by the solution thus, resulting into low specific capacitance. When compared with other carbon derived from biomass for CDI applications, JFAC electrode possesses enhanced EDL behavior and a higher specific capacitance compared to other materials as summarized in Table 6 in the literature review section. These results indicate that JFAC will not only be excellent CDI electrode material, but also a promising candidate as supercapacitor electrode materials.

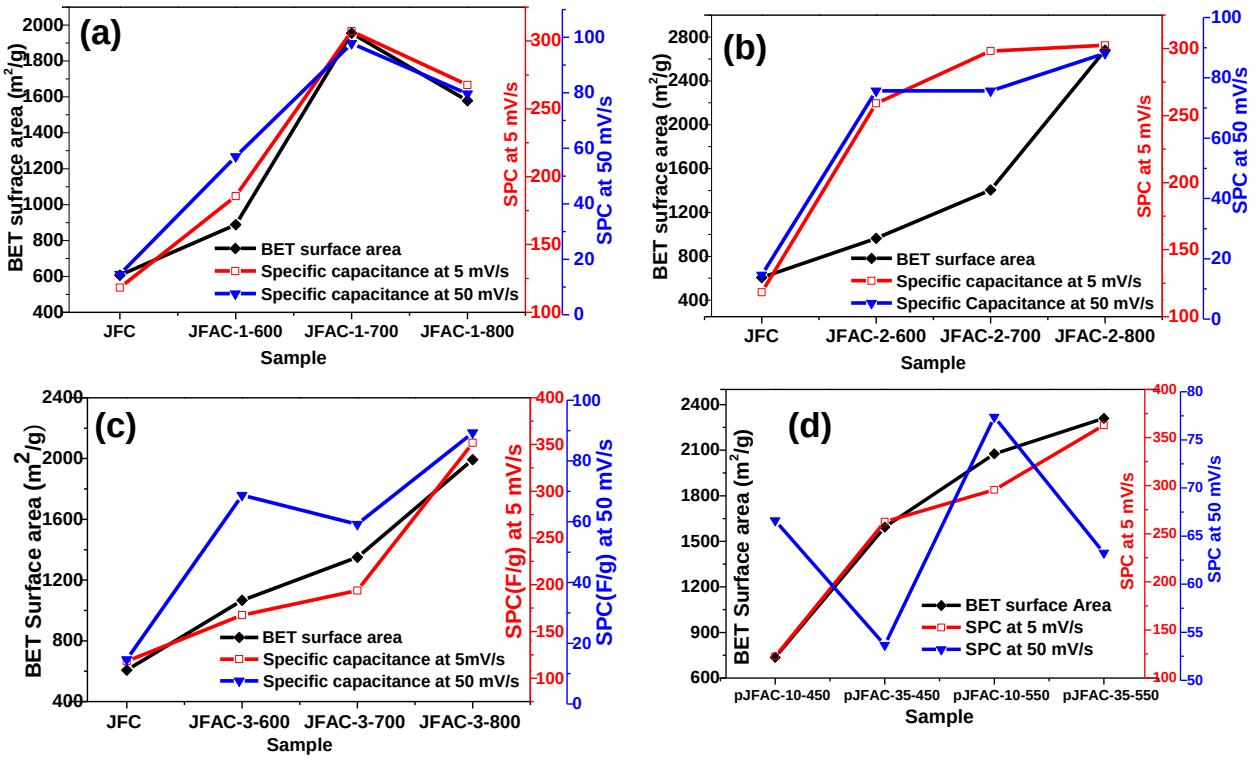

Figure 25: Relationship between BET surface area and specific capacitance of JFAC samples at 5 and 50 mV/s

The EIS analysis was carried out to further investigate the electrical conductivity of ACJF electrodes. The Nyquist plots for CJF and JFAC electrodes are presented in Fig. 26. The shape of the curves represents electrochemical supercapacitor with two main regions: the semi-circle region observed at high-frequencies and the non-vertical behavior at low frequency. The semi-circle at the high frequency range suggests that JFAC electrodes exhibit the resistive characteristic. The diameter of the semicircle corresponds to the charge-transfer resistance of the electrodes and the solution interface (Zornitta *et al.*, 2017). As seen from Fig. 26a, the diameter of the semicircle is small, which indicates the polarization resistance is low. For samples activated with KOH/C ratio of 2 and 3 (Fig. 26b and Fig. 26c), the semicircle at high frequency is observed to decrease as activation temperature increases from 600 to 800 ˚C indicating decreased charge transfer resistance. But with KOH/C ratio of 2, the semi-circle is much larger (Fig. 26b) compared to KOH/C ratio of 3 (Fig. 26c). JFAC-3-600, JFAC-3-700 and JFAC-3-800 show a smaller charge transfer resistance in comparison with JFAC-2-600, JFAC-2-700 and JFAC-2-800 due to an increased degree of graphitization consistent with Raman studies previously discussed. The non-vertical behavior at low frequency implies that JFAC electrodes possess non-ideal capacitive behavior.

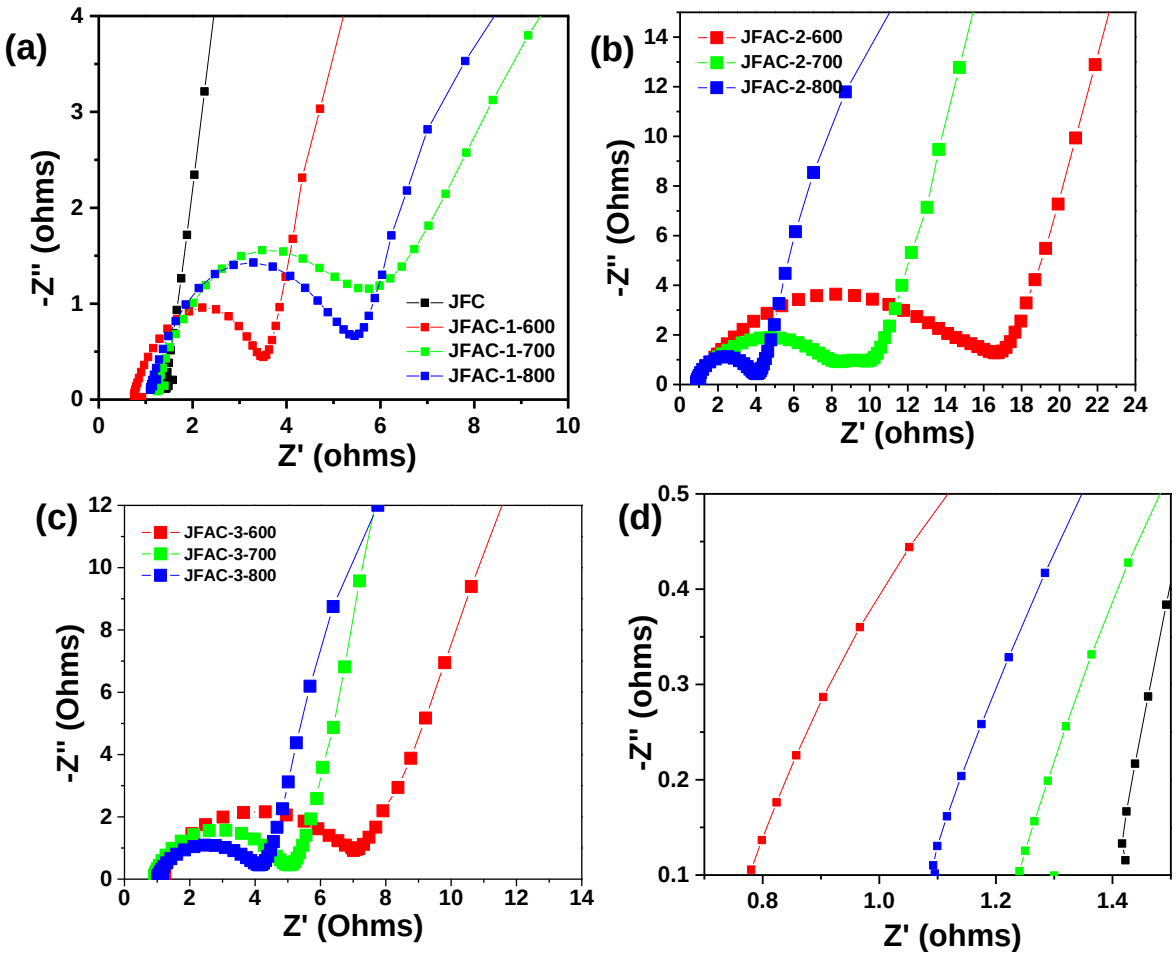

Figure 26: (a-c) Nyquist plots of JFAC activated at different KOH/C ratio and temperature (d) enlarged view of Fig. 18a in the high frequency range

Equivalent series resistances (ESR) of the electrodes are represented by the intersection of the curves at the real axis in the high frequency region. The ESR is a combination of the interfacial resistance between the electrode and the current collector, the electronic resistance of the electrode and the diffusion resistance of ions in the pores of electrode materials and the separator (Zhang *et al.*, 2012b). The smaller the ESR value, the smaller the internal resistance. From the Nyquist plots, it can be seen that the ESR values of all JFAC samples are less than 1.5 Ω. For example, the recorded ESR values as they appear in Fig. 26d are 1.42, 1.24, 1.09, and 0.78 Ω, for JFC, JFAC-1- 700, JFAC-1- 800 and JFAC-1- 600, respectively. These results show that there is a decrease in ESR value for JFAC carbons when compared to the ESR value of unactivated carbon (JFC). However, the decrease has no any specific trend with respect to increase in activation temperature. These values show that the produced carbon possesses small internal resistance and better electrical conductivity.

4.5 Desalination experiments

To investigate the CDI behavior, electrosorption experiment using CJF, JFAC-1-600, JFAC-1-700, JFAC-1-800, pJFAC-10-450, pJFAC-10-550, pJFAC-35-450 and pJFAC-35-450 electrodes were carried out with NaCl solution with a concentration of 30, 50, 100 and 500 mg/L with initial conductivity of 72.5, 102, 236 and 1085 µS/cm respectively. Different voltages of 1.2, 1.4 and 2.0 V were applied to the cell. Figure 27a illustrates the adsorption/desorption of JFAC-1-700 electrodes in 30 mg/L NaCl solution. As observed, the conductivity of NaCl solution decreases sharply during the electrosorption process suggesting that the salty ions were adsorbed by the electrodes. After 3 h of charging at 2 V, electrodes were discharged at 0 V whereby the adsorbed ions were released from the electrode surfaces back to the solution and the conductivity of the solution increased almost to its initial value.

Figure 27b shows the change in conductivity in NaCl solution with an initial concentration of 30 mg/L during batch-mode experiments using JFC, JFAC-1-600, JFAC-1-700 and JFAC-1-800 electrodes at 2 V. The JFC sample shows poor salt removal as no change in conductivity was observed. This is because JFC is having fewer pores and small surface area that would facilitate adsorption of ions as proved by SEM images and nitrogen desorption studies (Table 9). For JFAC-1-600 and JFAC-1-800 the conductivity decreased abruptly at the first 40 minutes to a constant value and increased slowly showing that the electrodes saturate easily.

Figure 27 c shows conductivity change of phosphoric acid activated samples with initial concentration of 500 mg/L at 1.2 V. It can be observed that conductivity drop abruptly during the first 3600 s for pJFAC-35-550 and the electrode saturates. For pJFAC-10-550 and pJFAC-10-450 conductivity first dropped and then starts to increase for the rest of the charging time. For pJFAC-35-450 conductivity also dropped slightly in the first 1800 s and then increased to a value greater than the initial conductivity of NaCl solution used. This increase related to the occurrence of a so-called “inversion effect” (i.e. a rise in effluent conductivity), resulting from ion desorption during charging as previously reported by Bouhadana *et al*. (2011).

Two factors have been reported which are responsible for inversion effect; i.e. changes in the electrodes and the distribution of the potential in the cell (Cohen *et al*., 2013). Changes in electrodes occurs when CDI cells comprising identical and symmetric pairs of AC electrodes lose their symmetry during charging and discharge cycles due to oxidation of the electrodes

their pore structures are destroyed. It is also reported that, the applied voltage is not divided equally to the cell, the positive electrodes gets more potential difference which accelerates their oxidation process, resulting into water oxidation and decrease in pH during charging step. To overcome the effect of positive electrode oxidation, it is recommended to apply low potential to cells. Nevertheless, applying low potential to the cell will result to a low electrosorption capacity. Therefore, pJFAC samples were not used for further electrosorption experiments. Figure 27d shows that when potentials of 1.2, 1.4 and 2 V were applied to the CDI cell with JFAC-1-700 electrodes, the conductivities were reduced to 207, 173 and 114 μS/cm respectively. The conductivity of solutions decreased significantly in the first 40 minutes, and reached equilibrium after about 90 minutes. The desalination performances of the JFAC-1-700 electrodes were further examined with 500 mg/L NaCl aqueous solution (~1085 μS/cm) at the applied voltage of 2 V as presented in Fig. 27e. The conductivity dropped from 1085 to 885 μS/cm in the first 90 minutes and then the electrode saturates.

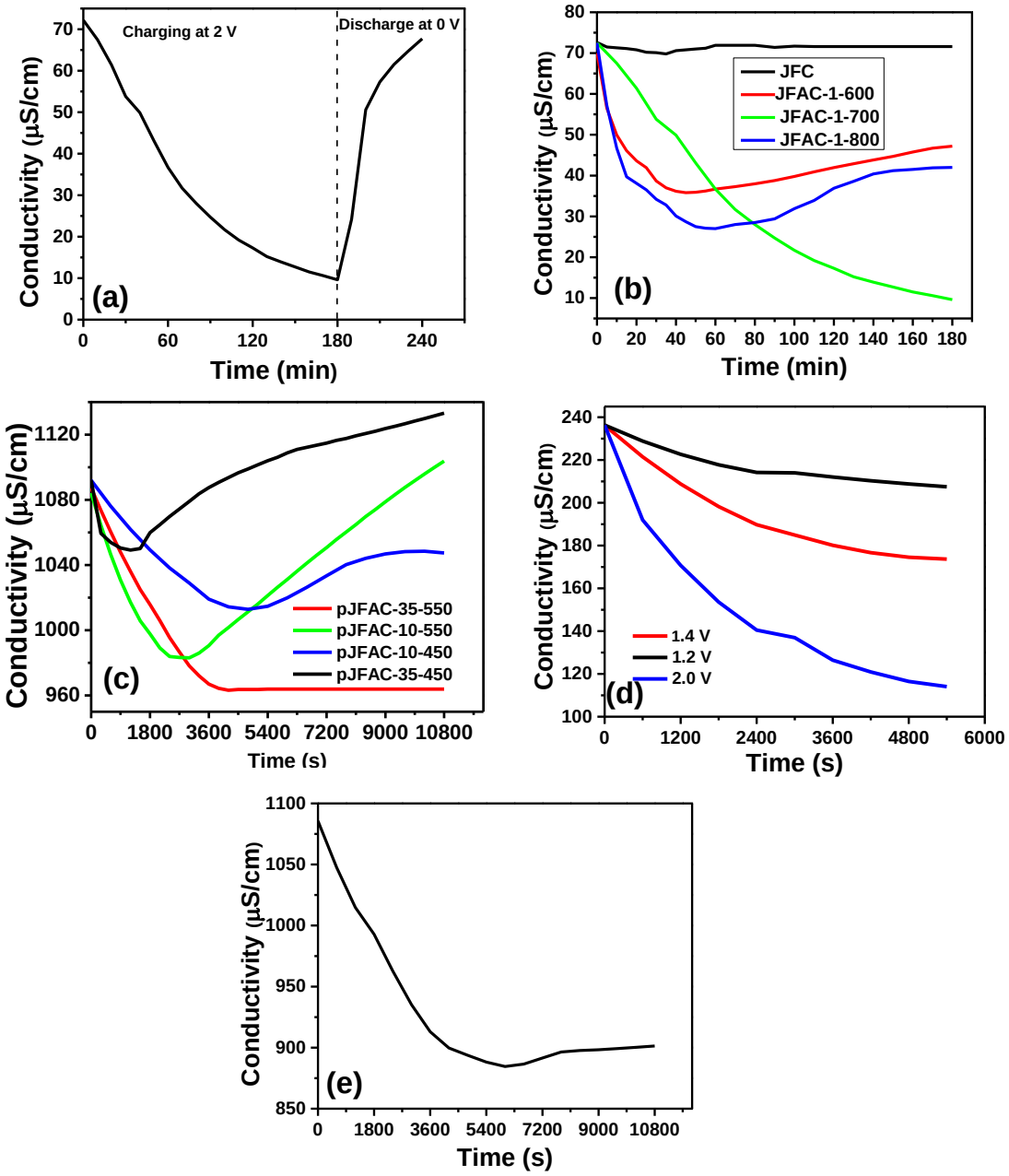

Figure 27: (a) Electrosorption/desorption profile of the JFAC-1-700 in 30 mg/L NaCl solution at 2 V (b) Electrosorption performance of JFC, JFAC-1-600, JFAC-1-700, JFAC-1-800 in 30 mg/L NaCl solution at 2 V(c) Electrosorption performance of pJFAC-10-450, pJFAC-10-550, pJFAC-35-450 and pJFAC-35-450 in 500 mg/L NaCl solution at 1.2 V (d) Electrosorptive performance of JFAC-1-700 in 100 mg/L NaCl at different applied potentials (e) Electrosorptive performance of JFAC-1-700 in 500 mg/L NaCl at 2 V

Figure 28 shows the CDI performance of JFAC electrodes with different concentration and applied voltage removal. With the initial concentration of 30 mg/L and 2 V (Fig. 28a and 28b), salt removal efficiency of the JFAC-1-600, JFAC-1-700 and JFAC-1-800 electrodes

were 56.2%, 95% and 67% and the electrosorption capacities were 0.78, 1.18 and 0.98 mg/g respectively. The order of electrosorption capacity is JFAC-1-700 > JFAC-1-800 > JFAC-1-600 > JFC. The salt removal efficiency and electrosorption capacity increased with activation temperature from 600 to 700ºC and then again dropped at 800ºC. JFAC-1-700 shows best salt removal efficiency of 95% and electrosorption capacity of 1.18 mg/g. The improved performance of JFAC-1-700 is attributed to its highest BET surface area and total pore volume as indicated in Fig. 28e together with its large specific capacitance and low internal resistance as indicated by electrochemical studies. This indicates that BET surface area and total pore volume are among the factors responsible for enhancing the deionization process in CDI.

The influence of initial concentration and applied voltage were studied on JFAC-1-700 electrodes. Results indicate that electrosorption capacities and removal efficiency were greatly influenced by the initial salt concentration and applied voltage as shown in Fig. 28c and 285d. Removal efficiency (RE) decreases with increase in salt concentration (Fig. 28d) while electrosorption capacity increases with the increase in salt concentration (Fig. 28c). As seen from Fig. 28c and Fig. 28d, when concentration increased from 50 to 500 mg/L at an applied voltage of 2 V, the electrosorption capacity increased from 1.35 to 5.74 mg/g whereas the RE decreased from 74 to 20% respectively. According to previous studies the electrosorption capacity increases as the concentration increases due to the reason that when concentration increases the solution resistance decreases resulting in increased concentration gradient and the EDL formation would be more easier (Lado *et al*., 2016; Zhao *et al*., 2017). In all cases when 2 V was applied, the removal efficiency and the electrosorption capacity were higher because of stronger Coulomb interaction introduced by the higher applied voltage. In addition, when the voltage of 2 V was applied there were no gas bubbles observed, indicating that water electrolysis was not taking place similar to what Li *et al*. (2010) observed.

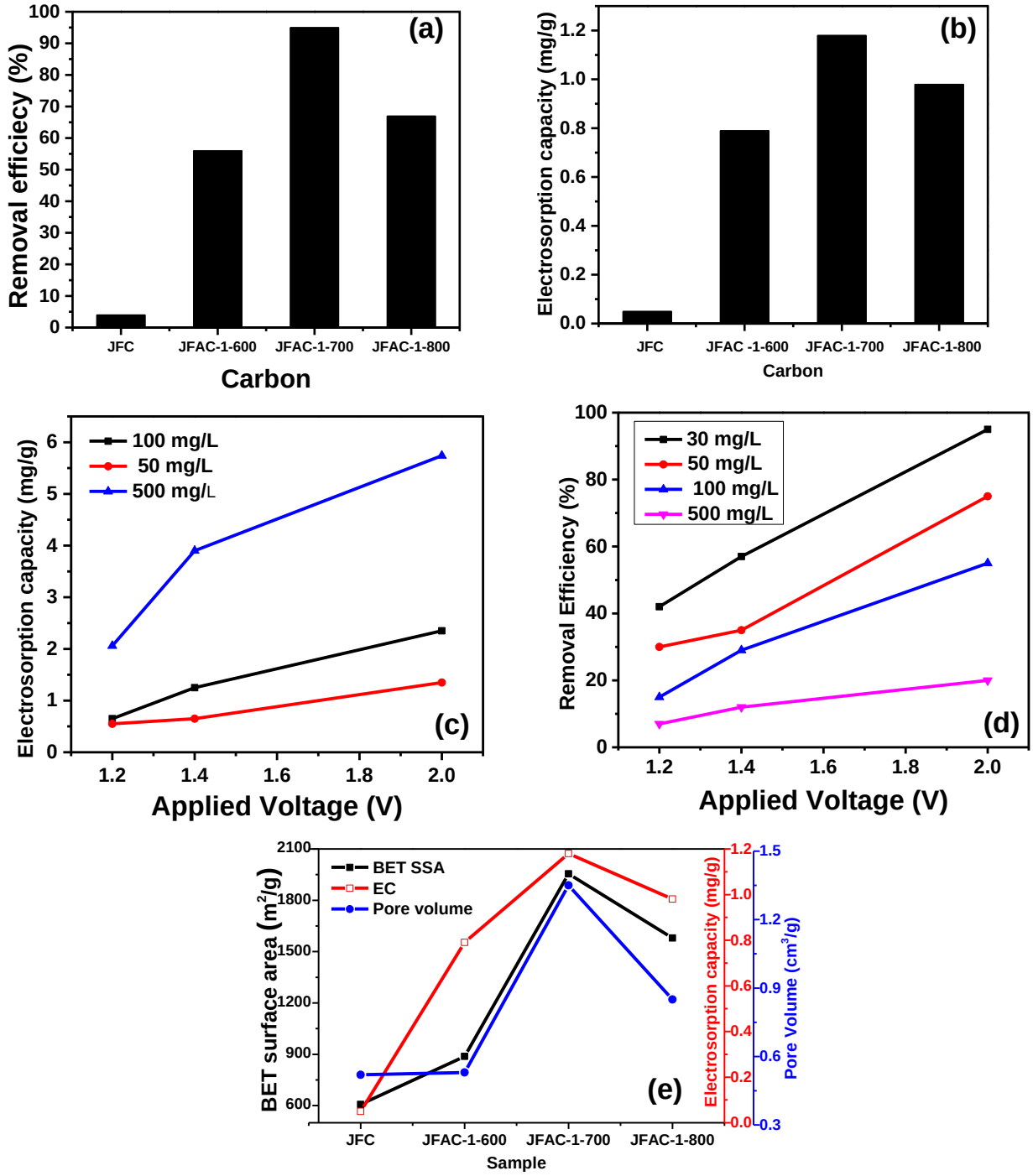

Figure 28: (a-b) Histogram showing removal efficiency and electrosorption capacity of JFAC samples in 30 mg/L (c-d) CDI performance of JFAC samples at different concentration and applied voltage (e) Comparison between BET surface area, total pore volume and electrosorption capacity of JFAC

It is reported that the pH of the effluent can change when faradaic reactions (oxidization and reduction) or water electrolysis is taking place at the electrodes (Choi, 2014; Lee & Choi, 2012). To verify if these reactions were taking place within the cell, pH of the effluent

solution was monitored when CDI was charged with 1.2 V and 2.0 V. Figure 29a shows that, when voltage of 1.2 V was applied, the pH increased from 6.5 to around 7.5 after the first 40 minutes and maintains at this value for the rest of the experimental time. However, when the charging potential was increased to 2 V, the pH changed from 6.5 to 7.5 after about 10 minutes before consistently decreasing to 6.5 (initial pH) and maintaining this initial value for 80 minutes. This little change in pH signifies that there was no electrode reaction (oxidation-reduction reaction) on the surface of the JFAC-1-700 electrode produced via KOH activation. For carbon produced through phosphoric acid activation, the pH of the solution change from the initial value of 6.5 to almost 3.5 (Fig. 29b) implying occurrence of Faradaic reactions and changes in surface properties of the positive electrode which lead into a decrease in electrode performance as previously reported by Cohen *et al*. (2013). Also, the observed pH changes may also be due to the reason that some of phosphoric acid remained in the sample which was then washed out during desalination experiments.

To investigate regeneration capacities of JFAC-1-700 electrodes, repeating charge-discharge experiment was carried out for 6 h at a constant cell potential of 2 V in 50 mg/L NaCl solution. Figure 29c shows the conductivity transient over 3 charge-discharge cycles. It was observed that the ions were released back to the solution after removing the voltage (discharge at 0 V) but the conductivity of the solution did not reach its initial value. Since the CDI process depends on electrostatic interactions, it is expected to be reversible; however, these results show that upon the removal of applied voltage some ions (25-35%) were not released back. Even though not all ions were releases back there was no significant decline in desalination performance observed after the first cycle indicating the potential of JFAC-1-700 electrodes to be re-used.

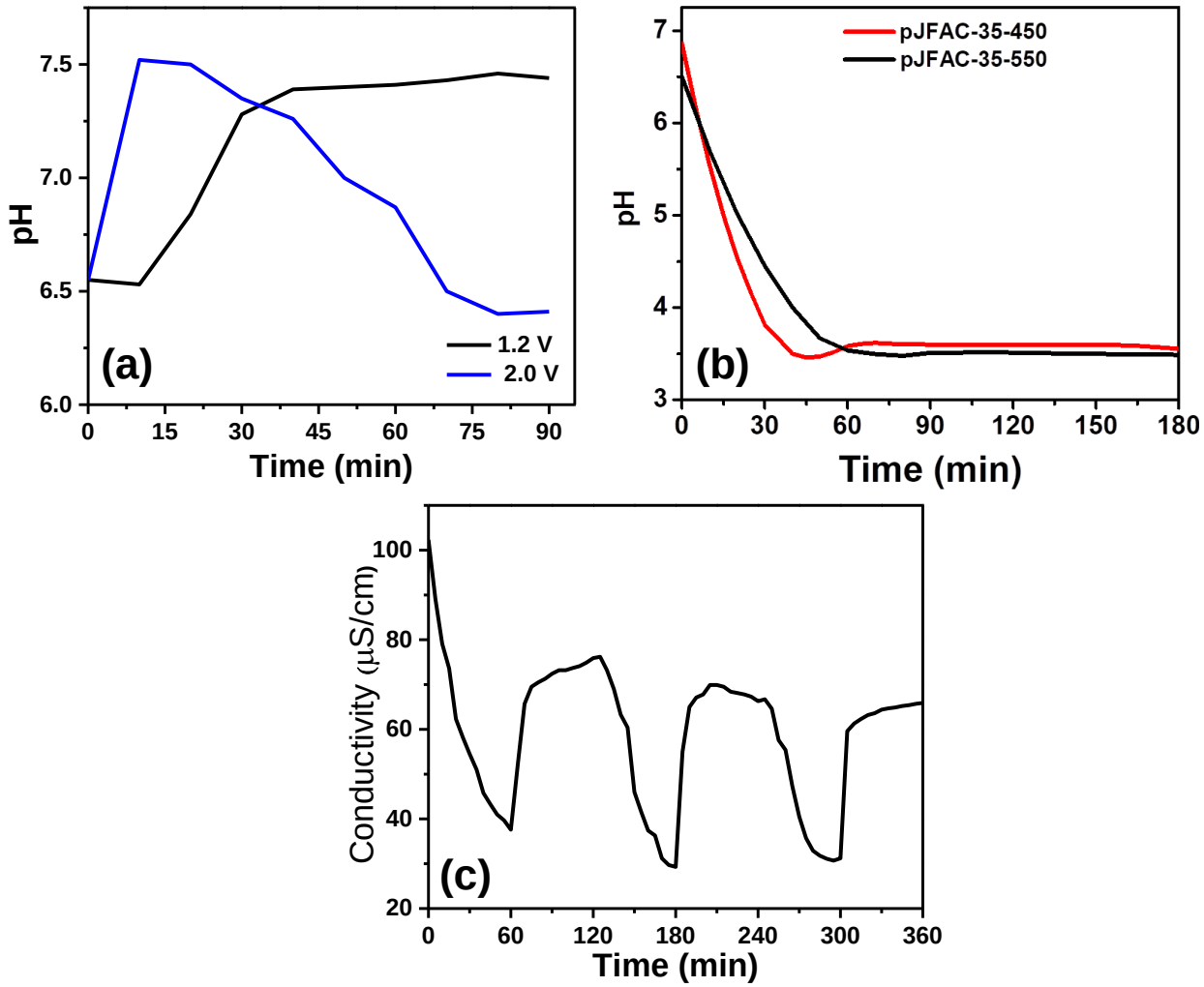

Figure 29: (a) Changes in effluent pH during the adsorption when (a) JFAC-1-700 electrodes was used and the potential of 1.2 V and 2 V was applied (b) pJFAC electrodes at 1.2 V (c) Conductivity and time profile of 50 mg/L NaCl solution measured in a CDI experiment with 2 h charge-discharge cycles at 2 V

The CDI performance of JFAC and other electrode materials derived from different biomass reported in the literature are summarized in Table 12. Quan *et al*. (2016) prepared electrode material from peanut shells and conduct desalination experiment with NaCl solution with an initial concentration of 20 mg/L. They reported electrosorption capacity of 1.96 mg/g and electrosorption efficiency of 97% when the potential of 1.2 V was applied. Similarly, Wang *et al*. (2013) tested electrodes prepared from commercial porous activated carbons originating from coconut shells and reported electrosorption capacity of 2.5-3.5 mg/g when the initial salt concentration of NaCl solution of 50 mg/L was used and potential of 1.6 V was applied to the CDI cell. Results of the present study are comparable to other carbon-based electrodes materials under almost similar operating conditions. It is evident that low cost biomass

materials can be used as a precursor for preparing activated carbon electrodes for CDI with improved electrosorption capacity. From Table 12 and Table 6 in the literature review it can be seen that factors including BET surface area, pore size, initial salt concentration, applied voltage and mass of the electrode contributes to the enhanced performance of the CDI electrodes. The higher the initial salt concentration the higher the electrosorption capacity, while the higher the mass of electrodes the lower the electrosorption capacity of the electrode material.

4.6 Charge efficiency and energy consumption

The charge efficiency and the energy consumption for desalinating different synthetic water (NaCl solution) with different concentrations in terms of kWh/m^3 water treated at the cell potential of 2 V was calculated using Eq. (6) and (7) and summarized in Table 11. It can be seen that charge efficiency increased when concentration increased from 30 to 100 mg/L and then dropped as concentration increase further to 500 mg/L. Energy consumption was observed to increase as the concentration of dissolved salt increase. The obtained charge efficiency is small compared to theoretical value of 100%, due to the presence of co-ions which repels each other from the electrodes and the weak adhesion between the electrode and current collector as previously reported by Xu *et al*. (2017).

Table 11: Charge efficiency and the energy consumption for desalinating synthetic water with different concentrations at 2 V

Concentration (mg/L)	Charge efficiency (%)	Energy (J)	Energy (kWh/m^3)
500	10.81	351.17	3.23E-03
100	19.37	52.70	4.88E-04
50	13.55	43.29	4.01E-04
30	7.72	66.40	6.15E-04

Table 12: The specific capacitance and electrosorption capacity of different carbon-based CDI electrode materials derived from biomass

Source of carbon	Scan rate (mV/s)	SCP (F/g)	C_i NaCl (mg/L)	Mass of Electrodes (g)	CDI mode	Voltage (V)	RE (%)	EC* (mg/g)	Reference
Pine pollen disruption powder	10	94.16	~25/250	0.16	Batch	2	92	7.25/19.43	(Liu *et al*., 2018b)
Watermelon peel	1	224	100 - 500	0.2	Batch	0.8-1.4	-	17.38	(Zhao *et al*., 2017)
Sugarcane bagasse	1-10	33-55	600		Batch	1.2		2.9-5.3	(Lado *et al*., 2016)
Peanut shells	10	44.9 - 83.2	20	0.8	Batch	1.2	97	0.22-1.96	(Quan *et al*., 2016)
Coconut shells	5–50	-	50	1.2	Batch	1.6		2.75 -3.75	(Wang *et al*., 2013)
	5	181.8	~30-500	0.1-0.4	Batch	1	-	9.72- 20.91	(Yeh *et al*., 2015)
Basswood blocks	1	87.1	100	0.7	Batch	1.2	-	5.7	(Liu *et al*., 2018a)
Loofa sponge	5	186	~500	-	Batch-(*MCDI)	1	40	22.5	(Feng *et al*., 2018)
Jackfruit peels	5-100	307-74	500	0.5	Batch	2	20	5.75	This study
			100	0.76		2	55	2.35	This study
			50	0.76		2	74	1.35	This study
			30	0.76		2	95	1.18	This study

4.7 Natural water defluoridation with CDI

4.7.1 Physicochemical properties of the water under study

The physicochemical properties of the collected water sample along with their WHO permissible limits of drinking water quality are summarized in Table 13. The collected water sample has conductivity, TDS and pH values of 762 µS cm^{-1} 498 mg/L and 7.4, respectively. Its F^- concentration is 3.11 mg/L which is above WHO drinking water permissible limit and total hardness of 112 mg/L (as $CaCO_3$) which are classified as moderately hard water. Water is considered to be soft if the concentration of calcium carbonate is below 60 mg/L, moderately hard if it is between 60–120 mg/L, hard if the concentration is between 120–180 mg/L and very hard if it is more than 180 mg/L (WHO, 2010). According to the WHO public drinking water standards magnesium, calcium, and chlorides level should not exceed the permissible limit of 50, 70 and 200 mg/L respectively. The concentration of hardness causing ions in our water sample is 78 mg/ L for Ca^{2+} which is above the WHO permissible limit and 16 mg/L for Mg^{2+}.

Table 13: The physicochemical properties of the water sample and the WHO permissible limits of drinking water quality

Parameter	Quantity	WHO permissible limit	Unit
pH	7.4	6.5-8.5	-
EC	762	-	uS/cm
TDS	498	-	mg/L
Total hardness as Ca-$CaCO_3$	112	500	mg/L
Calcium hardness	48	-	mg/L
Magnesium hardness	64	-	mg/L
Ca^{2+}	78	70	mg/l
Mg^{2+}	16	50	mg/L
F^-	3.11	1.5	mg/L

4.7.2 Conductivity change

When the potential was applied to the cell, ions in the water are adsorbed on the surface of JFAC electrodes and thus, conductivity drops correspondingly (Fig. 30) due to the lowered concentration of ions. When the voltage of 1.2 V was applied to JFAC electrodes (Fig. 30a)

the conductivity of water during the operation decreased sharply in the first 900 seconds and then slowly to 22, 11, 8, 6, and 3% of the initial value after 3 h. The same situation was observed when the potential of 2 V was applied to the JFAC electrodes (Fig. 30b), conductivity dropped abruptly for the first 900 seconds and then to 31 and 17% of the initial value when JFAC-3-700 and JFAC-3-600 electrodes were used respectively. For JFAC-3-800 electrode, conductivity dropped to 29% after 7200 seconds then rise slowly to a constant value. This indicates that the electrode saturates and cannot take more ions.

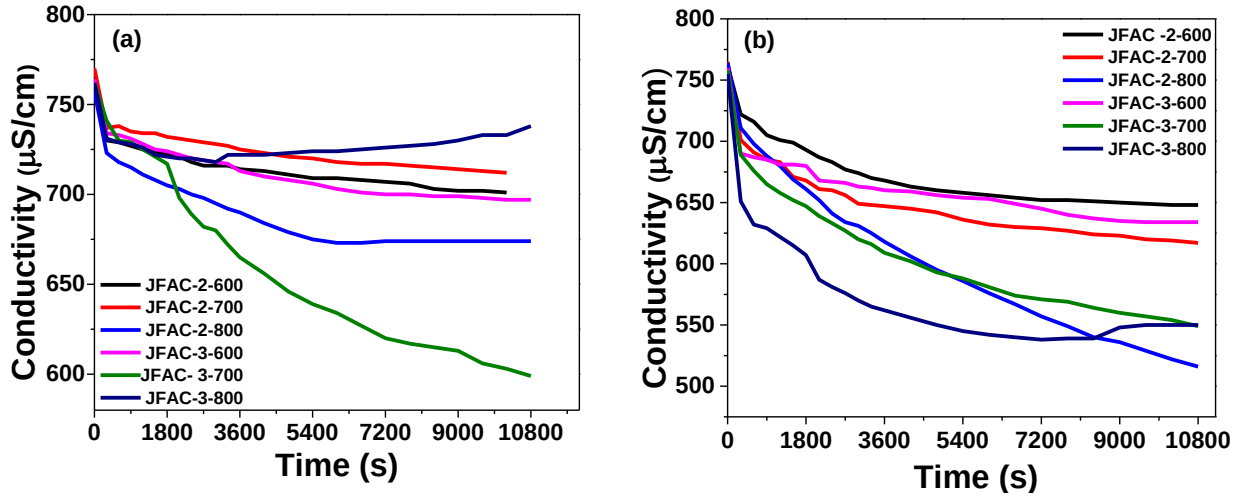

Figure 30: Conductivity change at an applied voltage of (a) 1.2 V (b) 2 V

4.7.3 Fluoride removal

The concentration of F^- after electrosorption experiment for all prepared electrodes is presented in Table 14. At 2.0 V JFAC-2-800, JFAC-3-700 and JFAC-3-800 reduce F^- concentration to 1.47, 1.18, 1.55 mg/L respectively. The values 1.47 and 1.18 mg/L are below the WHO permissible limit for drinking water quality of 1.5 mg/L. Thus, the CDI cell with JFAC biomass-based electrodes was used successfully for electrosorption of fluoride from tap water existing together with natural organic substances and other ions.

Table 14: The concentration of F^- after electrosorption experiment

Carbon		JFAC-2-600	JFAC-2-700	JFAC-2-800	JFAC-3-600	JFAC-3-700	JFAC-3-800
F^- (mg/L) at different applied Voltage	1.2 V	2.64	2.94	2.02	2.59	1.81	1.76
	2.0 V	2.28	1.7	1.47	1.91	1.18	1.55

Defluoridation efficiency of each electrode is presented in Fig. 31. It is observed that defluoridation efficiency increased with the increased applied potential. JFAC-3-700 shows the best defluoridation efficiency (62%) when the potential of 2 V was applied. One interesting thing is that JFAC-3-800 has highest capacitance as shown in Fig. 24c, but does not show the highest removal efficiency in the CDI test. This might be due to high charge transfer resistance and other intrinsic factors which may affect the performance of AC electrodes and limits its desalination performance as previously reported by Foo and Hameed (2009).

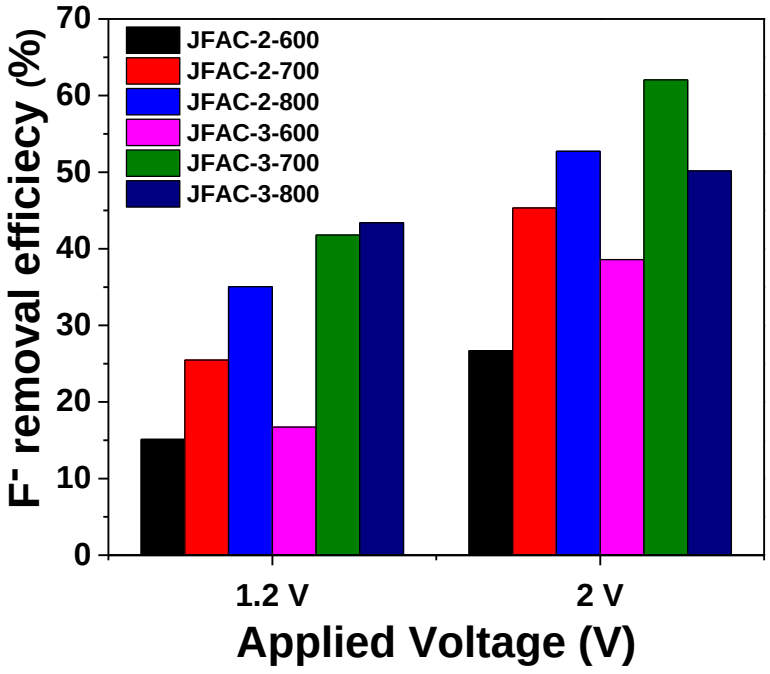

Figure 31: F^- removal efficiency by different JFAC electrodes at applied voltage of 1.2 V and 2 V

4.7.4 Removal of other co-existing ions in the water

Fluoride is not the only ion present in water under study; other charged ions, such as hardness causing cations ($Ca^{2+,}$ Mg^{2+}) were also present. Even though water hardness has an insignificant health impact, it can lead to scaling and cause failures in heat exchangers, pipelines of boilers and other electrical appliances as well as affecting the performance of cleaning detergents (Gabrielli *et al.*, 2006). Therefore, it is important to remove/minimize hardness causing ions from the water to the acceptable limits to avoid the aforementioned effects. In the charging step of the CDI process, these ions were adsorbed electrostatically by the oppositely charged JFAC electrodes and stored in EDLs on the electrode/solution

interface. That is why conductivity was decreasing as shown in Fig. 30 above. Figure 32(a-c) shows removal efficiency of total hardness (TH), Ca^{2+} and Mg^{2+} for each electrode type at different applied voltages. It can be seen that removal efficiency increases with increasing applied potential as presented in Fig. 32a. At 1.2 V JFAC-2-700, JFAC-2-800 and JFAC-3-700 has the same hardness removal efficiency. At 2 V the hardness removal efficiency increased for all electrodes whereby JFAC-3-700 outperforms others and hardness concentration reduction of 80% was reached. Removal efficiency for Mg^{2+} and Ca^{2+} also increased with applied voltage as shown in Fig. 32(c-d). The removal efficiency of different ions at 2 V for each JFAC electrode is shown in Fig. 32d. Mg^{2+} removal efficiency was higher than that of Ca^{2+} and F^{-} for JFAC-2-700 and JFAC-3-800.

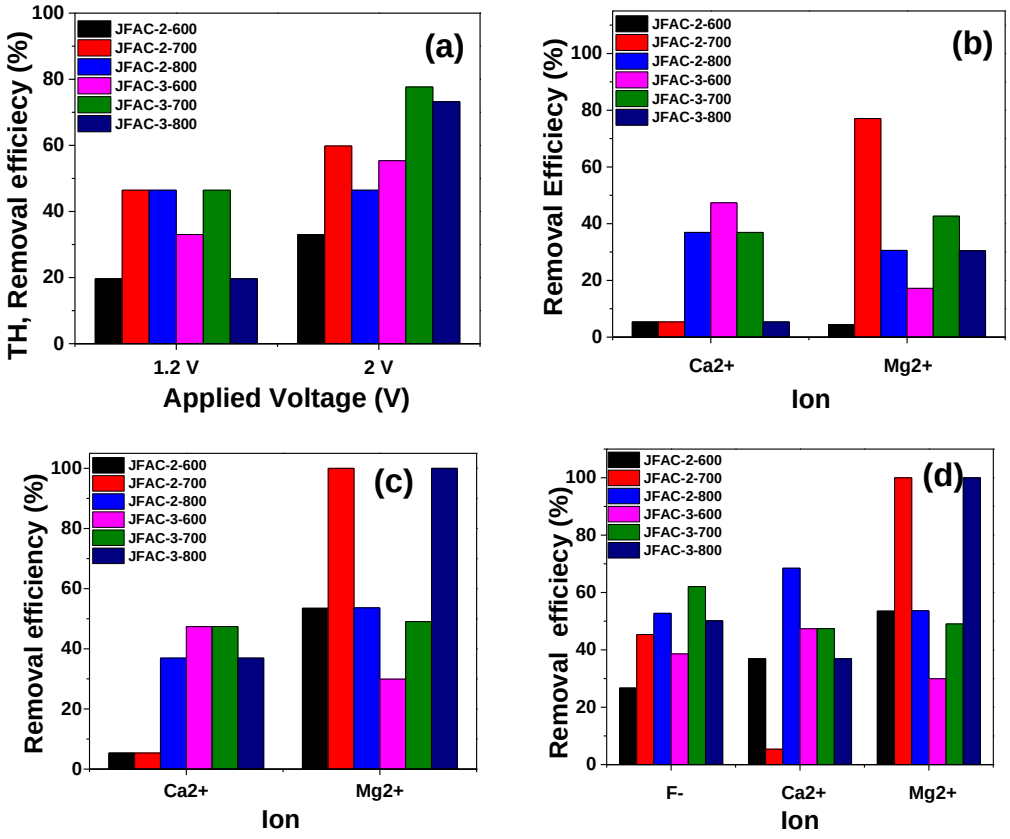

Figure 32: (a) Hardness removal efficiency of different JFAC electrodes (b) Removal efficiency for Ca^{2+} and Mg^{2+} at 1.2 V (c) Removal efficiency for Ca^{2+} and Mg^{2+} at 2 V (d) Removal efficiency for F^{-}, Ca^{2+} and Mg^{2+} ions at 2 V

The electrosorption processes in reverse osmosis and ion exchange technologies are well known. In these processes, ionic charge and molecular size dictate the salt removal in which the larger multivalent ions are preferably removed than the smaller ones (Gabelich *et al.*, 2002) however, in CDI it is not that much clear. Ion selectivity with CDI was firstly studied

by Gabelich *et al*. (2002) using carbon aerogel electrodes. Gabelich *et al*. (2002) generally concluded that in a competitive environment, ions with different valences the hydrated size of the ion in a solution controls the electrosorption preference. Smaller hydrated radii monovalent ions are removed more effectively than larger radii multivalent ions. Contrary, other studies revealed that ionic charge has a stronger effect on electrosorption ability than the hydrated ionic radius (Hou & Huang, 2013; Seo *et al*., 2010) in which multivalent ions are electrosorbed first resulting to a higher electrosorption capacity than monovalent ions due to their larger ionic size and greater charge. However, for ions with same initial concentrations and the charge, their hydrated radius dictates their selectivity and sometimes ions with higher feed concentration play a crucial role in ion electrosorption than the hydrated ionic radius (Xu *et al*., 2008; Ying *et al*., 2002). This is similar to what we observed in this study. The electrosorption capacity correlates well with the initial ion concentration in the feed water. Ion with higher hydrated radii i.e. Mg^{2+} (4.28 Å), was removed in large quantity compared to Ca^{2+} (4.12 Å) and F^{-} (3.52 Å) when JFAC electrodes were used. The electrosorption capacities of JFAC for different ions (shown in Table 15), nearly increased with increasing initial ion concentrations in the feed water except for JFAC-2-600, JFAC 2-700 and JFAC-3-800 in which EC of Ca^{2+} is small though its concentration is higher compared to that of Mg^{2+}. The CDI electrode JFAC-3-700 shows improved electrosorption capacity for Ca^{2+} (0.59 mg/g) due to its high concentration in the water sample followed by Mg^{2+} (0.50 mg/g) and F^{-} (0.13 mg/g). Hou and Huang (2013) previously reported that ions with higher concentrations in the water/solution had a higher driving force and can easily be transported from the solution to the pore structure leading to higher electrosorption capacity.

Table 15: Electrosorption capacities (EC) of JFAC for F^-, Ca^{2+} and Mg^{2+}

Sample/ Parameter	Ion	Initial conc. (mg/L)	JFAC-2-600	JFAC-2-700	JFAC-2-800	JFAC-3-600	JFAC-3-700	JFAC-3-800
BET SSA (m^2/g)			965	1405	2681	1067	1350	1993
Electrosoption capacity (mg/g) at 2.0 V	F^-	3.11	0.04	0.06	0.06	0.06	0.13	0.06
	Mg^{2+}	15.70	0.41	0.67	0.35	0.22	0.50	0.59
	Ca^{2+}	19.02	0.35	0.04	0.54	0.43	0.59	0.26

From Table 15, it can be seen that carbon sample with highest surface area (JFAC-2-800) did not achieve the highest EC for all ions. Sample JFAC-3-700 with BET SSA of 1350 m^2/g achieved the highest electrosorption capacity for F^- and Ca^{2+}. Therefore, we can say that not only high surface area required for efficient water defluoridation but also other material properties such as accessible pore size, the balanced structure between micropore and mesopore as previously reported by Seo *et al.* (2010). Furthermore, the CDI cell configuration and the mass of active materials used to make the electrodes, size, and thickness of electrodes could also probably be important parameters to consider for effective CDI performance. Since we utilize natural water without prior treatment, the presence of natural organic substances may be another factor which inhibits the JFAC surface and limits its effectiveness in water defluoridation and desalination.

4.7.5 pH changes

Figure 33 shows pH changes during defluoridation, the pH of the effluent during the electrosorption stage was observed to increase from 7.2 to 8.2 at all applied potentials. This range is within the WHO permissible limit for drinking water of 6.5-8.2. Considering that the pH of the effluent is retained within this range, it implies that no Faradaic reactions (e.g., redox reactions and water hydrolysis) were taking place when the voltage of 1.2 V (Fig. 33a) and 2 V (Fig. 33b) was applied to the JFAC electrodes. Thus, the fluoride and hardness removal in CDI generally occurs due to capacitive ion storage inside the pores and ion transport through the electrode material.

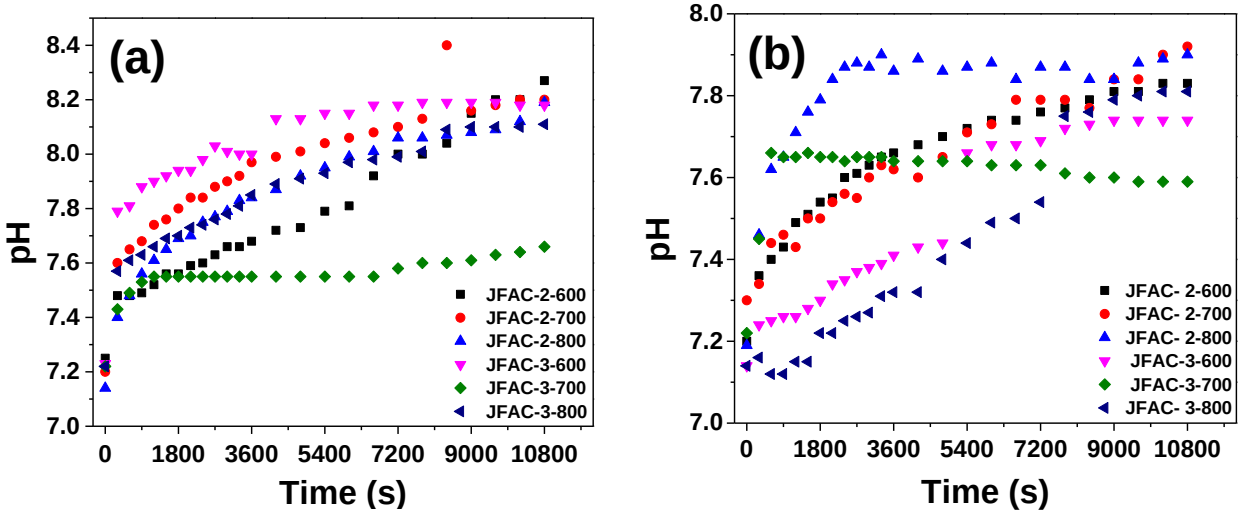

Figure 33: pH changes at an applied voltage of (a) 1.2 V (b) 2 V

CHAPTER FIVE

CONCLUSION AND RECOMMENDATIONS

5.1 Conclusion

In this work porous carbon has been successfully synthesized from abundant, low cost and environmentally friendly jackfruit peels precursor through chemical activation method and high activation temperature. The synthesis route, activation temperature and activating agent to carbon ratio had an important influence on the textural properties of porous carbon and the electrochemical properties of the electrodes. Nitrogen sorption studies prove that the synthesized JFAC composed of mainly mesopores. The formed JFAC acquired the honey comb like structure which is beneficial for ion adsorption. The JFAC electrodes synthesized exhibits good electrochemical performance. Samples prepared through phosphoric acid activation route (pJFAC) did not show promising desalination results due to occurrence of faradaic reactions which affect its desalination performance. Samples synthesized through KOH activation route have been shown to effectively remove NaCl from aqueous solutions with good electrosorption capacity and regeneration behavior. The mechanism of salt removal is generally due to electrostatic attraction of ions on the surface of the charged porous electrode because of EDL formation. The electrosorption capacity increased with increasing the applied potential and initial concentration of NaCl solution. From this work, it seems that the specific surface area is direct proportional to electrosorption capacity. Among KOH activated samples used for desalination, JFAC1-1-700 has the largest BET surface area and pore volume and exhibited the highest electrosorption capacity. Hence BET surface area and total pore volume are among the factors responsible for the deionization in the CDI process.

Furthermore, JFAC electrodes were studied in CDI for water defluoridation. It was found that JFAC based electrodes remove fluoride from natural water to standard required for drinking water as specified by the WHO. The presence of other ions in the water did not affect the defluoridation process, signifying that JFAC is good CDI electrode for fluoride removal. The JFAC electrodes showed a higher EC for magnesium absorption as compared to calcium due to its high concentration in the water. Generally, the ion removal efficiency of JFAC electrode depends not only on the surface area and pore volume but also on other factors including applied voltage and initial concentration of an ion in the water. The applied voltage enhances the electrosorption capacity of Mg^{2+}, Ca^{2+} and F^{-} and thus electrical double layer

adsorption dominate the electrosorption process since there was no significant change in pH observed during electrosorption stage. With a voltage of 2.0 V, the JFAC-3-700 electrode exhibits the highest electrosorption capacity for Ca^{2+}, Mg^{2+}, and F^{-}. Therefore, we can conclude that the carbon derived from jackfruit peels through KOH route can be considered as potential CDI electrode material for water desalination and defluoridation applications through CDI technology. Apart from being used as CDI electrode material, the synthesized JFAC may also be applied for energy storage in supercapacitor due to its high specific capacitance

5.2 Recommendations

This study evaluated performance of porous carbon derived from jackfruit peels as a cost effective electrode materials for CDI. Based on the findings of this study we recommend the following:

(i) Future work should explore the economic viability of producing porous carbon from jackfruit peels

(ii) Due to limited resources control system was not developed, therefore, future study should consider developing automated control system for the developed lab scale CDI cell

(iii) Wettability of the synthesized JFAC was not tested due to limitation of equipment; therefore future work should consider testing the wettability the electrodes using contact angle measurement system

(iv) Since electrode fabrication process was done manually, we recommend the process to be optimized by exploring the use of sophisticated equipment so that uniform electrodes can be obtained.

(v) More research on the electrode degradation when using natural water and regeneration is needed.

(vi) In this study, we studied effects applied voltage and initial concentration on CDI performance, we recommend future studies to investigate the impact of other parameters such as mode of operation, electrode thickness, mass of active electrode material and flow rate to obtain the optimal operating conditions for the present CDI cell.

(vii) Since the fabricated electrodes were used for removal of F^- from water which contain other co-ions, we recommend studies to functionalize the JFAC electrode materials for selective removal F^- ions.

(viii) Future work should consider developing a CDI cell prototype with JFAC electrodes for natural water desalination and defluoridation by increasing the dimensions of the cell.

REFERENCES

Abdul-Wahab, S. A., & Abdo, J. (2007). Optimization of multistage flash desalination process by using a two-level factorial design. *Applied Thermal Engineering, 27*(2-3), 413-421. https://doi.org/10.1016/j.applthermaleng.2006.07.010

Adinaveen, T., Kennedy, L. J., Vijaya, J. J., & Sekaran, G. (2013). Studies on structural, morphological, electrical and electrochemical properties of activated carbon prepared from sugarcane bagasse. *Journal of Industrial and Engineering Chemistry, 19*(5), 1470-1476. https://doi.org/10.1016/j.jiec.2013.01.010

Al-Karaghouli, A., & Kazmerski, L. L. (2013). Energy consumption and water production cost of conventional and renewable-energy-powered desalination processes. *Renewable and Sustainable Energy Reviews, 24*, 343-356.

Alkaisi, A., Mossad, R., & Sharifian-Barforoush, A. (2017). A Review of the Water Desalination Systems Integrated with Renewable Energy. *Energy Procedia, 110*, 268-274. https://doi.org/10.1016/j.egypro.2017.03.138

Anderson, M. A., Cudero, A. L., & Palma, J. (2010). Capacitive deionization as an electrochemical means of saving energy and delivering clean water. Comparison to present desalination practices: Will it compete? *Electrochimica Acta, 55*(12), 3845-3856. https://doi.org/10.1016/j.electacta.2010.02.012

Anton, Z., Marek, M., Slavomír, H., Michal, L., Zuzana, D., Milota, K., & Jaroslav, B. (2016). Preparation of chemically activated carbon from waste biomass by single-stage and two-stage pyrolysis. *Journal of Cleaner Production, 143*, 643-653. https://doi.org/10.1016/j.jclepro.2016.12.061

Bahar, R., Hawlader, M. N. A., & Woei, L. S. (2004). Performance evaluation of a mechanical vapor compression desalination system. *Desalination, 166*, 123-127. https://doi.org/10.1016/j.desal.2004.06.066

Barathi, M., Santhana Krishna Kumar, A., & Rajesh, N. (2013). Efficacy of novel Al–Zr impregnated cellulose adsorbent prepared using microwave irradiation for the facile defluoridation of water. *Journal of Environmental Chemical Engineering, 1*(4), 1325-1335. https://doi.org/10.1016/j.jece.2013.09.026

Biesheuvel, P. M., & Bazant, M. Z. (2010). Nonlinear dynamics of capacitive charging and desalination by porous electrodes. *Physical Review E: Statistical, Nonlinear, and Soft Matter Physics, 81*(3 Pt 1), 031502. http://www.ncbi.nlm.nih.gov/pubmed/20365735

Bouhadana, Y., Avraham, E., Noked, M., Ben-Tzion, M., Soffer, A., & Aurbach, D. (2011). Capacitive Deionization of NaCl Solutions at Non-Steady-State Conditions: Inversion Functionality of the Carbon Electrodes. *The Journal of Physical Chemistry C, 115*(33), 16567-16573. https://doi.org/10.1021/jp2047486

Brunson, L. R., & Sabatini, D. A. (2013). Practical considerations, column studies and natural organic material competition for fluoride removal with bone char and aluminum amended materials in the Main Ethiopian Rift Valley. *Science of the Total Environment, 488–489*, 580-587. https://doi.org/10.1016/j.scitotenv.2013.12.048

Cath, T., Childress, A., & Elimelech, M. (2006). Forward osmosis: Principles, applications, and recent developments. *Journal of Membrane Science, 281*(1-2), 70-87. https://doi.org/10.1016/j.memsci.2006.05.048

Chang, L. M., Duan, X. Y., & Liu, W. (2011). Preparation and electrosorption desalination performance of activated carbon electrode with titania. *Desalination, 270*(1-3), 285-290. https://doi.org/10.1016/j.desal.2011.01.008

Chao, L., Liu, Z., Zhang, G., Song, X., Lei, X., Noyong, M., Simon, U., Chang, Z., & Sun, X. (2015). Enhancement of capacitive deionization capacity of hierarchical porous carbon. *Journal of Materials Chemistry A, 3*(24), 12730-12737. https://doi.org/ 10.1039/c5ta01036e

Chen, W., Fan, Z., Gu, L., Bao, X., & Wang, C. (2010). Enhanced capacitance of manganese oxide via confinement inside carbon nanotubes. *Chemical Communications, 46*(22), 3905-3907.

Chen, Y., Zhu, Y., Wang, Z., Li, Y., Wang, L., Ding, L., Gao, X., Ma, Y., & Guo, Y. (2011). Application studies of activated carbon derived from rice husks produced by chemical-thermal process—A review. *Advances in Colloid and Interface Science, 163*(1), 39-52.

Chew, J. J., & Doshi, V. (2011). Recent advances in biomass pretreatment – Torrefaction fundamentals and technology. *Renewable and Sustainable Energy Reviews, 15*(8), 4212-4222. https://doi.org/10.1016/j.rser.2011.09.017

Choi, J. H. (2014). Determination of the electrode potential causing Faradaic reactions in membrane capacitive deionization. *Desalination, 347*, 224-229. https://doi.org/10.1016/j.desal.2014.06.004

Cohen, I., Avraham, E., Bouhadana, Y., Soffer, A., & Aurbach, D. (2013). Long term stability of capacitive de-ionization processes for water desalination: the challenge of positive electrodes corrosion. *Electrochimica Acta, 106*, 91-100.

Dehkhoda, A. M. (2016). *Development and Characterization of Activated Biochar as Electrode Material for Capacitive Deionization* [PhD Thessis, The University of British Columbia].

Dehkhoda, A. M., Ellis, N., & Gyenge, E. (2016). Effect of activated biochar porous structure on the capacitive deionization of NaCl and $ZnCl_2$ solutions. *Microporous and Mesoporous Materials, 224*, 217-228. https://doi.org/10.1016/j.micromeso.2015. 11. 041

Demirer, O. N., Naylor, R. M., Rios Perez, C. A., Wilkes, E., & Hidrovo, C. (2013). Energetic performance optimization of a capacitive deionization system operating with transient cycles and brackish water. *Desalination, 314*, 130-138. https://doi.org/10.1016/j.desal.2013.01.014

Deng, J., Xiong, T., Xu, F., Li, M., Han, C., Gong, Y., Wang, H., & Wang, Y. (2015a). Inspired by bread leavening: one-pot synthesis of hierarchically porous carbon for supercapacitors. *Green Chemistry, 17*(7), 4053-4060.

Deng, X., Zhao, B., Zhu, L., & Shao, Z. (2015b). Molten salt synthesis of nitrogen-doped carbon with hierarchical pore structures for use as high-performance electrodes in supercapacitors. *Carbon, 93*, 48-58. https://doi.org/10.1016/j.carbon.2015.05.031

Desale, G. R., Vasudevan, P., Pothal, J. K., Zala, K. S., Bhatti, B. A., Singh, S. N., & Sen, P. K. (2011). Purification of water using vertical multiple effect distillation unit. *Journal of Scientific and Industrial Research, 70*, 634-638. http://nopr.niscair.res.in /bitstream/123456789/12492/1/JSIR%2070(8)%20634-638.pdf

Eaton, A. D., Clesceri, L. S., Greenberg, A. E., & Franson, M. A. H. (2005). *Standard methods for the examination of water and wastewater* (21st ed., Vol. 21). American Public Health Association, American Water Works Association, Water Environment Federation.

El-Deen, A. G., Barakat, N. A., Khalil, K. A., & Kim, H. Y. (2014a). Hollow carbon nanofibers as an effective electrode for brackish water desalination using the capacitive deionization process. *New Journal of Chemistry, 38*(1), 198-205.

El-Deen, A. G., Boom, R. M., Kim, H. Y., Duan, H., Chan-Park, M. B., & Choi, J. H. (2016). Flexible 3D Nanoporous Graphene for Desalination and Bio-decontamination of Brackish Water via Asymmetric Capacitive Deionization. *ACS Applied Materials & Interfaces, 8*(38), 25313-25325. https://doi.org/10.1021/acsami.6b08658

El-Deen, A. G., Choi, J.-H., Khalil, K. A., Almajid, A. A., & Barakat, N. A. (2014b). A TiO_2 nanofiber/activated carbon composite as a novel effective electrode material for capacitive deionization of brackish water. *RSC Advances, 4*(110), 64634-64642.

Endarko, Fadilah, N., Anggoro, D., Rupiasih, N. N., Suharta, W. G., & Suyanto, H. (2016). Carbon electrode for desalination purpose in capacitive deionization. AIP Conference Proceedings,

Enock, T. K., King'ondu, C. K., Pogrbnoi, A., & Jande, Y. A. C. (2017a). Status of Biomass Derived Carbon Materials for Supercapacitor Application. *International Journal of Electrochemistry, 2017*, 1-14.

Enock, T. K., King'ondu, C. K., Pogrebnoi, A., & Jande, Y. A. C. (2017b). Biogas-slurry derived mesoporous carbon for supercapacitor applications. *Materials Today Energy, 5*, 126-137.

Ettouney, H. E.-D. H. (1999). Single-Effect Thermal Vapor-Compression Desalination Process: Thermal Analysis. *Heat Transfer Engineering, 20*(2), 52-68. https://doi.org/ 10.1080/014576399271583

Farmer, J. C., Fix, D. V., Mack, G. V., Pekala, R. W., & Poco, J. F. (1996). Capacitive deionization of NaCl and $NaNO_3$ solutions with carbon aerogel electrodes. *Journal of the Electrochemical Society, 143*(1), 159-169. https://doi.org/Doi 10.1149/1.1836402

Fechler, N., Fellinger, T. P., & Antonietti, M. (2013). "Salt templating": a simple and sustainable pathway toward highly porous functional carbons from ionic liquids. *Advanced Materials, 25*(1), 75-79. https://doi.org/10.1002/adma.201203422

Feng, C., Chen, Y. A., Yu, C. P., & Hou, C. H. (2018). Highly porous activated carbon with multi-channeled structure derived from loofa sponge as a capacitive electrode material for the deionization of brackish water. *Chemosphere, 208*, 285-293. https://doi.org/ 10.1016/j.chemosphere.2018.05.174

Ferrari, A. C., & Robertson, J. (2000). Interpretation of Raman spectra of disordered and amorphous carbon. *Physical Review B:, 61*(20), 14095-14107.

Fierro, V., Torné-Fernández, V., & Celzard, A. (2006). Kraft lignin as a precursor for microporous activated carbons prepared by impregnation with ortho-phosphoric acid: Synthesis and textural characterisation. *Microporous and Mesoporous Materials, 92*(1-3), 243-250. https://doi.org/10.1016/j.micromeso.2006.01.013

Foo, K. Y., & Hameed, B. H. (2009). A short review of activated carbon assisted electrosorption process: an overview, current stage and future prospects. *Journal of Hazardous Materials, 170*(2-3), 552-559. https://doi.org/ 10.1016/j.jhazmat.2009.05. 057

Foo, K. Y., & Hameed, B. H. (2012). Potential of jackfruit peel as precursor for activated carbon prepared by microwave induced NaOH activation. *Bioresource Technology, 112*, 143-150. https://doi.org/10.1016/j.biortech.2012.01.178

Frackowiak, E., & Beguin, F. O. (2001). Carbon materials for the electrochemical storage of energy in capacitors. *Carbon, 39*, 937–950.

Gabelich, C. J., Tran, T. D., & Suffet, I. H. M. (2002). Electrosorption of Inorganic Salts from Aqueous Solution Using Carbon Aerogels. *Environmental Science & Technology, 36*(13), 3010-3019. https://doi.org/10.1021/es0112745

Gabrielli, C., Maurin, G., Francy-Chausson, H., Thery, P., Tran, T. T. M., & Tlili, M. (2006). Electrochemical water softening: principle and application. *Desalination, 201*(1-3), 150-163. https://doi.org/10.1016/j.desal.2006.02.012

Gaikwad, M. S., & Balomajumder, C. (2016). Capacitive Deionization for Desalination Using Nanostructured Electrodes. *Analytical Letters, 49*(11), 1641-1655. https://doi.org/ 10.1080/00032719.2015.1118485

Gaikwad, M. S., & Balomajumder, C. (2017a). Simultaneous electrosorptive removal of chromium(VI) and fluoride ions by capacitive deionization (CDI): Multicomponent isotherm modeling and kinetic study. *Separation and Purification Technology, 186*, 272-281. https://doi.org/10.1016/j.seppur.2017.06.017

Gaikwad, M. S., & Balomajumder, C. (2017b). Tea waste biomass activated carbon electrode for simultaneous removal of Cr(VI) and fluoride by capacitive deionization. *Chemosphere, 184*, 1141-1149. https://doi.org/10.1016/j.chemosphere.2017.06.074

Gao, X., Landon, J., Neathery, J. K., & Liu, K. (2013). Modification of Carbon Xerogel Electrodes for More Efficient Asymmetric Capacitive Deionization. *Journal of the Electrochemical Society, 160*(9), E106-E112. https://doi.org/10.1149/2.111309jes

Gao, X., Omosebi, A., Holubowitch, N., Liu, A., Ruh, K., Landon, J., & Liu, K. (2016). Polymer-coated composite anodes for efficient and stable capacitive deionization. *Desalination, 399*, 16-20. https://doi.org/10.1016/j.desal.2016.08.006

Gao, X., Omosebi, A., Landon, J., & Liu, K. (2015). Surface charge enhanced carbon electrodes for stable and efficient capacitive deionization using inverted adsorption–desorption behavior. *Energy & Environmental Science, 8*(3), 897-909. https://doi.org/10.1039/c4ee03172e

Girgis, B. S., Temerk, Y. M., Gadelrab, M. M., & Abdullah, I. D. (2007). X-ray Diffraction Patterns of Activated Carbons Prepared under Various Conditions. *Carbon Science, 8* (2), 95-100.

Habuda-Stanic, M., Ravancic, M. E., & Flanagan, A. (2014). A Review on Adsorption of Fluoride from Aqueous Solution. *Materials 7*(9), 6317-6366. https://doi.org/10.3390 /ma7096317

He, D., Wong, C. E., Tang, W., Kovalsky, P., & Waite, T. D. (2016). Faradaic Reactions in Water Desalination by Batch-Mode Capacitive Deionization. *Environmental Science & Technology Letters, 3*(5), 222-226. https://doi.org/10.1021/acs.estlett.6b00124

Hou, C. H., & Huang, C. Y. (2013). A comparative study of electrosorption selectivity of ions by activated carbon electrodes in capacitive deionization. *Desalination, 314*, 124-129. https://doi.org/10.1016/j.desal.2012.12.029

Hou, C. H., Liu, N. L., & Hsi, H. C. (2015). Highly porous activated carbons from resource-recovered Leucaena leucocephala wood as capacitive deionization electrodes. *Chemosphere, 141*, 71-79. https://doi.org/10.1016/j.chemosphere.2015.06.055

Huang, P. H., Jhan, J. W., Cheng, Y. M., & Cheng, H. H. (2014). Effects of carbonization parameters of Moso-bamboo-based porous charcoal on capturing carbon dioxide. *The Scientific World Journal, 2014*, 937867. https://doi.org/10.1155/2014/937867

Huang, W. E. I., Zhang, Y., Bao, S., & Song, S. (2013). Desalination by Capacitive Deionization with Carbon-Based Materials as Electrode: A Review. *Surface Review and Letters, 20*(06), 1330003. https://doi.org/10.1142/s0218625x13300050

Hui, T. S., & Zaini, M. A. A. (2015). Potassium hydroxide activation of activated carbon: a commentary. *Carbon letters, 16*(4), 275-280.

Husain, B. (2017). *Water desalination: a review on major technologies*. Report from Technical University Munich.

Idropan-dell'Orto. (2015). *Idropan dell'Orto Depuratori S.r.l.* Retrieved Accessed on June 16, 2015 from www.idropan.com/en/

Im, J. S., Kim, J. G., & Lee, Y.-S. (2014). Effects of Pore Structure on the High-Performance Capacitive Deionization Using Chemically Activated Carbon Nanofibers. *Journal of Nanoscience and Nanotechnology, 14*(3), 2268–2273. https://doi.org/ 10.1166/jnn.2014.8474

Inbaraj, B. S., & Sulochana, N. (2004). Carbonised jackfruit peel as an adsorbent for the removal of Cd(II) from aqueous solution. *Bioresource Technology, 94*(1), 49-52. https://doi.org/10.1016/j.biortech.2003.11.018

Inbaraj, B. S., & Sulochana, N. (2006). Use of jackfruit peel carbon (JPC) for adsorption of rhodamine-B, a basic dye from aqueous solution. *Indian Journal of Chemical Technology, 13*, 17-23.

Jaehan Lee, Seoni Kim, Choonsoo Kim, & Yoon, J. (2014). Hybrid capacitive deionization to enhance the desalination performance of capacitive techniques. *Energy & Environmental Science*. https://doi.org/10.1039/C4EE02378A

Jain, A., Balasubramanian, R., & Srinivasan, M. P. (2016). Hydrothermal conversion of biomass waste to activated carbon with high porosity: A review. *Chemical Engineering Journal, 283*, 789-805. https://doi.org/10.1016/j.cej.2015.08.014

Jande, Y. A. C. (2015). *Modeling and Application of Capacitive Deionization in Desalination and CO_2 Capture* [PhD thesis, Hanyang University Graduate School].

Jande, Y. A. C., Asif, M., Shim, S. M., & Kim, W. S. (2014). Energy minimization in monoethanolamine-based CO_2 capture using capacitive deionization. *International Journal of Energy Research, 38*(12), 1531-1540. https://doi.org/10.1002/er.3168

Jande, Y. A. C., & Kim, W. S. (2013a). Desalination using capacitive deionization at constant current. *Desalination, 329*, 29-34. https://doi.org/10.1016/j.desal.2013.08.023

Jande, Y. A. C., & Kim, W. S. (2013b). Predicting the lowest effluent concentration in capacitive deionization. *Separation and Purification Technology, 115*, 224-230. https://doi.org/10.1016/j.seppur.2013.05.022

Jande, Y. A. C., & Kim, W. S. (2014). Modeling the capacitive deionization batch mode operation for desalination. *Journal of Industrial and Engineering Chemistry, 20*(5), 3356-3360. https://doi.org/10.1016/j.jiec.2013.12.020

Janssen, A. J. H., Schrader, G. A., & Verbeek, P. H. J. (2013). *Method and system for enhancing oil recovery (EOR) by injecting treated water into an oil bearing formation* (United States Patent No. WO/2013/098193)

Jia, B., & Zhang, W. (2016). Preparation and Application of Electrodes in Capacitive Deionization (CDI): a State-of-Art Review. *Nanoscale Research Letters, 11*(1), 64. https://doi.org/10.1186/s11671-016-1284-1

Jin, H. K. (2015). *Fabrication and characterization of nano carbonbased electrochemical double-layer capacitors* [PhD Thesis, University of Waterloo]. Ontario, Canada.

Johnson, A. M., & Newman, J. (1971). Desalting by Means of Porous Carbon Electrodes. *Journal of the Electrochemical Society, 118*(3), 510-517. http://jes.ecsdl.org/content/118/3/510.full.pdf+html

Jung, S. M., Choi, J. H., & Kim, J. H. (2012). Application of capacitive deionization (CDI) technology to insulin purification process. *Separation and Purification Technology, 98*, 31-35. https://doi.org/10.1016/j.seppur.2012.06.005

Karagiannis, I. C., & Soldatos, P. G. (2008). Water desalination cost literature: review and assessment. *Desalination, 223*(1-3), 448-456. https://doi.org/ 10.1016/j.desal.2007.02.071

Kaschemekat, J., Hilgendorff, W., Bőddeker, K., Hassan, A., & Malik, A. (1983). Two-stage reverse osmosis seawater desalination. *Desalination, 46*(1), 151-156.

Khairnar, M. R., Dodamani, A. S., Jadhav, H. C., Naik, R. G., & Deshmukh, M. A. (2015). Mitigation of fluorosis-a review. *Journal of Clinical and Diagnostic Research, 9*(6), 5-9.

Khan, Z. U., Yan, T., Shi, L., & Zhang, D. (2018). Improved capacitive deionization by using 3D intercalated graphene sheet–sphere nanocomposite architectures. *Environmental Science: Nano, 5*(4), 980-991. https://doi.org/10.1039/c7en01246b

Khayet, M. (2011). Membranes and theoretical modeling of membrane distillation: a review. *Advances in Colloid and Interface Science, 164*(1-2), 56-88. https://doi.org/10.1016/j.cis.2010.09.005

Kohli, D. K., Singh, R., Singh, M. K., Singh, A., Khardekar, R. K., Ram Sankar, P., Tiwari, P., & Gupta, P. K. (2012). Study of carbon aerogel-activated carbon composite electrodes for capacitive deionization application. *Desalination and Water Treatment, 49*(1-3), 130-135. https://doi.org/10.1080/19443994.2012.708210

Kong, W., Duan, X., Ge, Y., Liu, H., Hu, J., & Duan, X. (2016). Holey graphene hydrogel with in-plane pores for high-performance capacitive desalination. *Nano Research, 9*(8), 2458-2466. https://doi.org/10.1007/s12274-016-1132-8

Kumar, A., & Jena, H. M. (2016). Preparation and characterization of high surface area activated carbon from Fox nut (Euryale ferox) shell by chemical activation with H 3 PO 4. *Results in Physics, 6,* 651-658. https://doi.org/10.1016/j.rinp.2016.09.012

Lado, J. J., Zornitta, R. L., Calvi, F. A., Tejedor-Tejedor, M. I., Anderson, M. A., & Ruotolo, L. A. M. (2016). Study of sugar cane bagasse fly ash as electrode material for capacitive deionization. *Journal of Analytical and Applied Pyrolysis, 120,* 389-398. https://doi.org/10.1016/j.jaap.2016.06.009

Lee, J. G., & Kim, W.S. (2013). Numerical modeling of the vacuum membrane distillation process. *Desalination, 331,* 46-55. https://doi.org/10.1016/j.desal.2013.10.022

Lee, J. H., Bae, W. S., & Choi, J. H. (2010). Electrode reactions and adsorption/desorption performance related to the applied potential in a capacitive deionization process. *Desalination, 258*(1-3), 159-163. https://doi.org/10.1016/j.desal.2010.03.020

Lee, J. H., & Choi, J. H. (2012). The production of ultrapure water by membrane capacitive deionization (MCDI) technology. *Journal of Membrane Science, 409-410,* 251-256. https://doi.org/10.1016/j.memsci.2012.03.064

Leong, Z. Y., Lu, G., & Yang, H. Y. (2019). Three-dimensional graphene oxide and polyvinyl alcohol composites as structured activated carbons for capacitive desalination. *Desalination, 451,* 172-181. https://doi.org/10.1016/j.desal.2017.07.018

Leong, Z. Y., & Yang, H. Y. (2016). Porous carbon hollow spheres synthesized via a modified Stöber method for capacitive deionization. *RSC Advances, 6*(58), 53542-53549. https://doi.org/10.1039/c6ra06489b

Li, G. X., Hou, P. X., Zhao, S. Y., Liu, C., & Cheng, H. M. (2016). A flexible cotton-derived carbon sponge for high-performance capacitive deionization. *Carbon, 101*, 1-8. https://doi.org/http://dx.doi.org/10.1016/j.carbon.2015.12.095

Li, H., Liang, S., Li, J., & He, L. (2013). The capacitive deionization behaviour of a carbon nanotube and reduced graphene oxide composite. *Journal of Materials Chemistry A, 1*(21), 6335. https://doi.org/10.1039/c3ta10681k

Li, H., Lu, T., Pan, L., Zhang, Y., & Sun, Z. (2009). Electrosorption behavior of graphene in NaCl solutions. *Journal of Materials Chemistry, 19*(37), 6773. https://doi.org/ 10.1039/b907703k

Li, H., Pan, L., Lu, T., Zhan, Y., Nie, C., & Sun, Z. (2011). A comparative study on electrosorptive behavior of carbon nanotubes and graphene for capacitive deionization. *Journal of Electroanalytical Chemistry, 653*(1), 40-44.

Li, H., Zou, L., Pan, L., & Sun, Z. (2010). Novel graphene-like electrodes for capacitive deionization. *Environmental Science & Technology, 44*(22), 8692-8697.

Li, J., Wang, X., Wang, H., Wang, S., Hayat, T., Alsaedi, A., & Wang, X. (2017). Functionalization of biomass carbonaceous aerogels and their application as electrode materials for electro-enhanced recovery of metal ions. *Environmental Science: Nano, 4*(5), 1114-1123. https://doi.org/10.1039/c7en00019g

Li, Z., Song, B., Wu, Z., Lin, Z., Yao, Y., Moon, K. S., & Wong, C. P. (2015). 3D porous graphene with ultrahigh surface area for microscale capacitive deionization. *Nano Energy, 11*, 711-718. https://doi.org/10.1016/j.nanoen.2014.11.018

Liu, M., Chen, Y., Chen, K., Zhang, N., Zhao, X., Zhao, F., Dou, Z., He, X., & Wang, L. (2014). Biomass-derived activated carbon for rechargeable lithium-sulfur batteries. *BioResources, 10*(1), 155-168.

Liu, M., Xu, M., Xue, Y., Ni, W., Huo, S., Wu, L., Yang, Z., & Yan, Y. (2018a). Efficient Capacitive Deionization Using Natural Basswood Derived, Free Standing, Hierarchically Porous Carbon Electrodes. *ACS Applied Materials & Interfaces*. https://doi.org/10.1021/acsami.8b08232

Liu, N. L., Sun, S. H., & Hou, C. H. (2019a). Studying the electrosorption performance of activated carbon electrodes in batch-mode and single-pass capacitive deionization. *Separation and Purification Technology, 215*, 403-409. https://doi.org/10.1016/j.seppur.2019.01.029

Liu, P., Wang, H., Yan, T., Zhang, J., Shi, L., & Zhang, D. (2016). Grafting sulfonic and amine functional groups on 3D graphene for improved capacitive deionization. *Journal of Materials Chemistry A, 4*(14), 5303-5313. https://doi.org/10.1039/c5ta10680j

Liu, P., Yan, T., Shi, L., Park, H. S., Chen, X., Zhao, Z., & Zhang, D. (2017). Graphene-based materials for capacitive deionization. *Journal of Materials Chemistry A, 5*(27), 13907-13943. https://doi.org/10.1039/c7ta02653f

Liu, Q., Li, X., Wu, Y., Qing, M., Tan, G., & Xiao, D. (2018b). Pine pollen derived porous carbon with efficient capacitive deionization performance. *Electrochimica Acta, 298*, 360-371. https://doi.org/10.1016/j.electacta.2018.12.072

Liu, X., Liu, H., Mi, M., Kong, W., Ge, Y., & Hu, J. (2019b). Nitrogen-doped hierarchical porous carbon aerogel for high-performance capacitive deionization. *Separation and Purification Technology, 224*, 44-50. https://doi.org/10.1016/j.seppur.2019.05.010

Liu, Y., Chen, T., Lu, T., Sun, Z., Chua, D. H. C., & Pan, L. (2015a). Nitrogen-doped porous carbon spheres for highly efficient capacitive deionization. *Electrochimica Acta, 158*, 403-409. https://doi.org/10.1016/j.electacta.2015.01.179

Liu, Y., Nie, C., Liu, X., Xu, X., Sun, Z., & Pan, L. (2015b). Review on carbon-based composite materials for capacitive deionization. *RSC Advances, 5*(20), 15205-15225. https://doi.org/10.1039/c4ra14447c

Liu, Y., Xu, X., Wang, M., Lu, T., Sun, Z., & Pan, L. (2015c). Nitrogen-doped carbon nanorods with excellent capacitive deionization ability. *Journal of Materials Chemistry A, 3*(33), 17304-17311. https://doi.org/10.1039/c5ta03663a

Lixia, L., Linda, Z., Huaihe, S., & Gayle, M. (2009). Ordered mesoporous carbons synthesized by a modified sol–gel process for electrosorptive removal of sodium chloride. *Carbon, 47*(3), 775-781. https://doi.org/10.1016/j.carbon.2008.11.012

Lu, M., Liu, J. Y., Cheng, J., Wang, S.-P., & Yang, J.-M. (2014). Functionalized graphene/activated carbon composite electrodes for asymmetric capacitive deionization. *Acta Physico-Chimica Sinica*, *30*(12), 2263-2271.

Lu, Q., Lu, B., Chen, M., Wang, X., Xing, T., Liu, M., & Wang, X. (2018). Porous activated carbon derived from Chinese-chive for high energy hybrid lithium-ion capacitor. *Journal of Power Sources*, *398*, 128-136. https://doi.org/10.1016/j.jpowsour.2018.07.062

Mahendra S. Gaikwad, & Balomajumder, C. (2016). Current Progress of Capacitive Deionization for Removal of Pollutant Ions. *Electrochemical Energy Technology*, *2*, 17–23. https://doi.org/10.1515/eetech-2016-0004

Manocha, S., Manocha, L. M., Joshi, P., Patel, B., Dangi, G., & Verma, N. (2013). Activated carbon from biomass. AIP Conference

Marsh, H., & Reinoso, F. R. (2006). *Activated carbon*. Elsevier.

Matsubara, E. Y., Lala, S. M., & Rosolen, J. M. (2010). Lithium storage into carbonaceous materials obtained from sugarcane bagasse. *Journal of the Brazilian Chemical Society*, *21*(10), 1877-1884.

Mei, B. A., Munteshari, O., Lau, J., Dunn, B., & Pilon, L. (2017). Physical Interpretations of Nyquist Plots for EDLC Electrodes and Devices. *The Journal of Physical Chemistry C*, *122*(1), 194-206. https://doi.org/10.1021/acs.jpcc.7b10582

Mohamad Nor, N., Lau, L. C., Lee, K. T., & Mohamed, A. R. (2013). Synthesis of activated carbon from lignocellulosic biomass and its applications in air pollution control: a review. *Journal of Environmental Chemical Engineering*, *1*(4), 658-666. https://doi.org/10.1016/j.jece.2013.09.017

Mohanty, K., Jha, M., Meikap, B., & Biswas, M. (2005). Preparation and characterization of activated carbons from Terminalia arjuna nut with zinc chloride activation for the removal of phenol from wastewater. *Industrial & Engineering Chemistry Research*, *44*(11), 4128-4138.

Mohapatra, M., Anand, S., Mishra, B. K., Giles, D. E., & Singh, P. (2009). Review of fluoride removal from drinking water. *Journal of Environmental Management, 91*(1), 67-77.

Mohd Nor, N. S., Deraman, M., Omar, R., Awitdrus, Farma, R., Basri, N. H., Mohd Dolah, B. N., Mamat, N. F., Yatim, B., & Md Daud, M. N. (2015). Influence of gamma irradiation exposure on the performance of supercapacitor electrodes made from oil palm empty fruit bunches. *Energy, 79*, 183-194. https://doi.org/10.1016/j.energy.2014.11.002

Moon, A. S., & Lee, M. (2012). Energy consumption in forward osmosis-desalination compared to other desalination techniques. *World Academy of Science, Engineering and Technology, 65*, 537-539.

Nabais, J. M., Teixeira, J. G., & Almeida, I. (2011). Development of easy made low cost bindless monolithic electrodes from biomass with controlled properties to be used as electrochemical capacitors. *Bioresource Technology, 102*(3), 2781-2787. https://doi.org/10.1016/j.biortech.2010.11.083

Ng, K. C., Thu, K., Oh, S. J., Ang, L., Shahzad, M. W., & Ismail, A. B. (2015). Recent developments in thermally-driven seawater desalination: Energy efficiency improvement by hybridization of the MED and AD cycles. *Desalination, 356*, 255-270.

Nkuna, S. (2017). *Development of capacitive deionisation electrodes: optimization of fabrication methods and composition* [Degree of Magister Scientiae Thesis, University of Western Cape].

Noked, M., Avraham, E., Soffer, A., & Aurbach, D. (2009). The rate-determining step of electroadsorption processes into nanoporous carbon electrodes related to water desalination. *The Journal of Physical Chemistry C, 113*(51), 21319-21327.

Omosebi, A., Gao, X., Landon, J., & Liu, K. (2014). Asymmetric electrode configuration for enhanced membrane capacitive deionization. *ACS Applied Materials & Interfaces, 6*(15), 12640-12649. https://doi.org/10.1021/am5026209

Otowa, T., Tanibata, R., & Itoh, M. (1993). Production and adsorption characteristics of MAXSORB: high-surface-area active carbon. *Gas Separation & Purification, 7*(4), 241-245.

Paz-Garcia, J. M., Dykstra, J. E., Biesheuvel, P. M., & Hamelers, H. V. (2015). Energy from CO_2 using capacitive electrodes - a model for energy extraction cycles. *Journal of Colloid and Interface Science, 442*, 103-109. https://doi.org/10.1016/j.jcis.2014.11.045

Paz-Garcia, J. M., Schaetzle, O., Biesheuvel, P. M., & Hamelers, H. V. M. (2014). Energy from CO_2 using capacitive electrodes – Theoretical outline and calculation of open circuit voltage. *Journal of Colloid and Interface Science, 418*, 200-207. https://doi.org/http://dx.doi.org/10.1016/j.jcis.2013.11.081

Porada, S., Borchardt, L., Oschatz, M., Bryjak, M., Atchison, J., Keesman, K., Kaskel, S., Biesheuvel, P., & Presser, V. (2013a). Direct prediction of the desalination performance of porous carbon electrodes for capacitive deionization. *Energy & Environmental Science, 6*(12), 3700-3712.

Porada, S., Sales, B. B., Hamelers, H. V., & Biesheuvel, P. M. (2012a). Water Desalination with Wires. *J Phys Chem Lett, 3*(12), 1613-1618. https://doi.org/10.1021/jz3005514

Porada, S., Schipper, F., Aslan, M., Antonietti, M., Presser, V., & Fellinger, T. P. (2015). Capacitive Deionization using Biomass-based Microporous Salt-Templated Heteroatom-Doped Carbons. *ChemSusChem, 8*(11), 1867-1874.

Porada, S., Shrivastava, A., Bukowska, P., Biesheuvel, P. M., & Smith, K. C. (2017). Nickel Hexacyanoferrate Electrodes for Continuous Cation Intercalation Desalination of Brackish Water. *Electrochimica Acta, 255*, 369-378. https://doi.org/10.1016/j.electacta.2017.09.137

Porada, S., Weinstein, L., Dash, R., van der Wal, A., Bryjak, M., Gogotsi, Y., & Biesheuvel, P. M. (2012b). Water desalination using capacitive deionization with microporous carbon electrodes. *ACS Applied Materials & Interfaces, 4*(3), 1194-1199. https://doi.org/10.1021/am201683j

Porada, S., Zhao, R., van der Wal, A., Presser, V., & Biesheuvel, P. M. (2013b). Review on the science and technology of water desalination by capacitive deionization. *Progress in Materials Science, 58*(8), 1388-1442. https://doi.org/10.1016/j.pmatsci.2013.03.005

Prabaharan, S. R. S., Vimala, R., & Zainal, Z. (2006). Nanostructured mesoporous carbon as electrodes for supercapacitors. *Journal of Power Sources, 161*(1), 730-736. https://doi.org/10.1016/j.jpowsour.2006.03.074

Prahas, D., Kartika, Y., Indraswati, N., & Ismadji, S. (2008). Activated carbon from jackfruit peel waste by H3PO4 chemical activation: Pore structure and surface chemistry characterization. *Chemical Engineering Journal, 140*(1-3), 32-42. https://doi.org/ 10.1016/j.cej.2007.08.032

Qian, M., Xuan, X. Y., Pan, L. K., & Gong, S. Q. (2019). Porous carbon electrodes from activated wasted coffee grounds for capacitive deionization. *Ionics, 25*(7), 3443–3452.

Quan, G., Chu, L., Han, X., Ding, C., Chen, T., & Yan, J. (2016). Facile synthesis of novel hierarchically porous carbon derived from nature biomass for enhanced removal of NaCl. *Water Science and Technology, 74*(8), 1821-1831.

Quan,G., Wang,H.,. Zhu F., & Yan, J. (2018). Porous Biomass Carbon Coated with SiO_2 as High Performance Electrodes for Capacitive Deionization. *BioResources, 13*(1), 437-449.

Quan, X., Fu, Z., Yuan, L., Zhong, M., Mi, R., Yang, X., Yi, Y., & Wang, C. (2017). Capacitive deionization of NaCl solutions with ambient pressure dried carbon aerogel microsphere electrodes. *RSC Advances, 7*(57), 35875-35882.

Quist-Jensen, C. A., Macedonio, F., & Drioli, E. (2015). Membrane technology for water production in agriculture: Desalination and wastewater reuse. *Desalination, 364*(0), 17-32. https://doi.org/http://dx.doi.org/10.1016/j.desal.2015.03.001

Rijsberman, F. R. (2006). Water scarcity: Fact or fiction? *Agricultural Water Management, 80*(1-3), 5-22. https://doi.org/10.1016/j.agwat.2005.07.001

Rosas, J. M., Bedia, J., Rodríguez-Mirasol, J., & Cordero, T. (2010). On the preparation and characterization of chars and activated carbons from orange skin. *Fuel Processing Technology, 91*(10), 1345-1354. https://doi.org/10.1016/j.fuproc.2010.05.006

Rosli, N. A., Zawawi, M. H., Bustami, R. A., Hipni, F., & Kamruddin, M. A. (2015). Adsorption of Lead Using Jackfruit Peel Activated Carbon. *Applied Mechanics and Materials, 773-774,* 1079-1084. https://doi.org/10.4028/www.scientific.net/AMM.773-774.1079

Saleem, M. W., & Kim, W. S. (2018). Parameter-based performance evaluation and optimization of a capacitive deionization desalination process. *Desalination, 437,* 133-143. https://doi.org/10.1016/j.desal.2018.02.023

Selvaraju, G., & Bakar, N. K. A. (2017). Production of a new industrially viable green-activated carbon from Artocarpus integer fruit processing waste and evaluation of its chemical, morphological and adsorption properties. *Journal of Cleaner Production, 141,* 989-999. https://doi.org/10.1016/j.jclepro.2016.09.056

Seo, S. J., Jeon, H., Lee, J. K., Kim, G. Y., Park, D., Nojima, H., Lee, J., & Moon, S. H. (2010). Investigation on removal of hardness ions by capacitive deionization (CDI) for water softening applications. *Water Research, 44*(7), 2267-2275. https://doi.org/10.1016/j.watres.2009.10.020

Shatat, M., & Riffat, S. B. (2012). Water desalination technologies utilizing conventional and renewable energy sources. *International Journal of Low-Carbon Technologies, 9*(1), 1-19. https://doi.org/10.1093/ijlct/cts025

Shi, W., Ye, C., Xu, X., Liu, X., Ding, M., Liu, W., Cao, X., Shen, J., Yang, H. Y., & Gao, C. (2018). High-Performance Membrane Capacitive Deionization Based on Metal−Organic Framework-Derived Hierarchical Carbon Structures. *ACS Omega, 3*(8), 8506-8513. https://doi.org/10.1021/acsomega.8b01356

Singh, K., Porada, S., de Gier, H. D., Biesheuvel, P. M., & de Smet, L. C. P. M. (2019). Timeline on the application of intercalation materials in Capacitive Deionization. *Desalination, 455*, 115-134. https://doi.org/10.1016/j.desal.2018.12.015

Song, N., Gao, X., Ma, Z., Wang, X., Wei, Y., & Gao, C. (2018). A review of graphene-based separation membrane: Materials, characteristics, preparation and applications. *Desalination, 437*, 59-72. https://doi.org/10.1016/j.desal.2018.02.024

Souhaimi, M. K., & Matsuura, T. (2011). *Membrane distillation: principles and applications*. Elsevier.

Srimuk, P., Kaasik, F., Krüner, B., Tolosa, A., Fleischmann, S., Jäckel, N., Tekeli, M. C., Aslan, M., Suss, M. E., & Presser, V. (2016). MXene as a novel intercalation-type pseudocapacitive cathode and anode for capacitive deionization. *Journal of Materials Chemistry A, 4*(47), 18265-18271. https://doi.org/10.1039/c6ta07833h

Srimuk, P., Lee, J., Fleischmann, S., Choudhury, S., Jäckel, N., Zeiger, M., Kim, C., Aslan, M., & Presser, V. (2017a). Faradaic deionization of brackish and sea water via pseudocapacitive cation and anion intercalation into few-layered molybdenum disulfide. *Journal of Materials Chemistry A, 5*(30), 15640-15649. https://doi.org/10.1039/c7ta03120c

Srimuk, P., Zeiger, M., Jäckel, N., Tolosa, A., Krüner, B., Fleischmann, S., Grobelsek, I., Aslan, M., Shvartsev, B., Suss, M. E., & Presser, V. (2017b). Enhanced performance stability of carbon/titania hybrid electrodes during capacitive deionization of oxygen saturated saline water. *Electrochimica Acta, 224*, 314-328. https://doi.org/10.1016/j.electacta.2016.12.060

Sriramulu, D., Vafakhah, S., & Yang, H. Y. (2019). Activated Luffa derived biowaste carbon for enhanced desalination performance in brackish water. *RSC Advances, 9*(26), 14884-14892. https://doi.org/10.1039/c9ra01872g

Sui, Z., Meng, Q., Zhang, X., Ma, R., & Cao, B. (2012). Green synthesis of carbon nanotube–graphene hybrid aerogels and their use as versatile agents for water purification. *Journal of Materials Chemistry, 22*(18), 8767. https://doi.org/10.1039/c2jm00055e

Suss, M. E., Porada, S., Sun, X., Biesheuvel, P. M., Yoon, J., & Presser, V. (2015). Water desalination via capacitive deionization: what is it and what can we expect from it? *Energy & Environmental Science, 8*(8), 2296-2319. https://doi.org/10.1039/c5ee00519a

Tang, W., Kovalsky, P., Cao, B., He, D., & Waite, T. D. (2016a). Fluoride Removal from Brackish Groundwaters by Constant Current Capacitive Deionization (CDI). *Environmental Science & Technology*, 50(19), 10570-10579. https://doi.org/10.1021/acs.est.6b03307

Tang, W., Kovalsky, P., Cao, B., & Waite, T. D. (2016b). Investigation of fluoride removal from low-salinity groundwater by single-pass constant-voltage capacitive deionization. *Water Research, 99*, 112-121. https://doi.org/10.1016/j.watres.2016.04.047

Tang, W., Kovalsky, P., He, D., & Waite, T. D. (2015). Fluoride and nitrate removal from brackish groundwaters by batch-mode capacitive deionization. *Water Research, 84*, 342-349. https://doi.org/10.1016/j.watres.2015.08.012

Tang, Y., Guan, X., Su, T., Gao, N., & Wang, J. (2009). Fluoride adsorption onto activated alumina: Modeling the effects of pH and some competing ions. *Colloids and Surfaces A: Physicochemical and Engineering Aspects, 337*(1-3), 33-38.

Thamilselvan, A., Nesaraj, A. S., & Noel, M. (2016). Review on carbon-based electrode materials for application in capacitive deionization process. *International Journal of Environmental Science and Technology, 13*(12), 2961-2976. https://doi.org/10.1007/s13762-016-1061-9

Titirici, M. M., Funke, A., & Kruse, A. (2015). Hydrothermal Carbonization of Biomass. In *Recent Advances in Thermochemical Conversion of Biomass* (pp. 325-352). https://doi.org/10.1016/b978-0-444-63289-0.00012-0

Viswanathan, B., Neel, P. I., & Varadarajan, T. (2009). Methods of activation and specific applications of carbon materials. *India, Chennai*.

Voltea. (2015). *Voltea's Water Deionization Technology*. Retrieved Accessed on June 18, 2015 from http://www.voltea.com

Wagutu, A. W., Machunda, R., & Jande, Y. A. C. (2018). Crustacean derived calcium phosphate systems: Application in defluoridation of drinking water in East African rift valley. *Journal of Hazardous materials, 347*, 95-105. https://doi.org/10.1016/j.jhazmat.2017.12.049

Wang, G., Qian, B., Dong, Q., Yang, J., Zhao, Z., & Qiu, J. (2013). Highly mesoporous activated carbon electrode for capacitive deionization. *Separation and Purification Technology, 103*, 216-221.

Wang, H., Yan, T., Liu, P., Chen, G., Shi, L., Zhang, J., Zhong, Q., & Zhang, D. (2016). In situ creating interconnected pores across 3D graphene architectures and their application as high performance electrodes for flow-through deionization capacitors. *Journal of Materials Chemistry A, 4*(13), 4908-4919. https://doi.org/10.1039/c5ta10703b

Wang, J., & Kaskel, S. (2012). KOH activation of carbon-based materials for energy storage. *Journal of Materials Chemistry, 22*(45), 23710. https://doi.org/10.1039/c2jm34066f

Wang, L., Wang, M., Huang, Z.-H., Cui, T., Gui, X., Kang, F., Wang, K., & Wu, D. (2011). Capacitive deionization of NaCl solutions using carbon nanotube sponge electrodes. *Journal of Materials Chemistry, 21*(45), 18295. https://doi.org/10.1039/c1jm13105b

Wang, T., Zhai, Y., Zhu, Y., Li, C., & Zeng, G. (2018). A review of the hydrothermal carbonization of biomass waste for hydrochar formation: Process conditions, fundamentals, and physicochemical properties. *Renewable and Sustainable Energy Reviews, 90*, 223-247. https://doi.org/10.1016/j.rser.2018.03.071

Welgemoed, T. J. (2005). *Capacitive deionization technology™: Development and evaluation of an industrial prototype system* (Publication Number etd-02182005-130807) [Masters Dissertation, University of Pretoria]. Pretoria, South Africa. http://upetd.up.ac.za/thesis/available/etd-02182005-130807/

Welgemoed, T. J., & Schutte, C. F. (2005). Capacitive Deionization Technology™: An alternative desalination solution. *Desalination, 183*(1-3), 327-340. https://doi.org/10.1016/j.desal.2005.02.054

WHO. (2010). *Hardness in Drinking-water: Background document for development of WHO Guidelines for Drinking-water Quality*.

WHO. (2011). *Guidelines for drinking-water quality* (WHO chronicle 4th Edition).

Wimalasiri, Y., & Zou, L. (2013). Carbon nanotube/graphene composite for enhanced capacitive deionization performance. *Carbon, 59*, 464-471. https://doi.org/http://dx.doi.org/10.1016/j.carbon.2013.03.040

Xie, Z., Shang, X., Yan, J., Hussain, T., Nie, P., & Liu, J. (2018). Biomass-derived porous carbon anode for high-performance capacitive deionization. *Electrochimica Acta, 290*, 666-675. https://doi.org/10.1016/j.electacta.2018.09.104

Xing, F., Li, T., Li, J., Zhu, H., Wang, N., & Cao, X. (2017). Chemically exfoliated MoS_2 for capacitive deionization of saline water. *Nano Energy, 31*, 590-595. https://doi.org/10.1016/j.nanoen.2016.12.012

Xu, D., Tong, Y., Yan, T., Shi, L., & Zhang, D. (2017). N,P-Codoped Meso-/Microporous Carbon Derived from Biomass Materials via a Dual-Activation Strategy as High-Performance Electrodes for Deionization Capacitors. *ACS Sustainable Chemistry & Engineering, 5*(7), 5810-5819. https://doi.org/10.1021/acssuschemeng.7b00551

Xu, P., Drewes, J. E., Heil, D., & Wang, G. (2008). Treatment of brackish produced water using carbon aerogel-based capacitive deionization technology. *Water Research, 42*(10-11), 2605-2617.

Xu, X., Sun, Z., Chua, D. H., & Pan, L. (2015). Novel nitrogen doped graphene sponge with ultrahigh capacitive deionization performance. *Scientific Reports, 5*, 11225.

Yadav, A. K., Abbassi, R., Gupta, A., & Dadashzadeh, M. (2013). Removal of fluoride from aqueous solution and groundwater by wheat straw, sawdust and activated bagasse carbon of sugarcane. *Ecological Engineering, 52*, 211-218. https://doi.org/ 10.1016/j.ecoleng.2012.12.069

Yan, J., Zhang, H., Xie, Z., & Liu, J. (2017). Preparation of the Lentinus edodes-based porous biomass carbon by hydrothermal method for capacitive desalination. AIP Conference Proceedings

Yan, T., Xu, B., Zhang, J., Shi, L., & Zhang, D. (2018). Ion-selective asymmetric carbon electrodes for enhanced capacitive deionization. *RSC Advances, 8*(5), 2490-2497. https://doi.org/10.1039/c7ra10443j

Yang, J., Zou, L., & Choudhury, N. R. (2013). Ion-selective carbon nanotube electrodes in capacitive deionisation. *Electrochimica Acta, 91*, 11-19.

Yang, Z.-Y., Jin, L. J., Lu, G.-Q., Xiao, Q.-Q., Zhang, Y.-X., Jing, L., Zhang, X.-X., Yan, Y.-M., & Sun, K.-N. (2014). Sponge-Templated Preparation of High Surface Area Graphene with Ultrahigh Capacitive Deionization Performance. *Advanced Functional Materials, 24*(25), 3917-3925. https://doi.org/10.1002/adfm.201304091

Yasin, A. S., Mohamed, I. M. A., Mousa, H. M., Park, C. H., & Kim, C. S. (2018). Facile synthesis of TiO_2/ZrO_2 nanofibers/nitrogen co-doped activated carbon to enhance the desalination and bacterial inactivation via capacitive deionization. *Scientific Reports, 8*(1), 541. https://doi.org/10.1038/s41598-017-19027-w

Yasin, A. S., Obaid, M., Mohamed, I. M., Yousef, A., & Barakat, N. A. (2017). ZrO_2 nanofibers/activated carbon composite as a novel and effective electrode material for the enhancement of capacitive deionization performance. *RSC Advances, 7*(8), 4616-4626.

Yeh, C. L., Hsi, H.-C., Li, K.-C., & Hou, C. H. (2015). Improved performance in capacitive deionization of activated carbon electrodes with a tunable mesopore and micropore ratio. *Desalination, 367*, 60-68. https://doi.org/10.1016/j.desal.2015.03.035

Ying, T. Y., Yang, K. L., Yiacoumi, S., & Tsouris, C. (2002). Electrosorption of ions from aqueous solutions by nanostructured carbon aerogel. *Journal of Colloid and Interface Science, 250*(1), 18-27. https://doi.org/10.1006/jcis.2002.8314

Youssef, P. G., Al-Dadah, R. K., & Mahmoud, S. M. (2014). Comparative Analysis of Desalination Technologies. *Energy Procedia, 61*, 2604-2607. https://doi.org/10.1016/j.egypro.2014.12.258

Zhang, C., He, D., Ma, J., Tang, W., & Waite, T. D. (2018a). Faradaic reactions in capacitive deionization (CDI) - problems and possibilities: A review. *Water Research, 128*, 314-330. https://doi.org/10.1016/j.watres.2017.10.024

Zhang, D., Wen, X., Shi, L., Yan, T., & Zhang, J. (2012a). Enhanced capacitive deionization of graphene/mesoporous carbon composites. *Nanoscale, 4*(17), 5440-5446. https://doi.org/10.1039/c2nr31154b

Zhang, D., Yan, T., Shi, L., Peng, Z., Wen, X., & Zhang, J. (2012b). Enhanced capacitive deionization performance of graphene/carbon nanotube composites. *Journal of Materials Chemistry, 22*(29), 14696. https://doi.org/10.1039/c2jm31393f

Zhang, J., Fang, J., Han, J., Yan, T., Shi, L., & Zhang, D. (2018b). N, P, S co-doped hollow carbon polyhedra derived from MOF-based core–shell nanocomposites for capacitive deionization. *Journal of Materials Chemistry A, 6*(31), 15245-15252. https://doi.org/10.1039/c8ta04813d

Zhang, S., Tian, K., Cheng, B. H., & Jiang, H. (2017a). Preparation of N-Doped Supercapacitor Materials by Integrated Salt Templating and Silicon Hard Templating by Pyrolysis of Biomass Wastes. *ACS Sustainable Chemistry & Engineering, 5*(8), 6682-6691. https://doi.org/10.1021/acssuschemeng.7b00920

Zhang, W., Lin, N., Liu, D., Xu, J., Sha, J., Yin, J., Tan, X., Yang, H., Lu, H., & Lin, H. (2017b). Direct carbonization of rice husk to prepare porous carbon for supercapacitor applications. *Energy, 128*, 618-625. https://doi.org/10.1016/j.energy.2017.04.065

Zhang, X. F., Wang, B., Yu, J., Wu, X. N., Zang, Y. H., Gao, H. C., Su, P. C., & Hao, S. Q. (2018c). Three-dimensional honeycomb-like porous carbon derived from corncob for the removal of heavy metals from water by capacitive deionization. *RSC Advances, 8*(3), 1159-1167. https://doi.org/10.1039/c7ra10689k

Zhao, C., Liu, G., Sun, N., Zhang, X., Wang, G., Zhang, Y., Zhang, H., & Zhao, H. (2018). Biomass-derived N-doped porous carbon as electrode materials for Zn-air battery powered capacitive deionization. *Chemical Engineering Journal, 334*, 1270-1280. https://doi.org/10.1016/j.cej.2017.11.069

Zhao, R. (2013). *Theory and operation of capacitive deionization systems* [Thesis, Wageningen University].

Zhao, R., Biesheuvel, P. M., & Van der Wal, A. (2012). Energy consumption and constant current operation in membrane capacitive deionization. *Energy & Environmental Science, 5*(11), 9520. https://doi.org/10.1039/c2ee21737f

Zhao, R., Porada, S., Biesheuvel, P. M., & Van der Wal, A. (2013a). Energy consumption in membrane capacitive deionization for different water recoveries and flow rates, and comparison with reverse osmosis. *Desalination, 330*, 35-41. https://doi.org/10.1016/j.desal.2013.08.017

Zhao, R., Satpradit, O., Rijnaarts, H. H., Biesheuvel, P. M., & van der Wal, A. (2013b). Optimization of salt adsorption rate in membrane capacitive deionization. *Water Research, 47*(5), 1941-1952. https://doi.org/10.1016/j.watres.2013.01.025

Zhao, S., Yan, T., Wang, Z., Zhang, J., Shi, L., & Zhang, D. (2017). Removal of NaCl from saltwater solutions using micro/mesoporous carbon sheets derived from watermelon peel via deionization capacitors. *RSC Advances, 7*(8), 4297-4305.

Zornitta, R. L., García-Mateos, F. J., Lado, J. J., Rodríguez-Mirasol, J., Cordero, T., Hammer, P., & Ruotolo, L. A. M. (2017). High-performance activated carbon from polyaniline for capacitive deionization. *Carbon, 123*, 318-333. https://doi.org/ 10.1016/j.carbon. 2017.07.071

Zou, L., Li, L., Song, H., & Morris, G. (2008a). Using mesoporous carbon electrodes for brackish water desalination. *Water Research, 42*(8-9), 2340-2348. https://doi.org/10. 1016/ j.watres.2007.12.022

Zou, L., Morris, G., & Qi, D. (2008b). Using activated carbon electrode in electrosorptive deionisation of brackish water. *Desalination, 225*(1-3), 329-340.

Zou, R., Quan, H., Wang, W., Gao, W., Dong, Y., & Chen, D. (2018). Porous carbon with interpenetrating framework from Osmanthus flower as electrode materials for high-performance supercapacitor. *Journal of Environmental Chemical Engineering, 6*(1), 258-265. https://doi.org/10.1016/j.jece.2017.11.080